NATIONAL ADVISORY COMMITTEE FOR AERONAUTICS

—

REPORT 1340

INVESTIGATION OF DOWNWASH, SIDEWASH, AND MACH NUMBER DISTRIBUTION BEHIND A RECTANGULAR WING AT A MACH NUMBER OF 2.41

By DAVID ADAMSON and WILLIAM B. BOATRIGHT

1957

REPORT 1340

INVESTIGATION OF DOWNWASH, SIDEWASH, AND MACH NUMBER DISTRIBUTION BEHIND A RECTANGULAR WING AT A MACH NUMBER OF 2.41

By DAVID ADAMSON and WILLIAM B. BOATRIGHT

Langley Aeronautical Laboratory
Langley Field, Va.

National Advisory Committee for Aeronautics

Headquarters, 1512 H Street NW., Washington 25, D. C.

Created by Act of Congress approved March 3, 1915, for the supervision and direction of the scientific study of the problems of flight (U. S. Code, title 50, sec. 151). Its membership was increased from 12 to 15 by act approved March 2, 1929, and to 17 by act approved May 25, 1948. The members are appointed by the President and serve as such without compensation.

REPORT 1340

INVESTIGATION OF DOWNWASH, SIDEWASH, AND MACH NUMBER DISTRIBUTION BEHIND A RECTANGULAR WING AT A MACH NUMBER OF 2.41 [†]

By DAVID ADAMSON [1] and WILLIAM B. BOATRIGHT

SUMMARY

An investigation of the nature of the flow field behind a rectangular wing of circular arc cross section has been conducted in the Langley 9-inch supersonic tunnel. Pitot- and static-pressure surveys covering a region of flow behind the wing have been made together with detailed pitot surveys throughout the region of the wake. In addition, the flow direction has been measured by means of a weathercocking vane.

Theoretical calculations have been made to obtain the variation of both downwash and sidewash with angle of attack by using the superposition method of Lagerstrom, Graham, and Grosslight. In addition the effect of the wing thickness on the sidewash with the wing at 0° angle of attack has been evaluated. Near an angle of attack of 0°, agreement between theory and experiment is good, particularly for the downwash results, except in the plane of the wing, inboard of the tip. In this region the proximity of the shed vortex sheet and the departure of the spanwise distribution of vorticity from theory would account for the disagreement. At higher angles of attack prediction of downwash depends on a knowledge of the location of the trailing vortex sheet, in order that the downwash may be corrected for its displacement and distortion. The theoretical location of the trailing vortex sheet, based on the theoretical downwash values integrated downstream from the wing trailing edge, is shown to differ widely from the experimentally determined location.

The rolling-up of the trailing vortex sheet behind the wing tip is evidenced by both the wake surveys and the flow-angle measurements.

INTRODUCTION

In order to assess the stability characteristics of an aircraft or missile configuration, it is necessary that the nature of the flow field existing in the region of the tail plane be known. As far as the subsonic flow is concerned, much attention has been given in the past to this problem (e.g., ref. 1) and, for the conventional subsonic aircraft configuration, downwash effects can be predicted with sufficient accuracy to serve the practical needs of designers. For configurations in which the ratio of wing span to tail span is small, as is the usual case for supersonic-missile configurations, the downwash problem is not so fully developed. Only fairly recently have research investigations in this important field been undertaken with any degree of thoroughness.

The application of the linearized theory to the problem of predicting the downwash field existing behind wings of various shapes has been studied by Lagerstrom, Graham, and Grosslight (refs. 2 and 3) using the method of superposition, by Mirels and Haefeli (ref. 4) using a surface of potential discontinuity (represented by a distribution of vortices over the vortex sheet), and by Lomax and Sluder (ref. 5) using the discontinuity as represented by a distribution of doublets.

In addition, several experimental investigations of the downwash field behind lifting surfaces in a supersonic flow have been made within the past year. In reference 6 a somewhat indirect approach is made to the problem, the average downwash over a tail surface being measured by force tests of a variable configuration of a body, wing, and tail. In references 7 and 8, direct measurements at a Mach number of 1.53 of the downwash angle of the flow have been made at a limited number of locations behind a rectangular wing and behind a triangular wing. In addition a survey of the pitot pressure across the wake of the two wings was made. A similar investigation of the flow in the region of the tip of a trapezoidal wing at a Mach number 1.91 was made in reference 9.

Except for these few studies, experimental data pertinent to the problem are very limited. The primary purpose in undertaking the present investigation is to supplement the available experimental data. For this investigation a number of measurements of both the downwash and sidewash components of the flow angle have been made in the Langley 9-inch supersonic tunnel for locations in the plane of the wing and in planes above and below the plane of the wing. These measurements were obtained by using a floating vane that would weathercock in the stream in the direction of the local flow angle. In addition, pitot-pressure measurements throughout the region of the viscous wake and static- and pitot-pressure measurements for a region covering the general flow field behind the wing were made. All tests were conducted at a stream Mach number of 2.41 and a Reynolds number of 640,000. A secondary purpose of this investigation is to compare the theoretical evaluation of the flow field with the experimental data and to examine the regions of validity of linearized theory. In order to calculate these theoretical results the superposition method of reference 2 has been used. These results have been extended to calculate

the flow direction in planes above and below the plane of the wing. The effect of the wing thickness on the values of side-wash and downwash in causing a departure from the results of the theory presented by reference 2 is shown and discussed. A comparison of the measured wake characteristics with those of a subsonic flow is included and an attempt to show the effect of the wake on the downwash field has been made.

SYMBOLS

α wing angle of attack, deg

α_B angle of attack of vane about its axis, when its axis is inclined in roll so that the bottom mirror of the vane is vertical, deg

α_T angle of attack of vane about its axis, when its axis is inclined in roll so that the top mirror of the vane is vertical, deg

b wing span, in.

c wing chord, in.

ϵ downwash angle, deg

M Mach number of flow

$\mu = \dfrac{1}{\sqrt{M^2-1}}$

p stream static pressure, in. Hg

Δp change in static-pressure reading due to tube misalinement

$p_{t,c}$ tunnel stagnation pressure (measured in settling chamber of tunnel), in. Hg

p_t' total pressure as measured by a total-pressure tube (uncorrected for the normal shock at nose of tube)

R Reynolds number (based on wing chord)

S wing area, sq in.

σ sidewash angle, deg

ϕ angle of inclination of vane axis in roll, deg

t wing thickness, in.

u perturbation velocity component of flow along the longitudinal axis, fps

v perturbation velocity component of flow along the lateral axis, fps

w perturbation velocity component of flow along the vertical axis, fps

U free-stream velocity, fps

x longitudinal coordinate

y lateral coordinate

z vertical coordinate

APPARATUS AND TEST METHODS

TEST APPARATUS

Wind tunnel.—All tests were made in the Langley 9-inch supersonic tunnel, which is a continuously operating, closed-circuit tunnel in which the stream pressure, temperature, and humidity can be controlled and regulated. Different test Mach numbers are provided by interchanging nozzle blocks which form test sections approximately 9 inches square. Throughout the present tests the moisture content in the tunnel was kept sufficiently low to make the effects of condensation in the supersonic nozzle negligible.

Wing model and boundary-layer bypass plate.—The measurements of the flow field were made behind a rectangular, semispan wing of circular-arc section. The geometric characteristics of the wing are as follows:

Semispan, inches _____ 3.50
Aspect ratio (complete wing, including image) _____ 2.34
Thickness, percent chord _____ 6
Chord, inches _____ 2.98

The semispan wing was mounted on a boundary-layer bypass plate so that boundary-layer interference effects were reduced to a minimum. The boundary-layer bypass plate used in these tests is shown in figures 1, 2, and 3. It had a semiapex angle of 32° and was beveled on its underside to an angle of 4.6° normal to the leading edge. Thus its leading edge was supersonic and the tips of the plate should not affect any of the points where test data were taken. The side of the boundary-layer bypass plate toward the wing was flat and parallel to the tunnel wall over its entire area to within 0.005 inch.

The wing and the spindle on which it was mounted were of one-piece solid-steel construction. Adjacent to the wing root, the spindle was ¾ inch in diameter and passed through the hole of this size drilled and reamed in the boundary-layer bypass plate. Between the bypass plate and the tunnel wall the spindle had a ¾-inch chord and a ¼-inch-thick diamond-shaped cross section. The part of the spindle piercing the tunnel side wall and projecting beyond was a ½-inch-diameter shaft. A sector plate was clamped to the part of the spindle projecting beyond the side wall. A clinometer was placed on the edge of the sector plate so that it could be used for setting the angle of attack of the wing. The zero reference angle was obtained by using a cathetometer to aline a carefully scribed mean chord line on the tip cross section with the horizontal center line of the tunnel.

Pressure survey rakes.—Total and static pressures were first measured with a rake consisting of five pitot-static tubes, each 0.090 inch in diameter. The static-pressure orifices were located 1.5 inches rearward of the nose of the tube. Some doubt existed as to the dependability of the static-pressure measurements made with a tube so large in relation to the model size; consequently, a second five-prong rake consisting of 0.040-inch-diameter tubes, each vented with four 0.010-inch-diameter orifices at a distance ⅜ inch behind a sharp ogival nose, was also used to measure the static pressures. The static pressures obtained by using this small rake checked closely those obtained by using the large rake, with the exception of the entire spanwise set of measurements made 0.5 chord to the rear of the wing trailing edge and 0.363 chord above the plane of the wing. The disagreement in the static pressures for this set of points resulted because one tube on the small rake at this station was faulty. If these faulty measurements are ruled out, 90 percent of all remaining measurements agreed within ±2 percent and of the other 10 percent none differed by more than 6 percent. The static-pressure and Mach number data presented are those obtained by using the 0.040-diameter tubes, with the exception of those faulty points
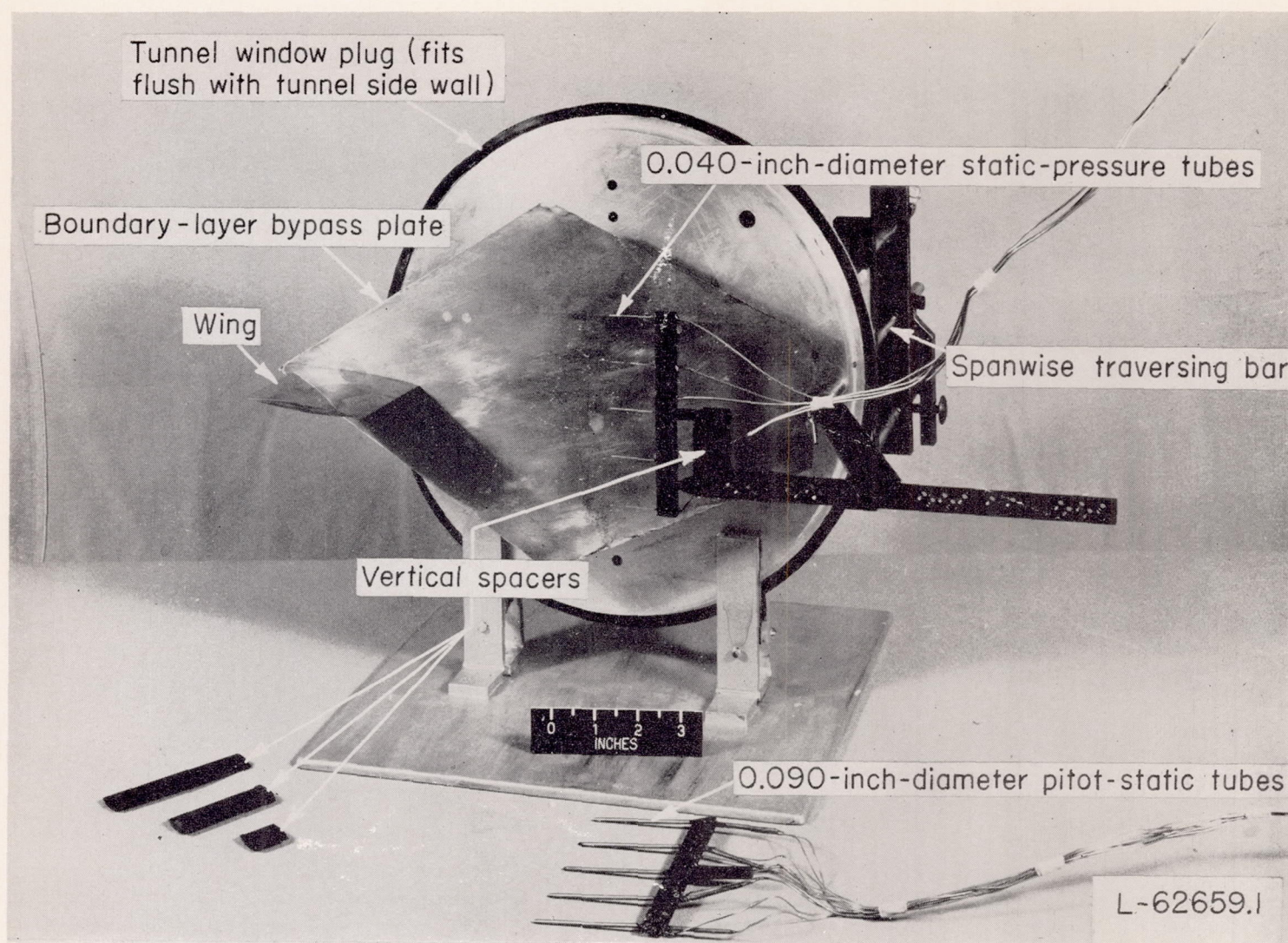
FIGURE 1.—Illustration of apparatus for the general survey behind the wing.

referred to above, for which the data of the 0.090-inch-diameter tube were substituted. The test setup is shown in figure 1.

The total-pressure distribution throughout the viscous wake behind the wing was measured with a rake of 7 tubes, each of 0.040-inch outside diameter (fig. 2). The seven tubes in this rake were spaced ¼ inch apart. For this spacing, there should be no mutual interference between the tubes. The front part of the rake, on which the tubes were mounted, was linked to the rear part with flexible plates in such a manner that the tubes could be traversed up or down the ⅛ inch necessary for a complete measurement of the pressures vertically throughout the wake. Cables attached to the bell cranks (fig. 2) actuated the system so that the traverse might be made while the tunnel was running.

The presence of steep pressure gradients encountered in the wake in preliminary test runs in which the 0.040-inch-diameter tubing was used suggested that the large tubing might not yield a true local pressure; consequently, a smaller rake of 0.010-inch-outside-diameter tubes 1/16 inch apart was

attached to the larger rake and a check test was made through the wake at the station ½ chord to rear of the trailing edge and $0.571\frac{b}{2}$ from the wing root. At this point, the measurements of the pressures through the peak check within 0.7 percent. Since this check was made closest to the trailing edge where the pressure peak through the wake is sharpest, it is believed that the data pertaining to the pressures in the wake are reliable.

Floating vane used for measurement of flow direction.— For the measurements of the stream angle throughout the flow field, a vane that would "weathercock" in the stream was used. A photograph of the entire installation is given in figure 3 and a detailed sketch of the vane itself in figure 4.

In order to keep the aerodynamic center of pressure of the vane as far behind its axis as possible and still have it mass balanced about this axis, the vane was fabricated from different materials. The forecone and central part were of stainless steel, the aftercone of magnesium, and the flat triangular wing part was made from 0.010-inch-thick aluminum. The stainless-steel central part was of square cross section with
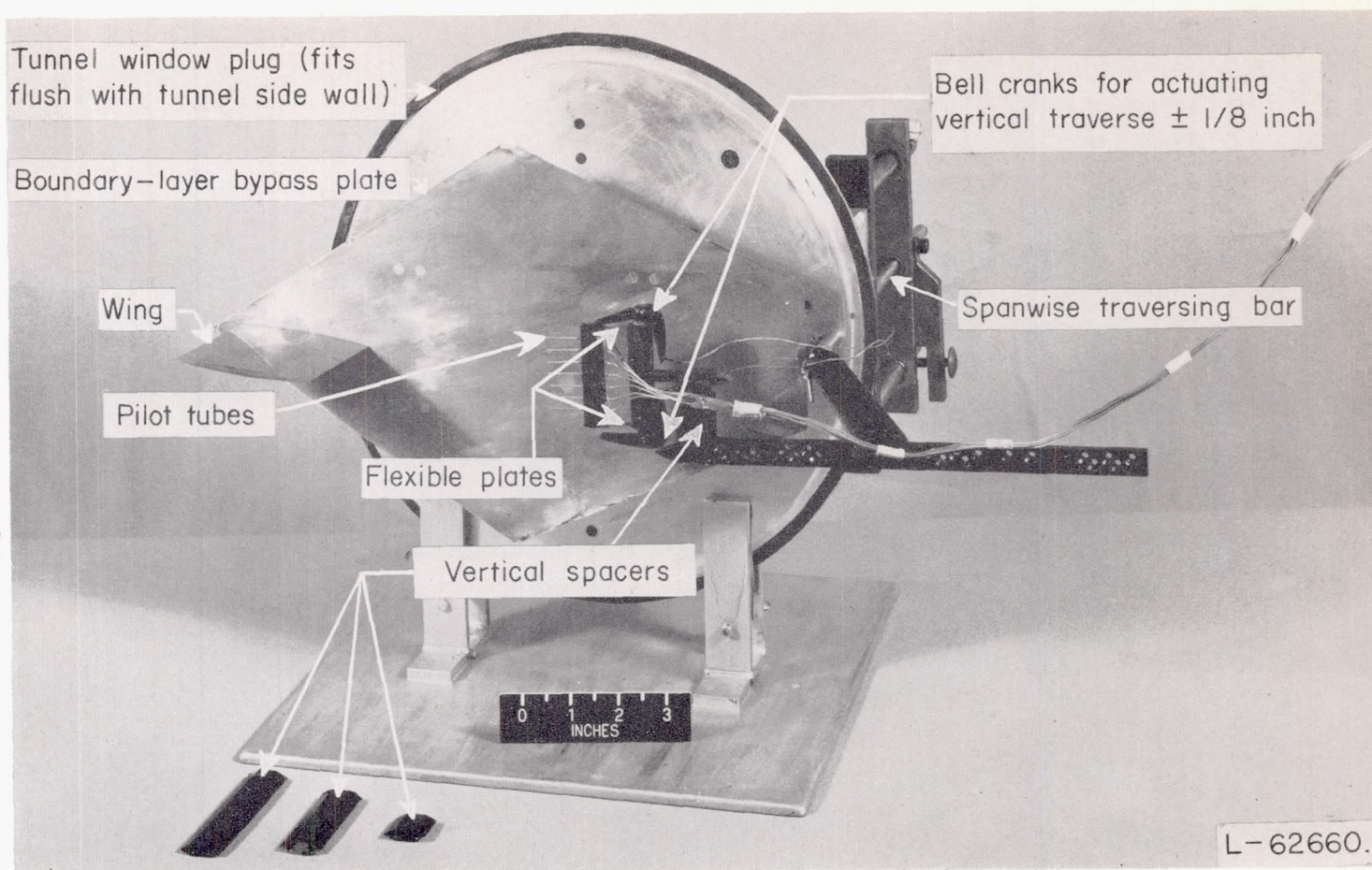
Figure 2.—Illustration of wake survey apparatus.

its faces inclined at 45° to the vane pivot axis and each face was polished to a mirror finish. The axis about which this vane was free to pivot was contained in a vertical plane perpendicular to the free-stream flow and was first inclined in roll 45° from the vertical in one direction then 45° in roll in the opposite direction from the vertical. This orientation of the axis was actuated while the tunnel was in operation by means of two cables, which were led out through a hole in the tunnel side wall. One or the other of these cables was pulled to rotate the vane yoke in either direction against a stop. When the vane spindle was oriented at 45° to the horizontal, one of the four mirrored surfaces was always vertical. A light source giving approximately parallel light was located 80 inches from the vane. The incident light passed through a glass window in the tunnel side wall and was reflected from the mirrored face onto a ruled grid which had been set up outside the tunnel. The position of the reflected light spot on the ruled grid determined the deflection of the flow in the plane perpendicular to the vane spindle. When this measurement had been taken with the vane axis 45° one way, the procedure was repeated with the vane axis reoriented to 45° the other way. The downwash and side-wash could then be obtained from these two measurements.

In order to facilitate the conversion of the measurements of coordinates of the light spot to values of angular displacement of the vane, charts were prepared as described in appendix A. In order that a single series of calibration curves

might be used in the reduction of the test data it was necessary that the distance between the vane and the reference grid, to which the light source was rigidly attached, remain unchanged throughout the entire tests. This restriction necessitated that the grid be moved whenever a change was made in the spanwise or chordwise location of the vane. For the purpose of facilitating these adjustments, a plan view of the tunnel test section was mapped on the top of the table on which the reference grid was supported. In this way the movement of the grid corresponding to each movement of the vane within the working section could be made rapidly.

In order to attain the required degree of accuracy in the measurement of the direction of the flow by using a vane, it was necessary that the relative location of the vane light source and graduated scale be known with exactness. This demanded that care be exercised in setting up the apparatus. It was also necessary to know the orientation of the normals to the mirror surfaces of the vane relative to the vane axis of rotation. The method of making these measurements is described in appendix A.

TEST PROCEDURE

Surveys.—The procedure used in making the pressure surveys with the five-tube rake was to set the wing angle of attack, then, by sliding the shaft through the tunnel, to vary the spanwise position of the rake in 0.5-inch increments from 0.5 inch from the root to 2 inches beyond the tip. The
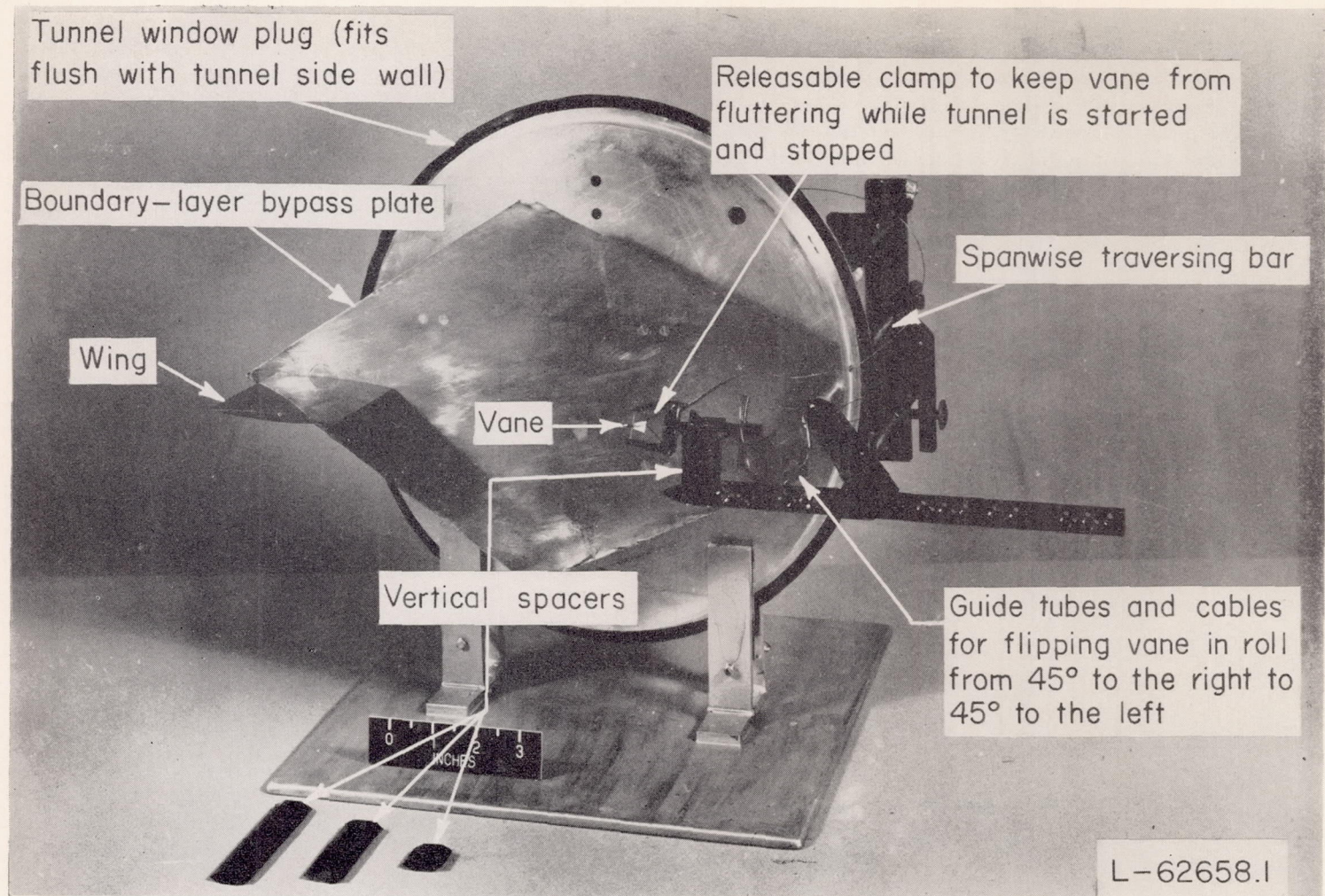
FIGURE 3.—Illustration of the vane setup used in the tunnel for measuring flow direction.
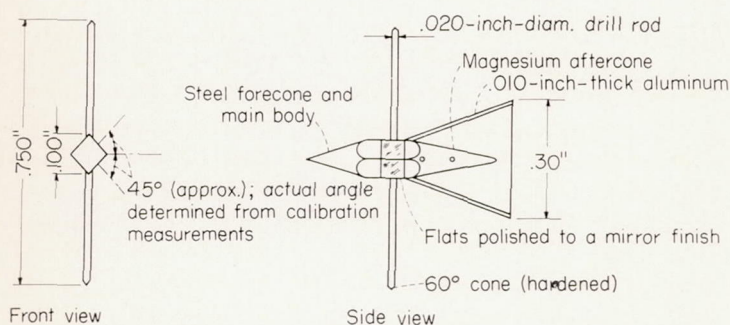

FIGURE 4.—Magnified sketch of vane showing pertinent dimensions.

pressures at the five vertical locations were read at each spanwise position. With the tunnel operating, the wing angle of attack was adjusted to a new value and the procedure repeated. When spanwise traverses at the four angles of attack were completed, the tunnel flow was stopped in order that the rake might be moved to a new chordwise location. Measurements of stagnation pressure and static pressure were thus obtained for five vertical locations, ten spanwise stations, and for wing angles of attack of 0°, 3°, 6°, and 10° at chordwise stations from 0.5 chord to 3 chords rearward of the wing trailing edge in 0.5-chord increments.

Exploration of wake.—The wake survey was conducted in a similar manner, except that at each spanwise station a vertical traverse of the wake was made. Special attention was given to this vertical traverse in order to cover adequately the region of minimum pressures in the wake and to get a number of test points at each edge of the wake. The vertical location of the center tube in the seven-tube rake was measured with a cathetometer for each set of readings and the location of each of the seven tubes was known from measurements of the tube spacing made before each test. Data defining the wake were obtained at the same ten spanwise stations and the same four angles of attack as in the pitot-static survey, but at only three of the chordwise locations, that is, at 0.5 chord, 1.5 chords, and 2.5 chords downstream of the wing trailing edge.

Measurement of flow angles.—The test procedure followed in making measurements of flow angle was the following. With the vane located at any spanwise station, the wing angle of attack was adjusted to each of the four angles of attack in turn. This adjustment to wing angle of attack was made by rotating the sector attached to the wing spindle until a hole in the sector was brought opposite a hole drilled in the tunnel wall and inserting a pin to hold it in position.

At each angle of attack, the x- and y-coordinates of the light spot of the beam reflected from the vane were noted with the vane yoke rolled first against one stop then against the other. After these measurements were taken for the four wing angles of attack, the spanwise positions of the vane and of the grid were changed and the process was repeated. After each spanwise movement of the vane, a check was made by using the cathetometer to ensure that the vane axis of rotation remained in a vertical plane with the vane rolled against either stop.

The tunnel had to be stopped to change either the chordwise or the vertical position of the vane. Angle data were taken for the same ten spanwise stations and the same four wing angles of attack as in the case of the pressure surveys, but only for the vertical locations on the tunnel center line and 0.363 chord above and 0.363 chord below the tunnel center line and for chordwise locations of 0.5 chord, 1.5 chords, and 2.5 chords behind the wing trailing edge.

PRECISION OF DATA

The data to be presented consist of (a) static- and total-pressure measurements throughout the general flow field behind the wing, (b) detailed measurements of total pressure throughout the region of the viscous wake, and (c) measurements of the direction of the flow throughout the general flow field. The errors associated with each of these three categories of measurements are discussed in the sections that follow.

STATIC- AND TOTAL-PRESSURE MEASUREMENTS OF GENERAL FLOW FIELD

The errors involved in measurements of pressures in the general flow field behind the wing are traceable to three sources:

First, it is known from past experience that the error involved in reading the heights of the mercury manometer may make the static pressure in doubt by ± 0.5 percent and the stagnation pressures in doubt by ± 0.06 percent. Since the Mach number was determined by the ratio of these pressures, a cumulative error could introduce an error in free-stream Mach number of ± 0.006.

Second, in the presence of large pressure gradients in the flow, the error due to the finite size of any pressure-measuring device might be appreciable. For the static-pressure measurements, where this effect would be most noticeable, the tests with the two different tube diameters should indicate the order of magnitude of the errors due to this source of inaccuracy. In the section entitled "Apparatus and Test Methods" the inconsistencies in the static-pressure measurements with the two sizes of tube are pointed out.

A third source of error might result from misalinement of the tube with the local stream direction. Previous experience has shown that a pitot tube is insensitive to variations in alinement of the flow with respect to the tube of as much as 7°, the maximum deflection encountered in these tests; however, since no reliable data existed as to the errors attributable to misalinement of tubes in obtaining static measurements, a separate series of tests was run to obtain such data. For this purpose each tube of the five-tube rake was rotated about its axis by amounts varying between 0° and 45°. The rake was then placed in the empty tunnel

and static-pressure measurements taken with the rake inclined at various angles to the tunnel axis. The results are presented in figure 5 in the form of plots of $\Delta p/p_{t,c}$ against α for various angles of roll. This figure shows that the correction is negligible up to flow angles of 3°, irrespective of location of the four orifices equally spaced around the periphery. At those points where measurement of sidewash and downwash exceeded 3°, the angle of the flow with respect to the tube (or tunnel axis) was computed in polar coordinates and appropriate corrections applied. Since in most parts of the downwash field the flow angle was less than this, most of the pressure data did not need to be corrected. At stations 0.726 chord above and below the tunnel center line, no measurements were made of downwash or sidewash and corrections to the static pressures could not be applied. However, it is probable that in these planes only the data for the station 0.5 chord to the rear of the trailing edge would require any correction, because the angle of the flow at the 1.5- and 2.5-chord stations was probably less than 3°.

MEASUREMENTS OF PITOT PRESSURE ACROSS WAKE

The total-pressure readings made in the wake surveys were, of course, of the same order of accuracy as the pitot pressure readings of the general survey. For the wake survey, the most critical source of error was the measurement of the location of the point where the pressure was being read with respect to the wing. A cathetometer with a vertical scale, which, by means of a vernier, could be read to 0.001 inch, was used for all measurements of location of the test points. It is believed that the locations of the pressure readings in the wake are correct as plotted with respect to the wing to within ± 0.003 inch. The smoothness of the curves of the measurement of the pitot pressures across the wake and the excellent check that was obtained with the small 0.010-inch-diameter-tube rake seem to bear this out.

MEASUREMENTS OF FLOW DIRECTION

The measurements of flow angle with the vane were subject to four main sources of error: (1) a possible error due to friction of the conical pivots of the vane shaft in the pivot holes of the yoke, (2) a possible error in the angular measurement of normals to the polished flats of the vane relative to
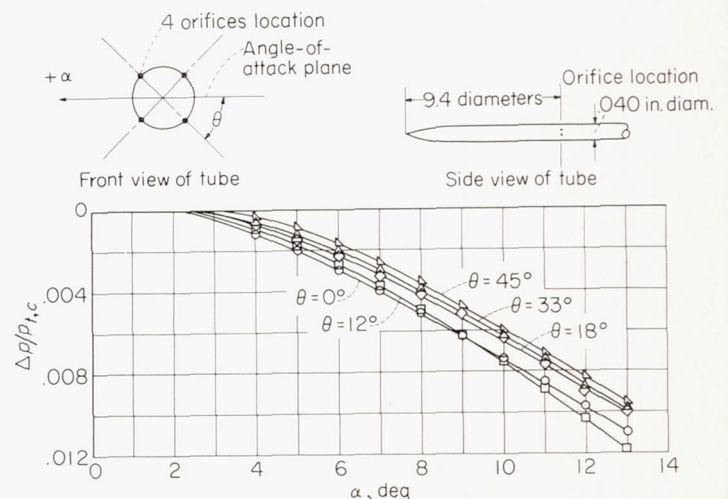

FIGURE 5—Effect of misalinement with flow direction on 0.040-inch-diameter static-pressure tube. $M = 2.41$.

the vane axis, (3) a possible error due to the possibility that the plane containing the axes of rotation of the vane in its two positions was not normal to the free stream, and (4) a possible error due to the finite size of the vane which might influence the results in regions of large pressure or angle gradients. Since 1° of vane rotation resulted in a movement of the light spot of about 2 inches any reading error was negligible. These sources of error are discussed separately in the following paragraphs.

The first source of error considered (i.e., error due to pivot friction) was calculated to be about ±0.05°. This in itself would be reduced by any vibration which is always present in the tunnel.

The second source of error (i.e., the accuracy of the measurement of the angle of the normals to the polished flats of the vane body) was a function of the accuracy of each step in these measurements. The accuracy involved in each step of the calibration has been assessed and, by using the theorem of least squares, it is estimated that the measurement of the angle of the reflected light beam from any flat was correct to within ±0.07° in the horizontal plane and ±0.03° in the vertical plane. Checking by repeating the measuring procedure seemed to bear out these estimates.

The third source of error could arise from the vane axis not being normal to the stream in its two rolled positions. This alinement was checked during the tests by means of a cathetometer and it is believed the precision of this measurement was kept to ±0.05°.

The fourth source of error, the finite vane dimensions, would cause the vane to indicate an average value of the angularity of the flow over its finite area instead of the point value which is presented in the results. The point on the vane used as reference in plotting the results as point locations was the point where the vane spindle intersected the center line of the vane fuselage. The vane was constructed as small as was practical in order to minimize the effect of its finite size; the excellent check between theory and experiment for the downwash results just outboard of the tip, where a large gradient in flow angularity exists, suggests that any errors due to the finite size of the vane were small. A large pressure gradient over the area of the vane would serve to weight the angle gradient existing over the area of the vane in such a manner that it would indicate a different average angle of flow than the average angle it would indicate in a uniform pressure. For this reason the results for locations in the viscous wake might be expected to be slightly more in error than results elsewhere in the flow field.

Application of the theory of least squares indicates that the over-all precision of the measurement of the angle of the flow is ±0.1°, although the inaccuracy may be slightly more in the wake.

RESULTS AND DISCUSSION
TEST-POINT LOCATIONS WITH RESPECT TO TRAILING-EDGE SHOCKS AND TIP MACH CONES

The locations of the test points at which static and total pressure were measured are shown in side view in figure 6 and in plan view in figure 7 in relation to the wing and to the
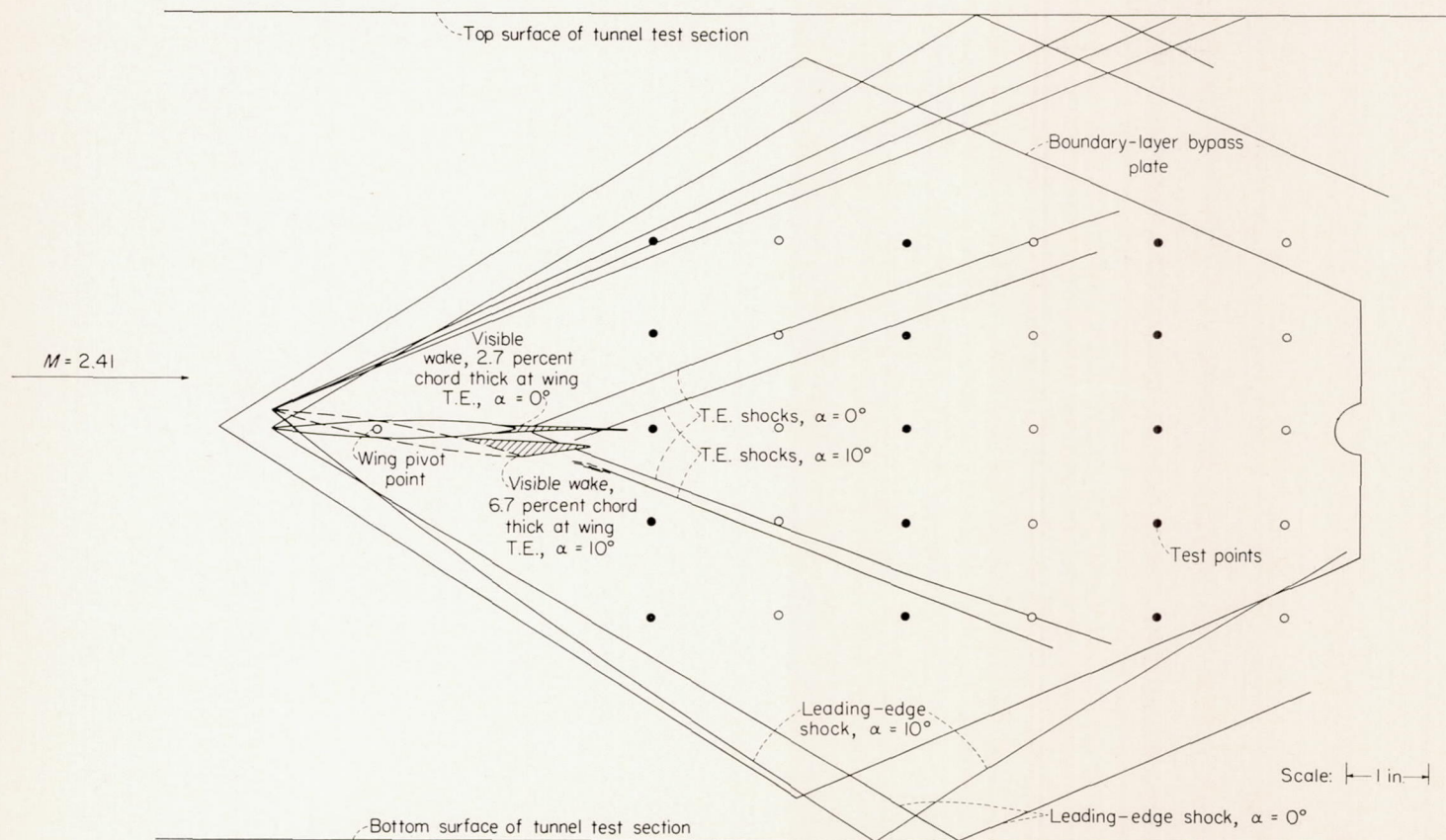

FIGURE 6.—Side view of test section showing relation of test points to wing-trailing-edge shock pattern as seen in a shadowgraph. Solid symbols indicate survey locations for both Mach number and flow angle. Open circles indicate survey locations for only flow angle.

discontinuities existing in the field of flow behind the wing. Knowledge of the locations of these discontinuities is of great value in analyzing the downwash and sidewash data. The trailing-edge shock waves shown in figure 6 are copies of the shadows of these shock disturbances on the bypass plate obtained when parallel light, normal to the surface of the plate, is projected through the test section. The measured inclination of the shock waves checked closely with the calculated values. However, at both $\alpha=0°$, and more particularly at $\alpha=10°$, the trailing-edge shock waves do not originate at the trailing edge. At $\alpha=10°$ the laminar separation at the trailing edge and the resulting overexpansion of the flow from the high-pressure side of the wing leading to the shock wave downstream of the trailing edge are discussed in detail in reference 10. The strength of this shock wave which arises only from viscosity of the flow is comparable with that of the expected nonviscous shock at the trailing edge from the upper surface.

The boundaries of the regions of the tip effects shown in plan view in figure 7 are not as accurate as are those in the side view of figure 6 since their locations were not visible to an observer and were not measured directly. On the wing surface their location was plotted by using the Mach number distribution as obtained from section theory. Reference 11 shows that the experimental locations conform closely to those predicted by this method. Downstream of the trailing

edge the experimental values of Mach number, which were known at streamwise stations 0.5 chord apart, were used in constructing the tip Mach cones. This type of construction would thus represent the forward limit of the disturbances from the tip. In planes above or below the horizontal plane through the wing trailing edge, it is known that the boundaries are approximately hyperbolic (they would be exactly hyperbolic if the Mach cone were right circular in form). The nose of this hyperbola was obtained by revolving the trace of the trailing-edge shocks (as obtained from the shadowgraph sketch of fig. 6) about the cone axis into the plane of the test points. Where the legs of the hyperbola become almost straight lines, the method previously described (based on Mach number measurements) can be used to extend the boundaries. The principal uncertainties involved in the application of this method of construction lie in the construction of the nose portion of the hyperbola and for this reason these portions of the boundary are shown dotted in figure 7 (a). However, since the nose portion of the hyperbola is relatively small, the errors introduced are correspondingly small and the approximate boundaries as drawn in figure 7 are believed quite adequate for tracing discontinuities existing in sidewash and downwash data to their source.

Results obtained with wing absent.—Measurements of static and total pressures made at the stations defined above indicated that there is only a slight departure from uniformity
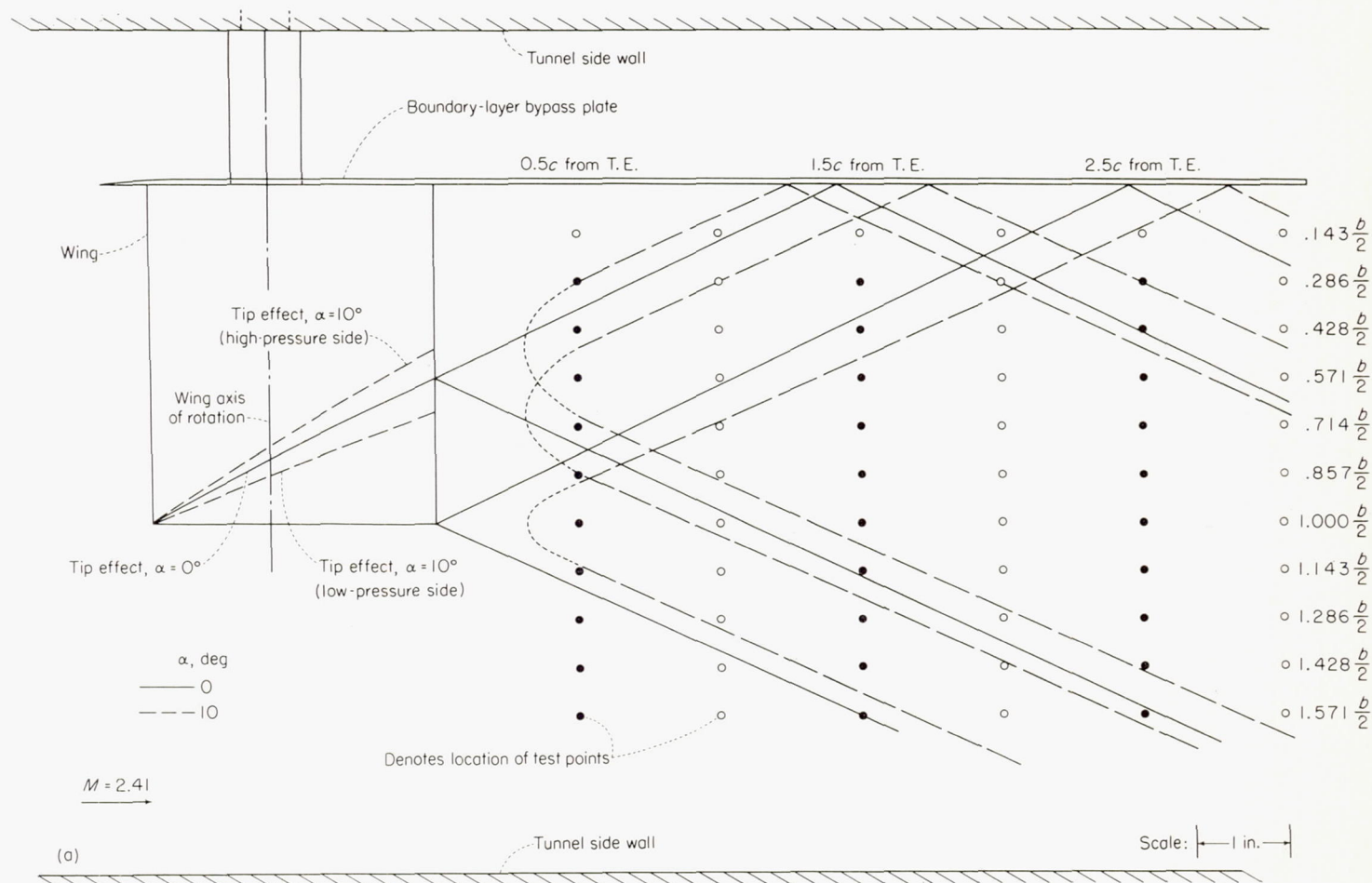
(a) Horizontal plane of tunnel center line.

FIGURE 7.—Location of tip-effect regions behind wing in relation to test points. Solid symbols indicate survey locations for both Mach number and flow angle. Open circles indicate survey locations for only flow angle.

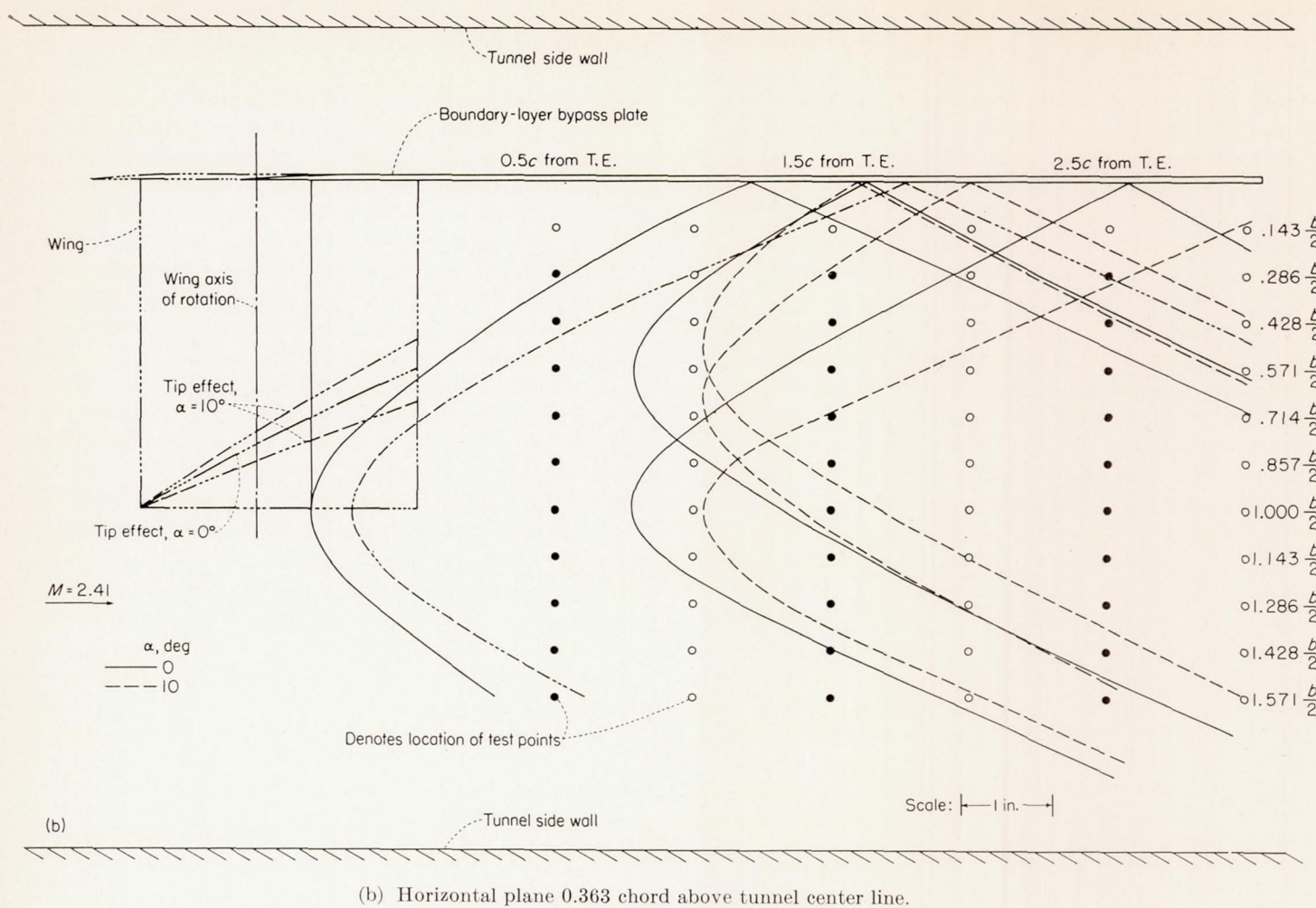(b) Horizontal plane 0.363 chord above tunnel center line.

FIGURE 7.—Continued.

throughout the region of flow investigated, and that, therefore, as far as pressure distribution is concerned, the presence of the boundary-layer plate does not, to any significant extent, destroy the uniformity of flow. Within the region investigated, the Mach number was found to be 2.41 within limits of ±0.01. No measurements of the flow angle were made with the wing absent; however, indications from previous experiments where the flow angle was measured at a limited number of points are that the deviations of the flow from the alinement with the tunnel horizontal center line are small.

Results obtained with wing present.—Plots of the pressure ratio $p/p_{t,c}$ against each vertical location of the test point are shown for all angles of attack and test-point locations in figure 8. The experimental points have been joined with straight lines only to assist in distinguishing the points appropriate to the various wing angles of attack. Actually the presence of shocks gives rise to finite discontinuities in static-pressure distribution.

Within the strictly two-dimensional region of flow, the static pressures as measured conform closely to the theoretical values. Wherever discontinuities do occur they can be traced to the presence of shock waves either emanating from the wing or reflected from the boundary-layer bypass plate or tunnel walls. The reflections of the disturbances due to the wing from the bypass plate correspond to an opposite wing or total-span condition. In those instances

where the center tube of the five-tube rake falls within the wake boundaries, it is found that, for most of the data, the pressure as recorded by this tube does not differ markedly from the pressure as recorded by the two tubes adjacent to the center tube. This result implies that the static pressure is fairly constant over the wake thickness. (An observation in this connection is made in the next section.)

In addition to the static-pressure measurements, measurements of total pressure were made at the same locations and for the same wing angle-of-attack conditions as for the static pressures. From these data, the Mach number has been evaluated and plotted in figure 9 in a similar manner, and for the same locations, as for plots of the static pressure ratios just described.

WAKE

The measured total pressures across the wake have been plotted against vertical distance in figure 10. Owing to the presence of shocks across the mouth of the measuring tubes these are not the true stagnation pressures. Plotted in this manner (i.e., uncorrected for the shock at the nose of the tubes) the large jumps in the curves above and below the wake at the station 0.5 chord behind the trailing edge clearly define the vertical location of the trailing-edge shocks. Figure 11 shows the same curves of pressure ratio against vertical location presented in an oblique view. This figure gives a better visualization of the pitot pressures throughout the whole wake to be obtained.
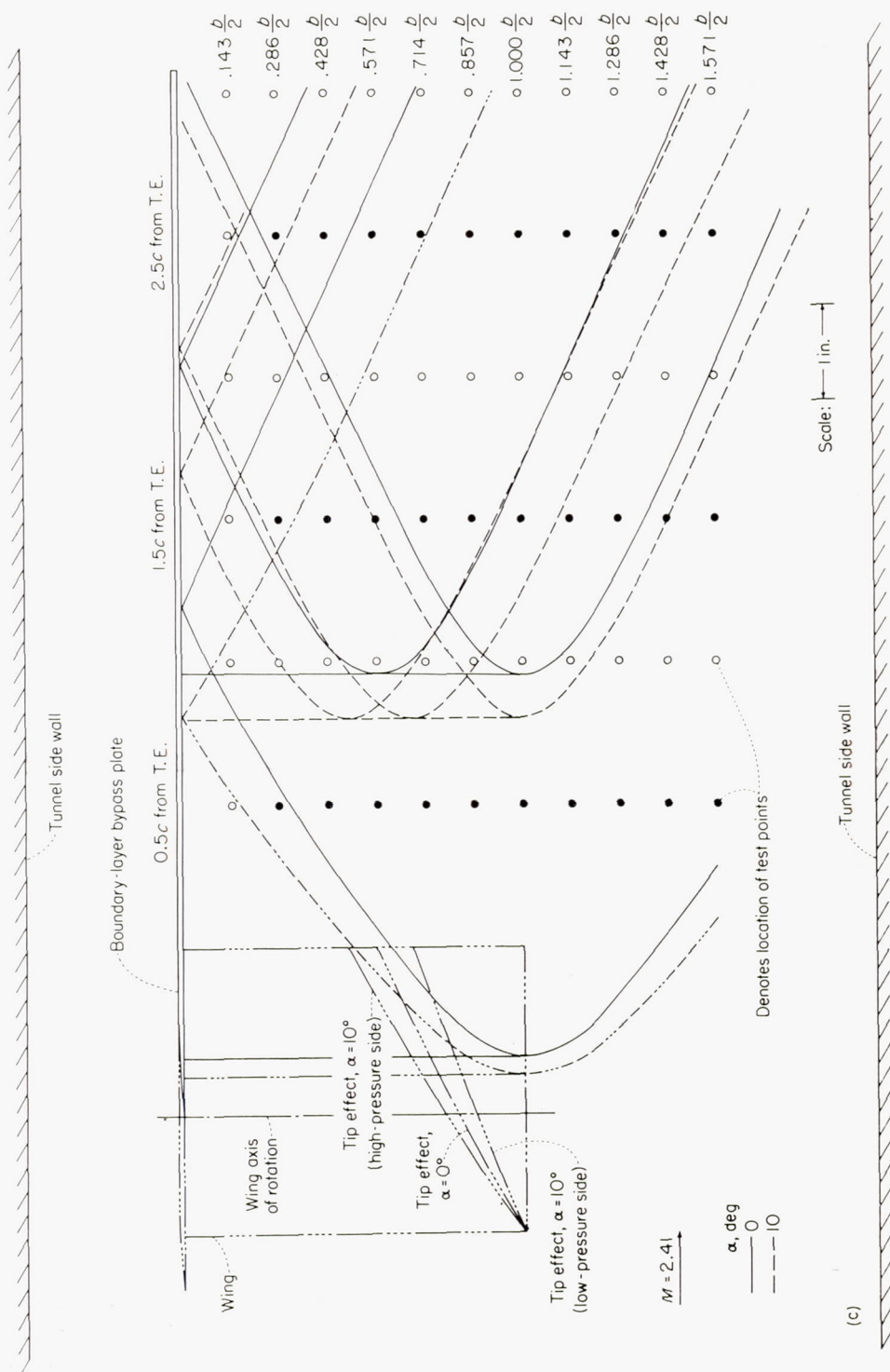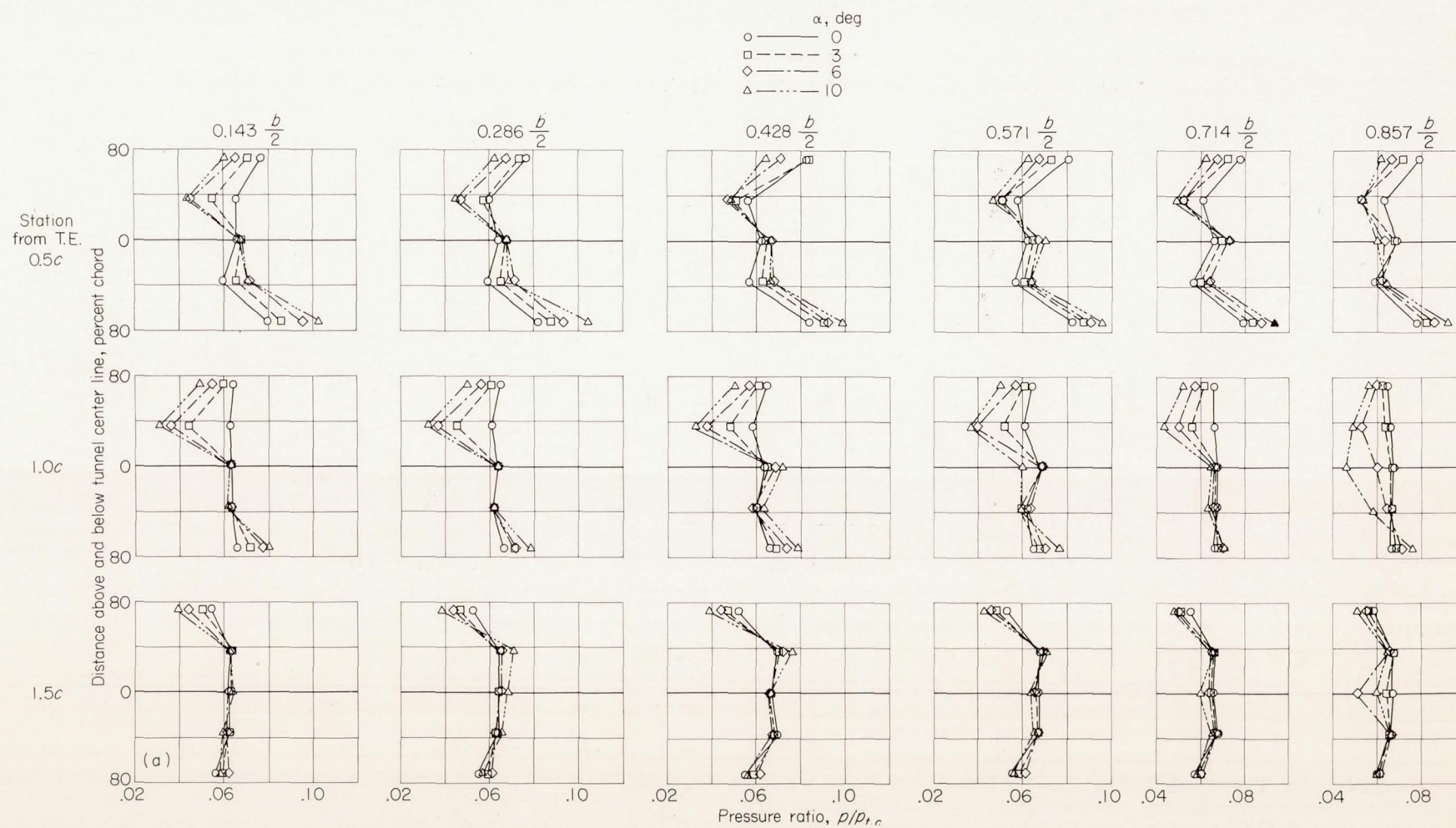
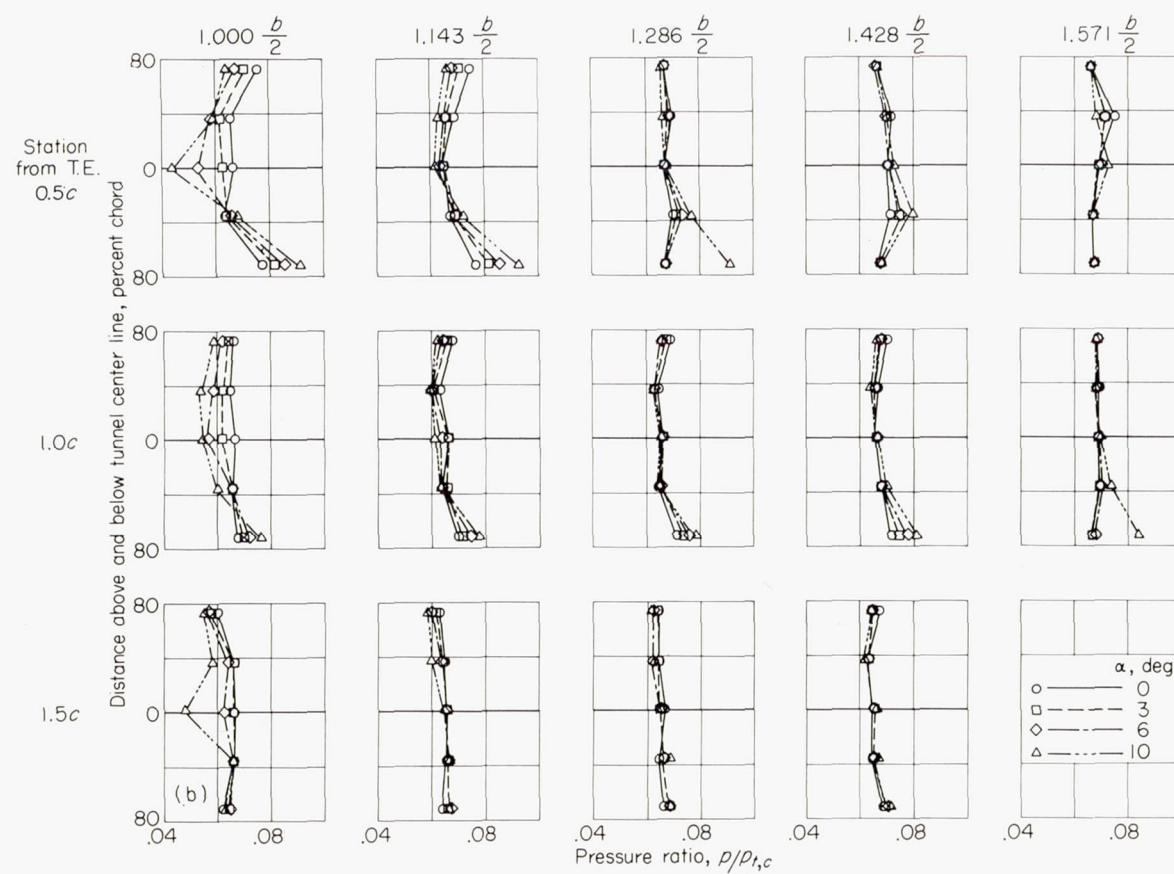(c) Horizontal plane 0.363 chord below tunnel center line.

Figure 7.—Concluded.

(a) Survey stations 0.5, 1.0, and 1.5 chords behind wing trailing edge.   Inboard of tip.

FIGURE 8.—Static-pressure distribution behind rectangular wing.   Stream Mach number=2.41.
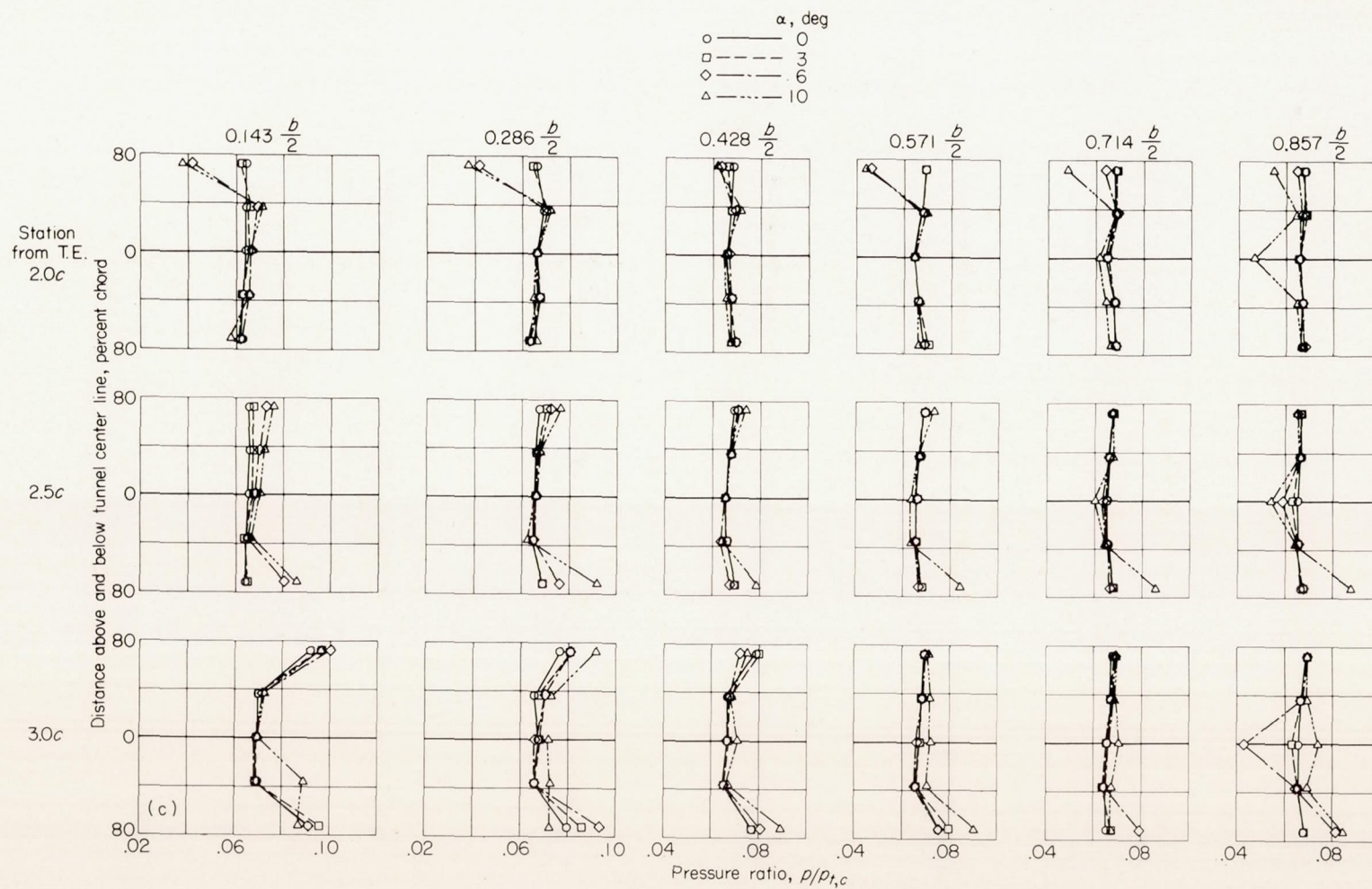
(b) Survey stations 0.5, 1.0, and 1.5 chords behind wing trailing edge.   Outboard of tip.
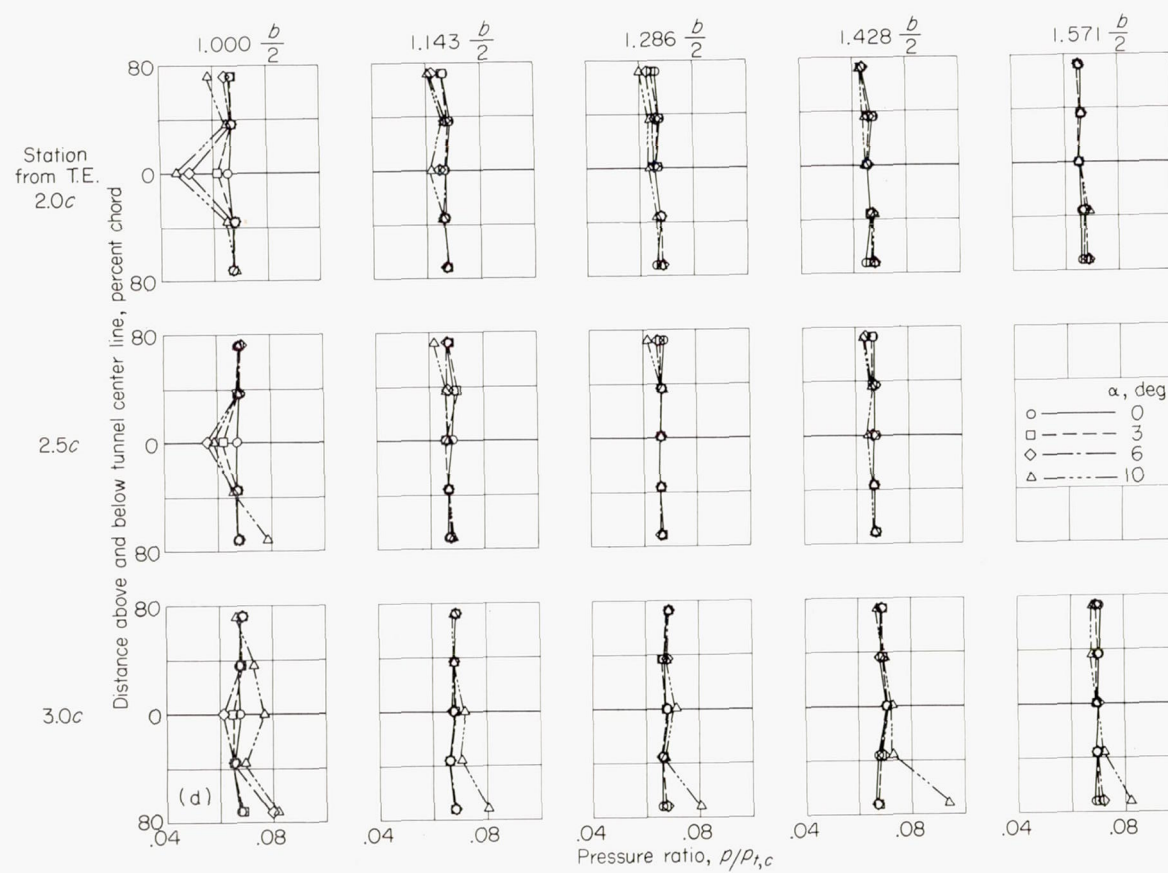
FIGURE 8.—Continued.

(c) Survey stations 2.0, 2.5, and 3.0 chords behind wing trailing edge.   Inboard of tip.

FIGURE 8.—Continued.

(d) Survey stations 2.0, 2.5, and 3.0 chords behind trailing edge. Outboard of tip.

FIGURE 8.—Concluded.

(a) Survey stations 0.5, 1.0, and 1.5 chords behind wing trailing edge. Inboard of tip.

FIGURE 9.—Mach number distribution behind rectangular wing. Undisturbed stream Mach number, 2.41.

(b) Survey stations 0.5, 1.0, and 1.5 chords behind wing trailing edge.   Outboard of tip.
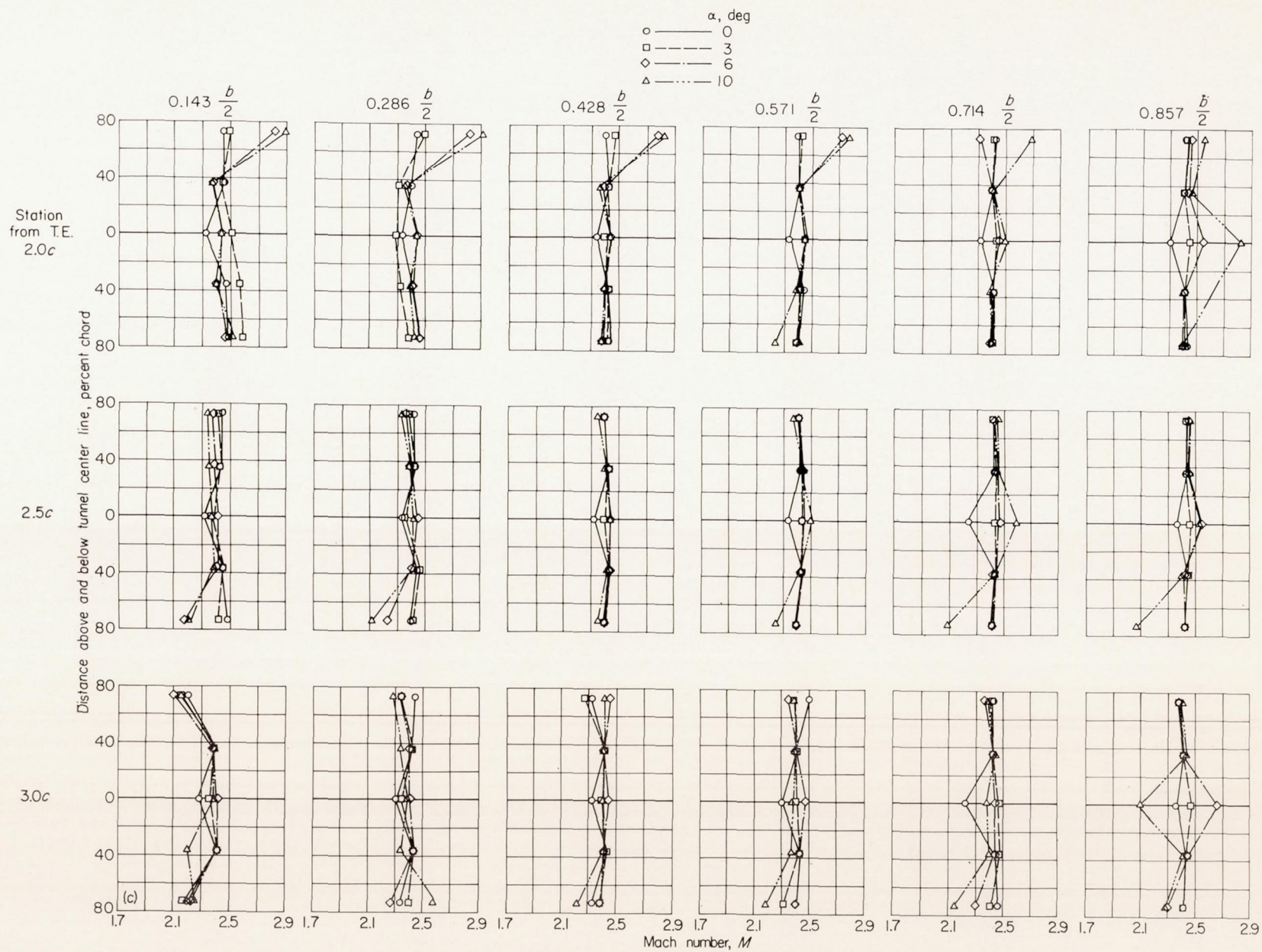
FIGURE 9.—Continued.

(c) Survey stations 2.0, 2.5, and 3.0 chords behind wing trailing edge. Inboard of tip.
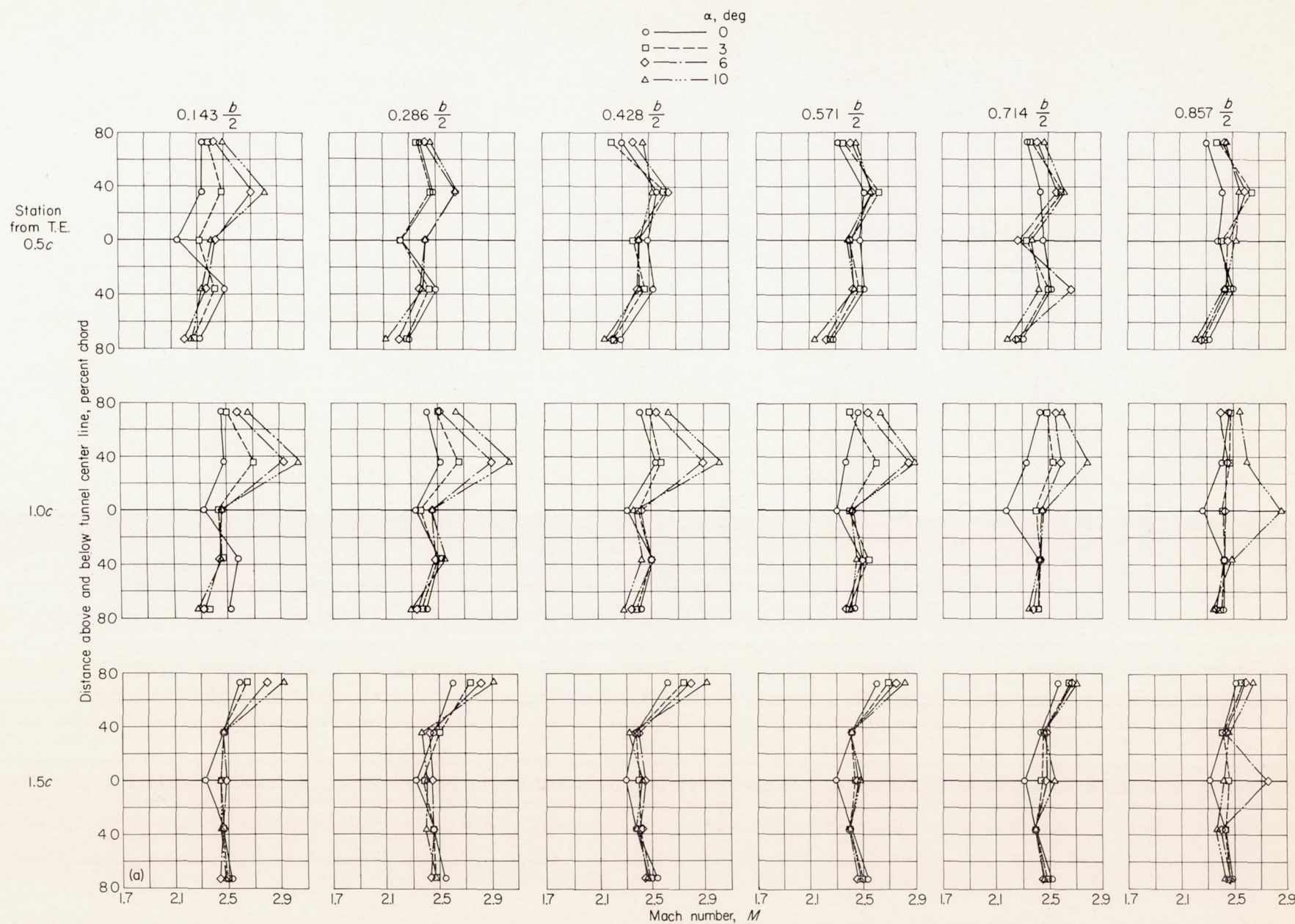
FIGURE 9.—Continued.

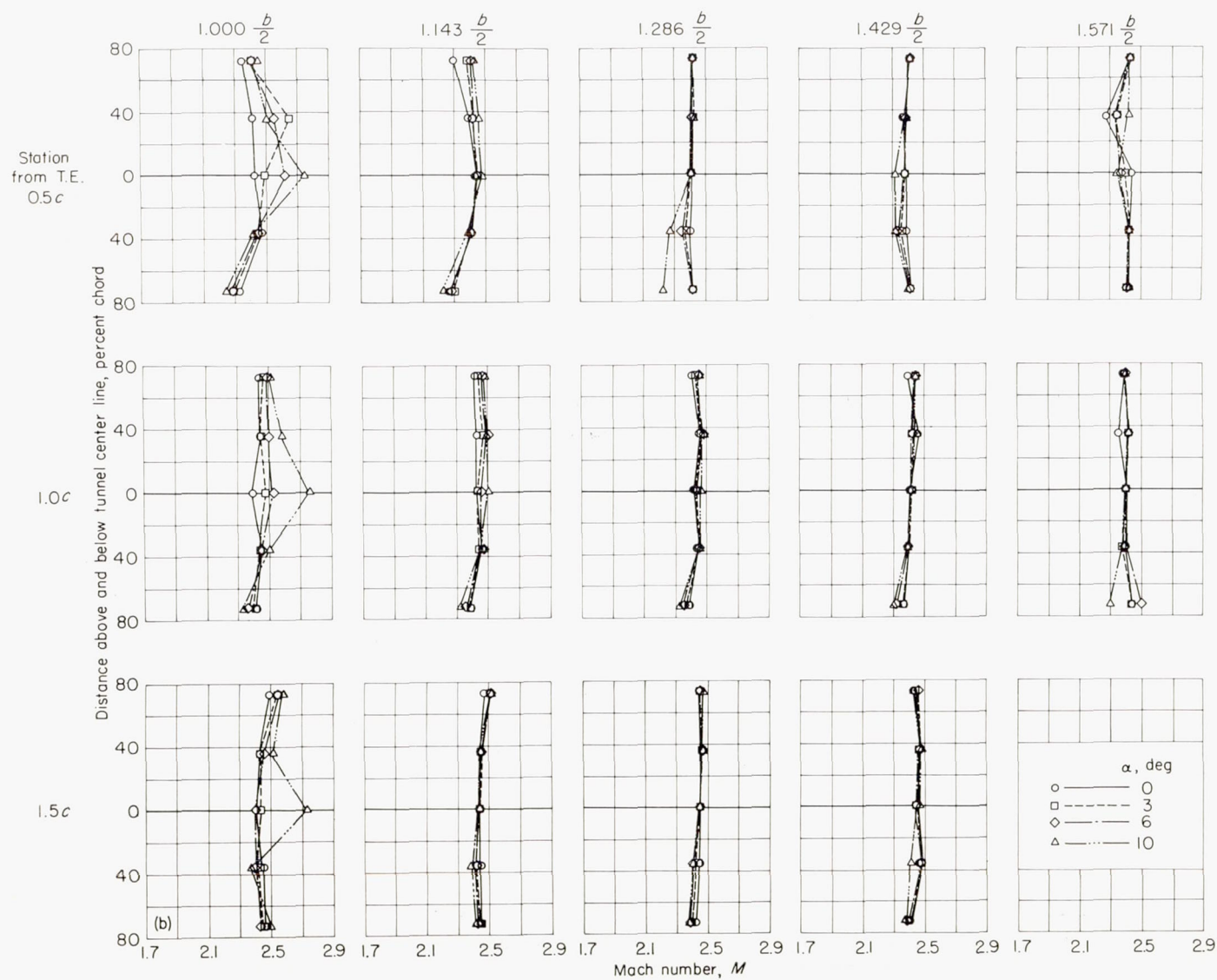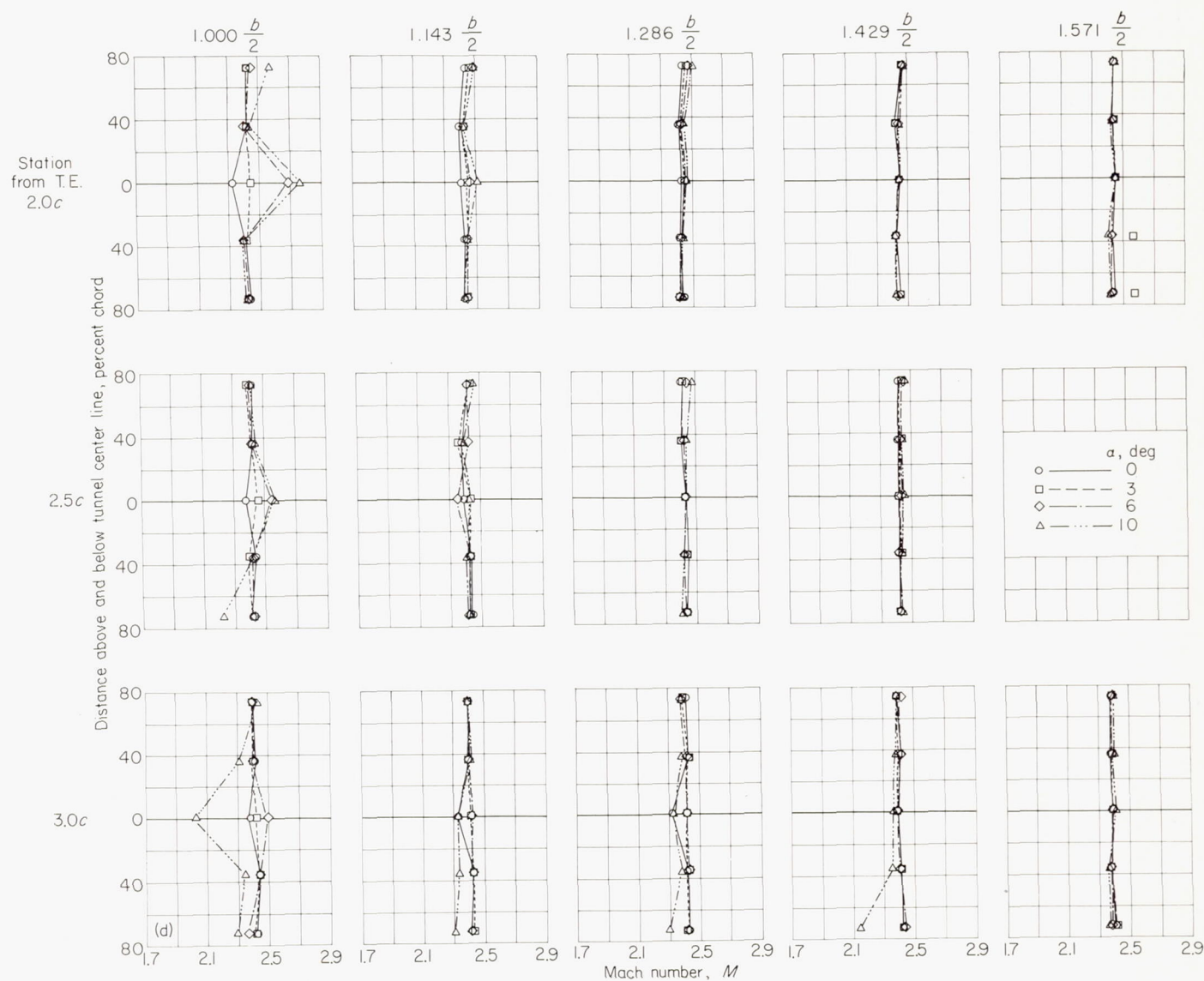(d) Survey stations 2.0, 2.5, and 3.0 chords behind wing trailing edge.   Outboard of tip.

FIGURE 9.—Concluded.
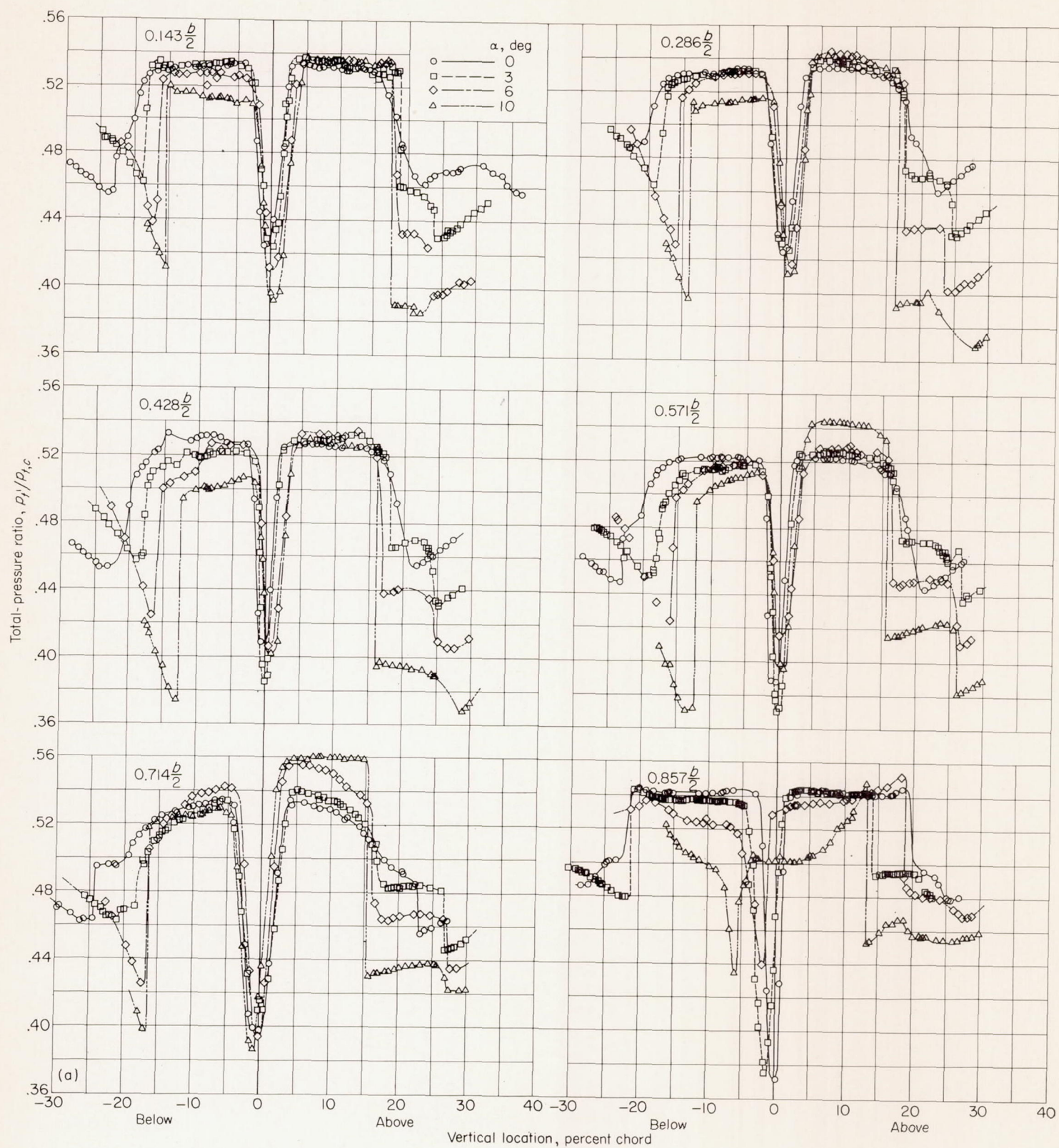
(a) Station 0.5 chord behind wing trailing edge; spanwise stations $0.143 \frac{b}{2}$ through $0.857 \frac{b}{2}$.

FIGURE 10.—Pitot pressure distribution across wake (pressures uncorrected for shock at nose of tube).
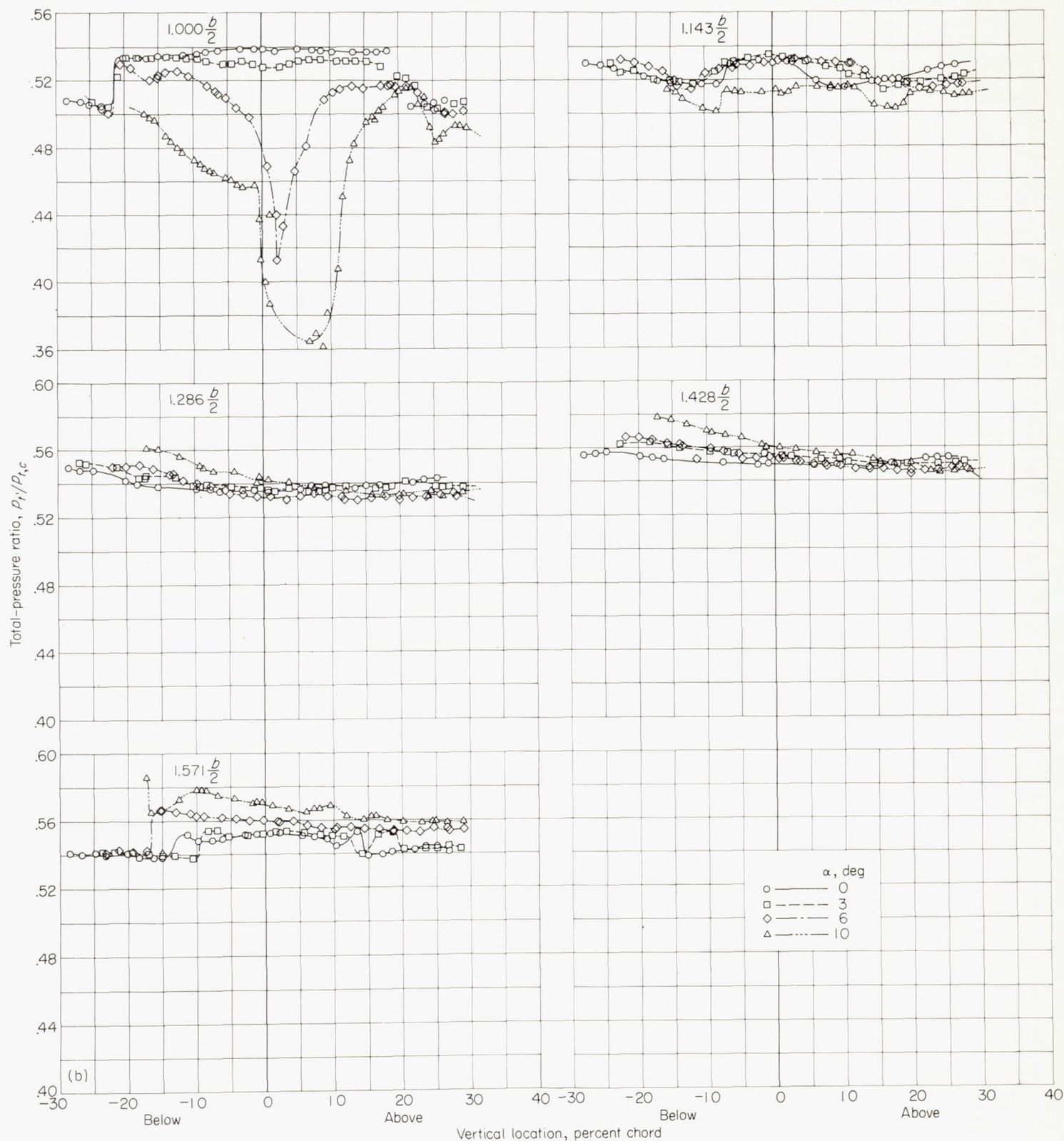
(b) Station 0.5 chord behind wing trailing edge.   Spanwise stations $1.000\frac{b}{2}$ through $1.571\frac{b}{2}$.

FIGURE 10.—Continued.

(c) Station 1.5 chords behind wing trailing edge. Spanwise stations $0.143\frac{b}{2}$ through $0.857\frac{b}{2}$.

FIGURE 10.—Continued.
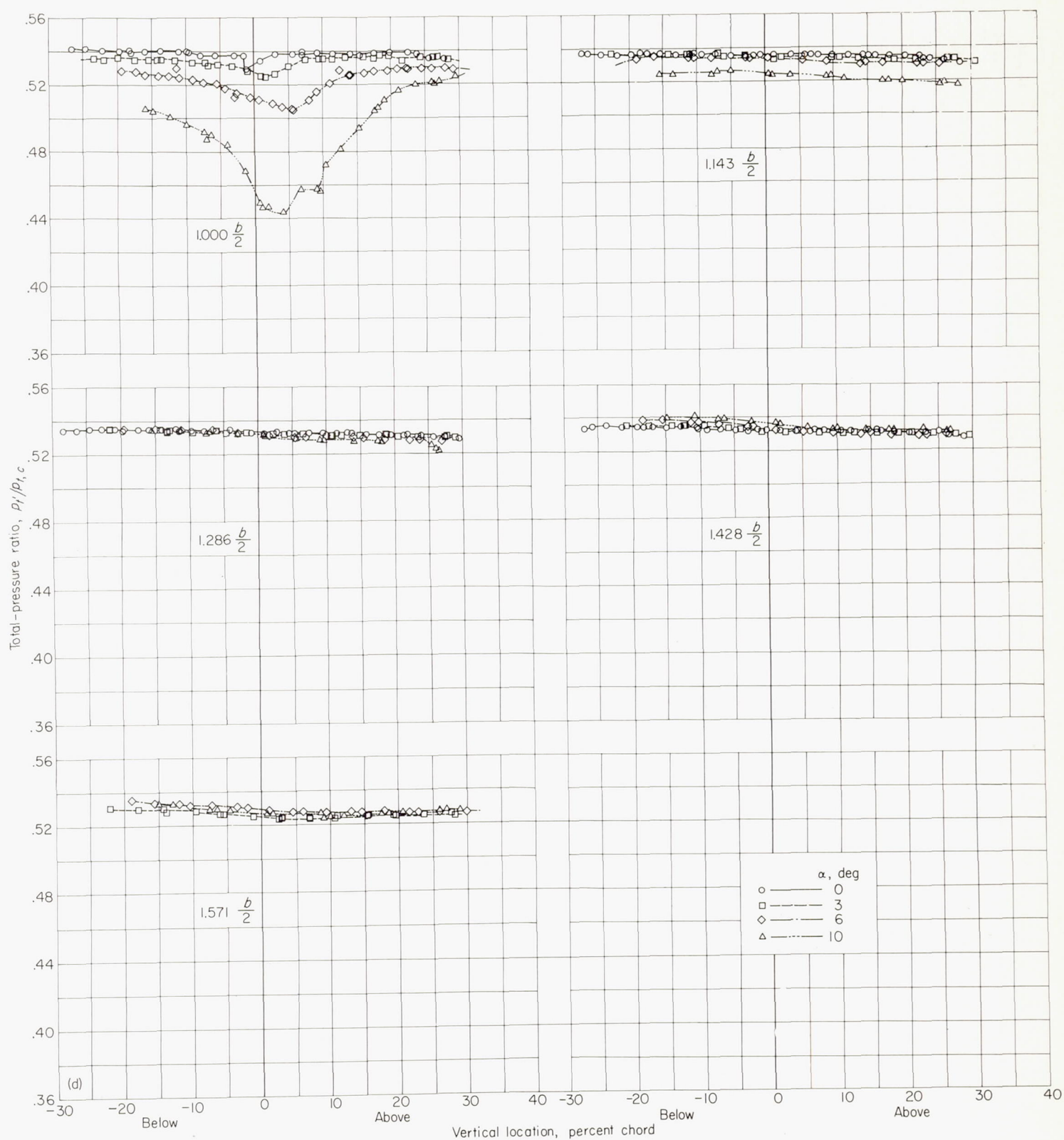
(d) Station 1.5 chords behind wing trailing edge.   Spanwise stations $1.000 \frac{b}{2}$ through $1.571 \frac{b}{2}$.

FIGURE 10.—Continued.

(e) Station 2.5 chords behind wing trailing edge. Spanwise stations $0.143 \frac{b}{2}$ through $0.857 \frac{b}{2}$.

FIGURE 10.—Continued.

(f) Station 2.5 chords behind wing trailing edge.   Spanwise stations $1.000\,\frac{b}{2}$ through $1.571\,\frac{b}{2}$.

FIGURE 10.—Concluded.
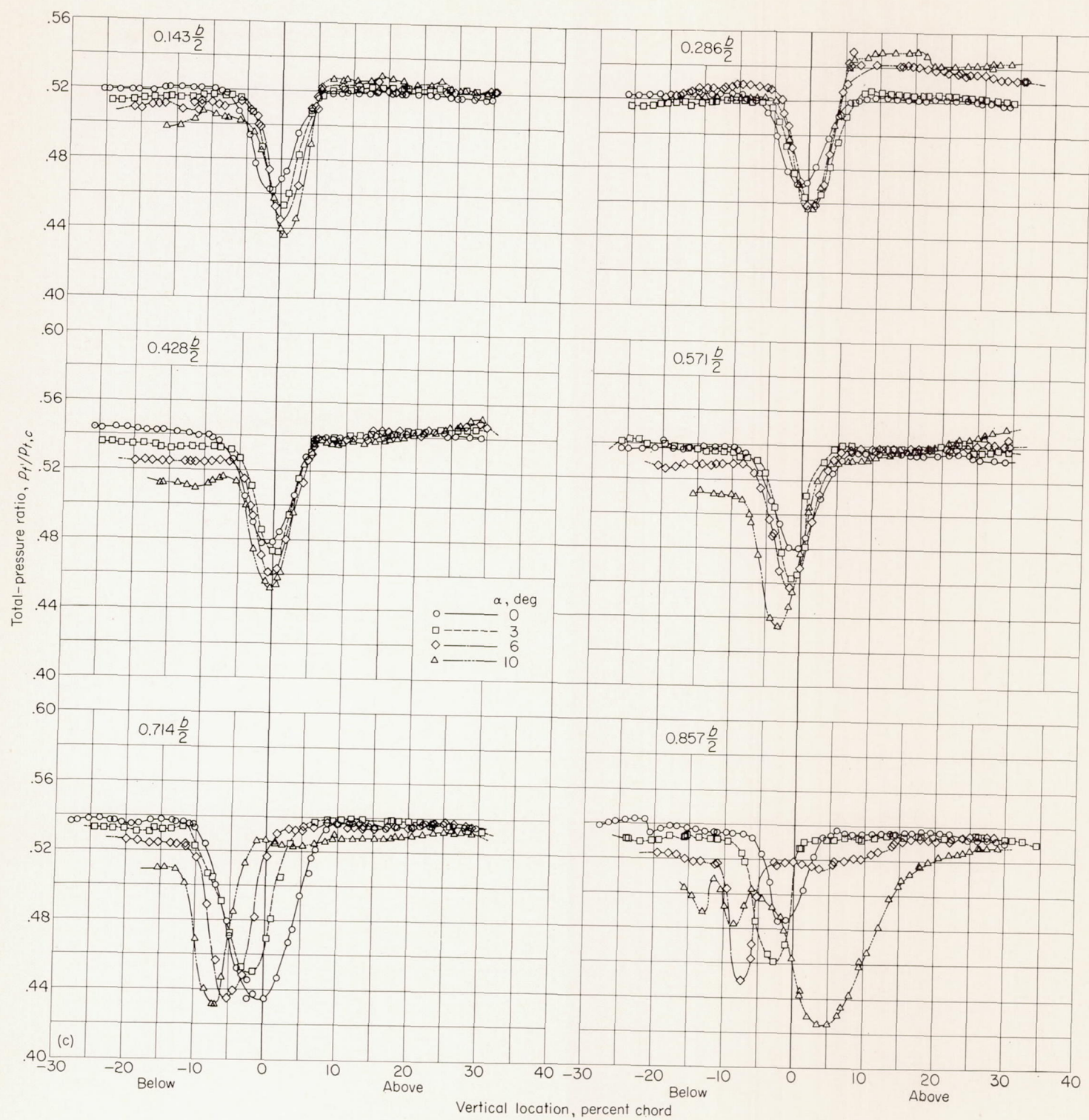
(a) $\alpha=0°$.

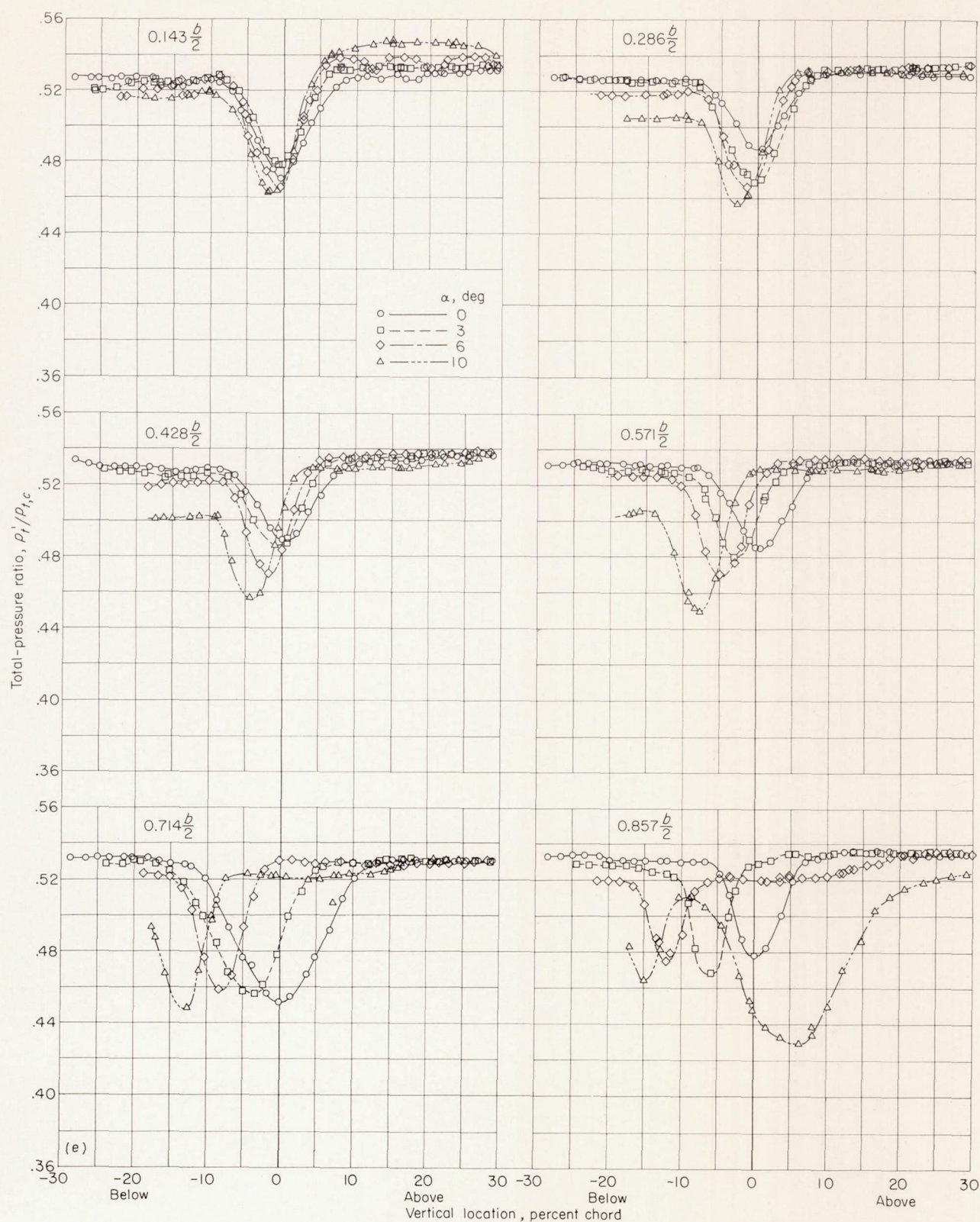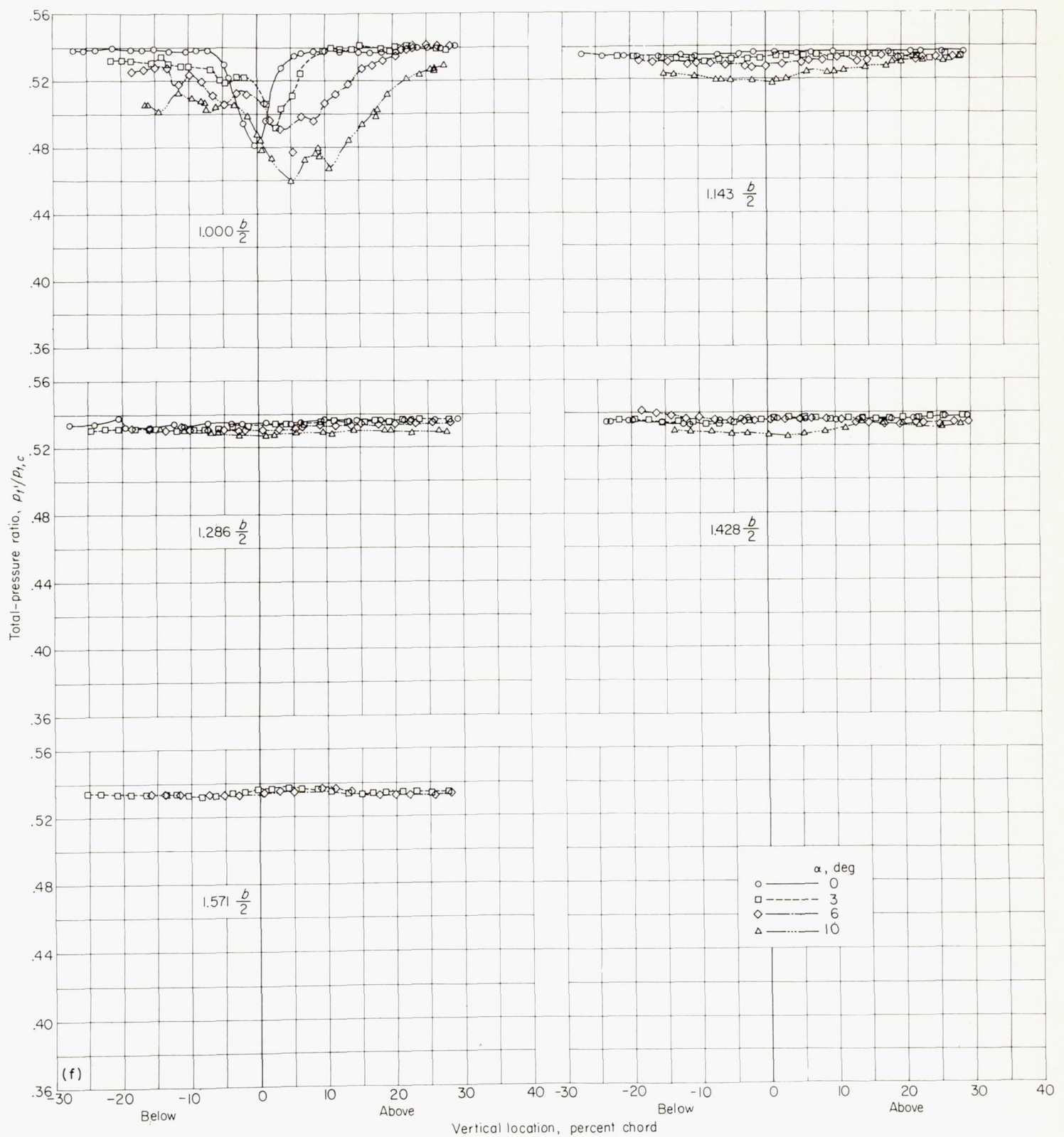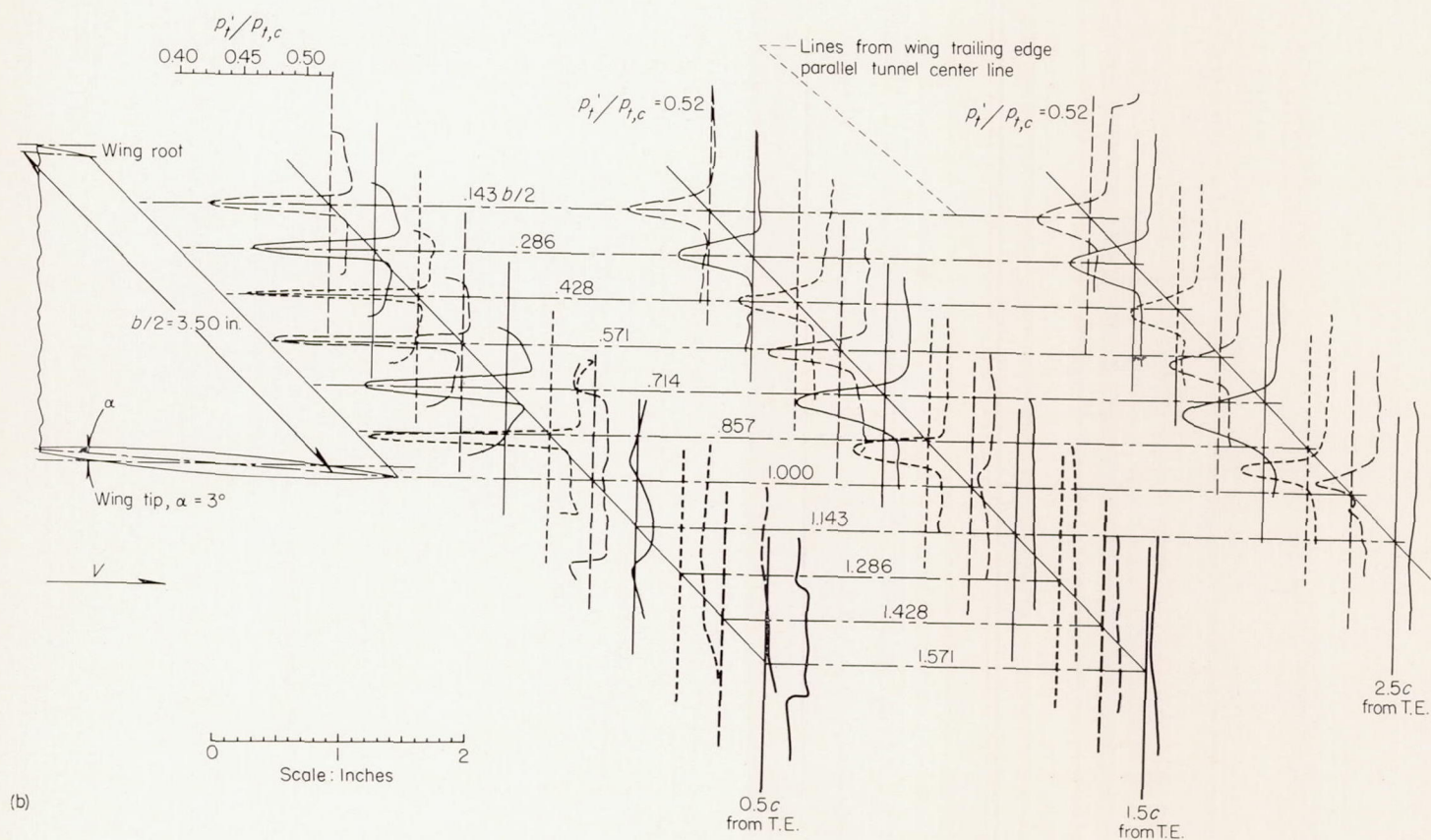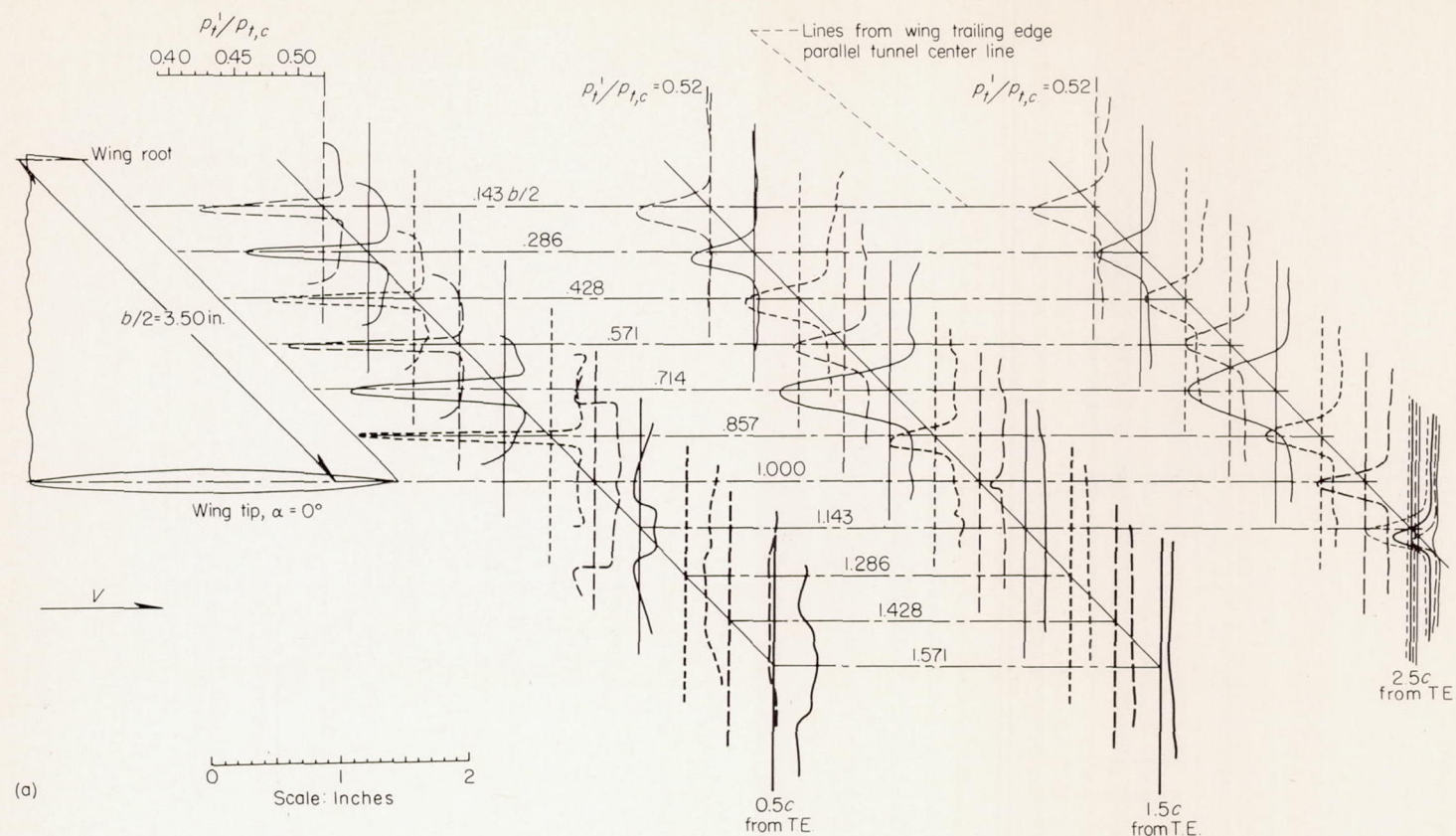(b) $\alpha=3°$.

FIGURE 11.—Oblique view of the plots of pitot pressure distribution measured vertically across the wake. (Pressures uncorrected for shock at nose of tube.) $M=2.41$.

(c) $\alpha = 6°$.

(d) $\alpha = 10°$.
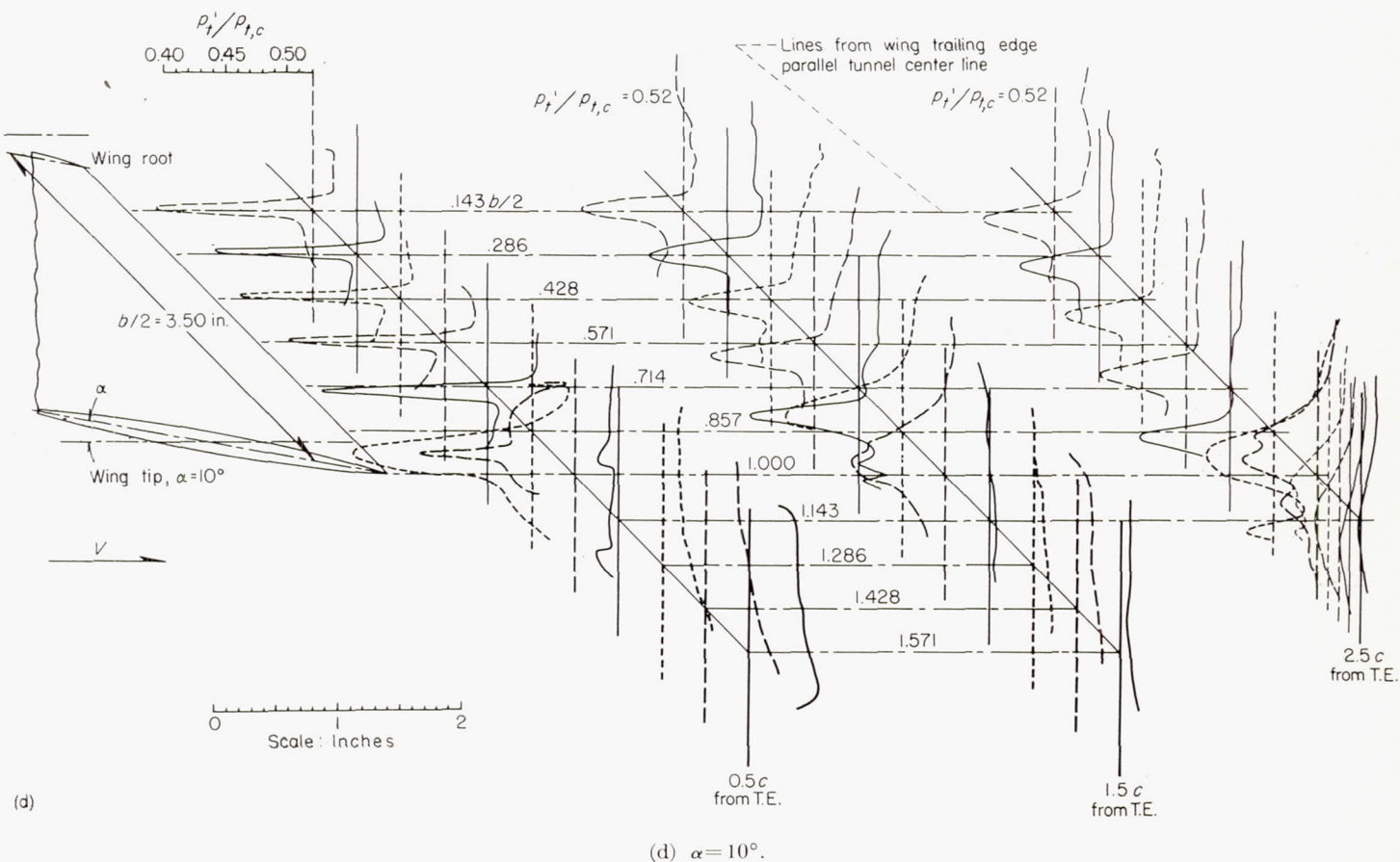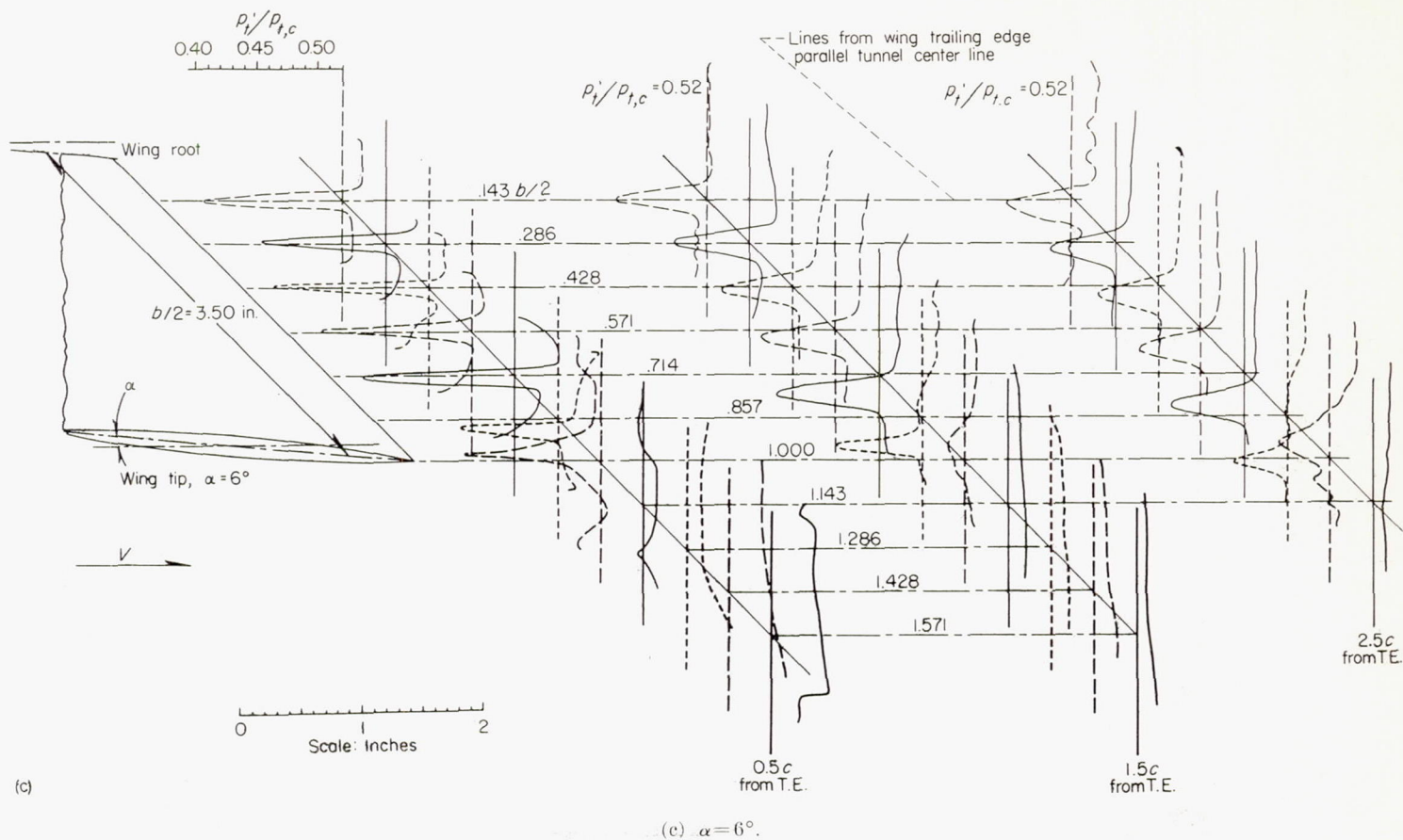
FIGURE 11. Concluded.

In figure 12 are mapped the locations of the wake boundaries and the wake center line in relation to the wing for each of the four test values of α. In those regions where the incompleteness of the wake traverse introduced rather large uncertainties in the estimation of the wake boundaries, a dashed line is used in figure 12 to trace the boundary.

The rolling-up of the trailing vortex sheet manifests itself on the wake pressures, as can be observed by the double peaks in the wake total-pressure profiles at stations downstream of the tip (fig. 11). The distance behind a wing at which the vortex sheet becomes essentially rolled up is a function of wing lift coefficient and aspect ratio as was recently pointed out in reference 12. As a qualitative check on these calculations it can be seen that at $\alpha=6°$ double

peaks are discernible in figures 10 and 11 only at the station 2.5 chords behind the trailing edge; whereas at $\alpha=10°$, double peaks are clearly defined at both the 1.5- and 2.5-chord stations downstream of the trailing edge.

Comparison of wake characteristics in subsonic and supersonic flow.—In reference 1, it is shown that the growth in thickness of the wake of a wing in subsonic flow follows a parabolic shape closely. In figure 13 a comparison between the growth in wake thickness for subsonic and supersonic flows indicates that the growth in wake thickness in supersonic flow is of a different nature. The wake thickness at the trailing edge shown in this figure was obtained from a shadowgraph. In general, figure 13 shows that the growth of wake thickness is almost linear from the trailing

(a) $\alpha=0°$.

(b) $\alpha=3°$.
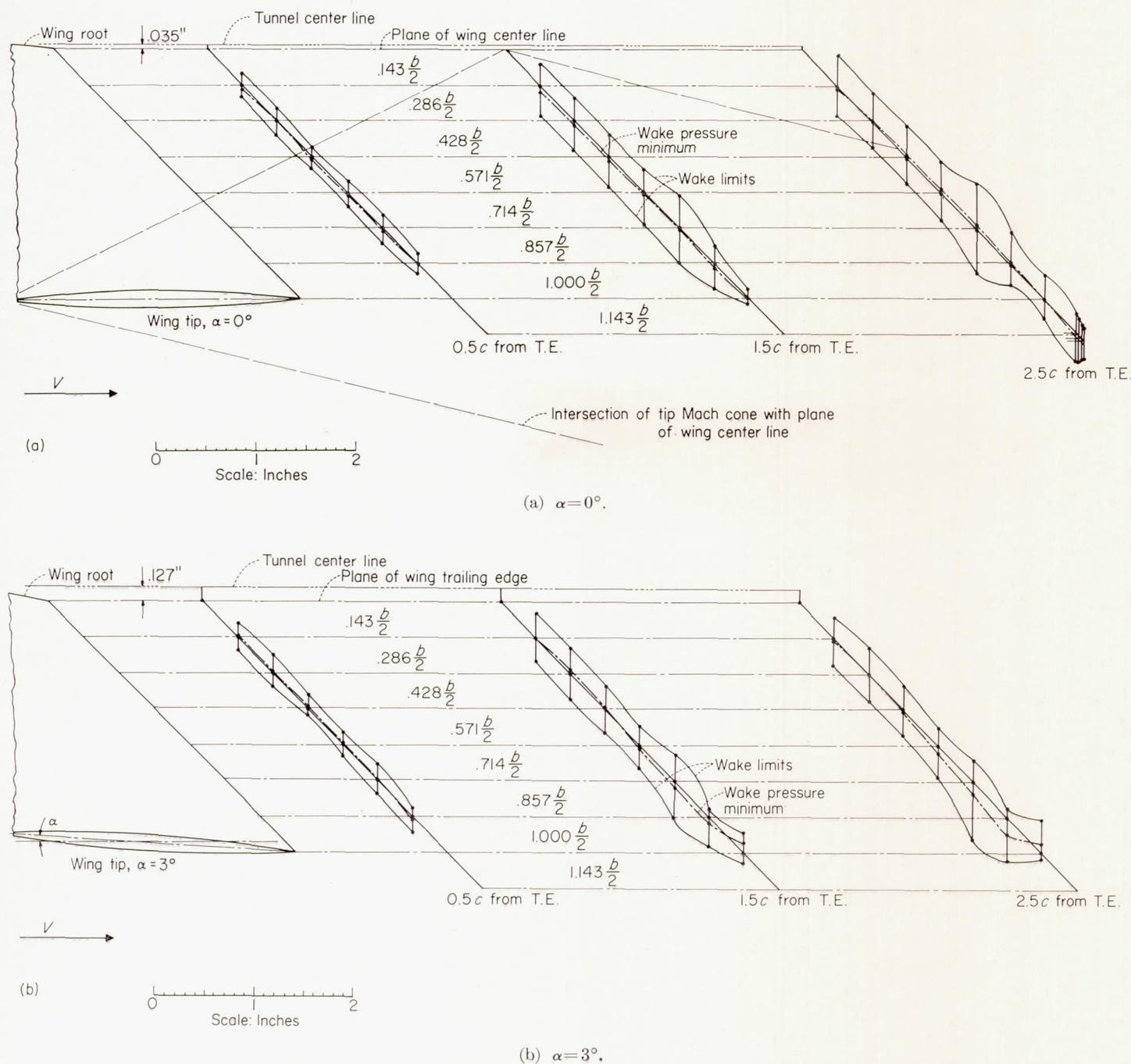
FIGURE 12.—Oblique view of wake boundaries and wake center line in relation to wing.

(c) $\alpha = 6°$.

(d) $\alpha = 10°$.

FIGURE 12.—Concluded.

edge to 1.5 chords behind the wing trailing edge and that it grows more rapidly in supersonic flow than in subsonic flow; however, this high rate of growth falls off rapidly and at some distance downstream becomes less than that in the subsonic flow.

A comparison is also made in figure 13 of the rate of recovery of the total-pressure loss with distance downstream in the subsonic and supersonic flows. For the purpose of this comparison the total-pressure measurements in the wake were corrected for the presence of shock waves at the mouth of the measuring tubes. These corrections were applied by assuming the static pressures across the entire wake width to be constant and equal to those measured by

the 0.040-inch-diameter static-pressure tubes of the general survey behind the wing. When this assumption was used, the data indicated a gain in total pressure at the edge of the wake of the order of 4.5 percent at 0.5 chord behind the trailing edge and of about 0.5 percent at 1.5 and 2.5 chords behind the trailing edge. The assumption of constant static pressure across the wake is therefore probably slightly in error.

Effect of wake on downwash field.—In a discussion of the wake, not only are its location, size, and the pressure gradients within it of importance but also its effect on the downwash field. This latter effect cannot be accurately assessed from the data of this experiment; however, with the wing at
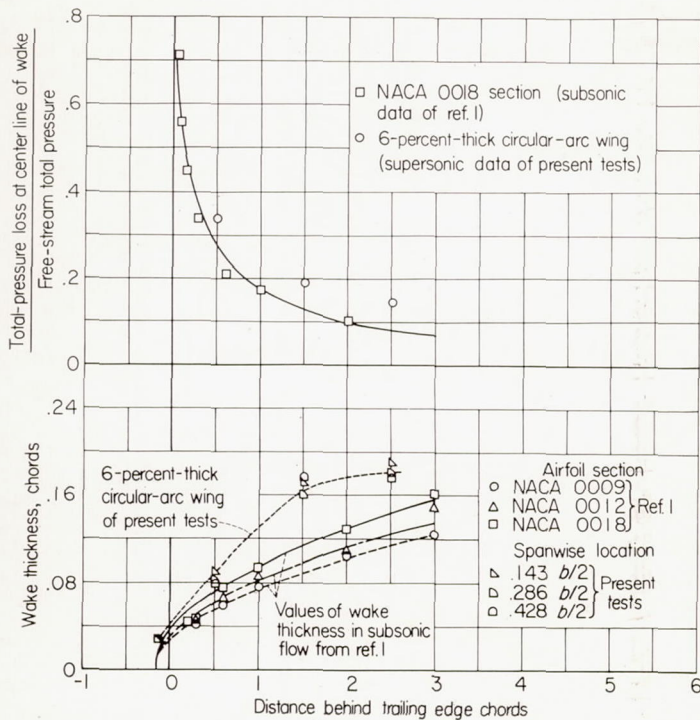
FIGURE 13.—Comparison of growth in wake thickness and decrease in total-pressure deficiency with distance behind wing trailing edge in subsonic and supersonic flow. $\alpha=0°$.

0° angle of attack, downwash angles up to $-1.1°$ were measured in the horizontal plane 0.363 chord above and 0.8° in the plane 0.363 chord below the plane of the wing. These sizable values of downwash are attributable to three causes: (1) the effect of the wake on the downwash field, (2) the

fact that downstream of a finite-span wing with thickness, even at $\alpha=0°$, there exists a downwash field varying from 0° in the plane of the wing to finite values above and below the plane of the wing, and (3) the tunnel tare angles that might be present, but which are believed to be small.

DOWNWASH AND SIDEWASH

Theoretical considerations.—A detailed account of the method of evaluating the downwash and sidewash field by use of the linearized superposition theory of reference 2 is given in appendix B. By this method, the downwash and sidewash angles were evaluated in vertical planes at a number of chordwise locations to the rear of the wing trailing edge (namely, 0.5, 1.0, 1.5, 2.0, 2.5, and 3.0 chords). The results of these computations are given in nondimensional form for locations 0.5, 1.5, and 2.5 chords behind the trailing edge in figures 14, 15, and 16. (Use of these figures allows the downwash to be computed at any point of a flow field of a rectangular wing of given aspect ratio and at a specified Mach number.) A graphic presentation of these theoretical results is given in figure 17.

In the calculation of the theoretical variation of downwash and sidewash with wing angle of attack, the wing is assumed to remain in one plane throughout the angle-of-attack range. The most logical choice for locating this datum plane in order to compare the results with experimental measurements would be along the trailing vortex sheet. Apart from the slight variation in vertical location resulting from the flexibility of the supporting arm, all points of measurement of the flow direction in the experiment remained fixed relative to the tunnel axis. The wing itself was pivoted about a point

(a) Sidewash, $d\sigma/d\alpha$. (Signs reversed below plane of wing.)
(b) Downwash, $d\epsilon/d\alpha$. (Signs same below plane of wing.)

FIGURE 14.—Theoretical values of $d\sigma/d\alpha$ and $d\epsilon/d\alpha$ in a vertical plane 0.5 chord behind the trailing edge of a semi-infinite rectangular wing of zero thickness.

(a) Sidewash, $d\sigma/d\alpha$.   (Signs reversed below plane of wing.)
(b) Downwash, $d\epsilon/d\alpha$.   (Signs same below plane of wing.)
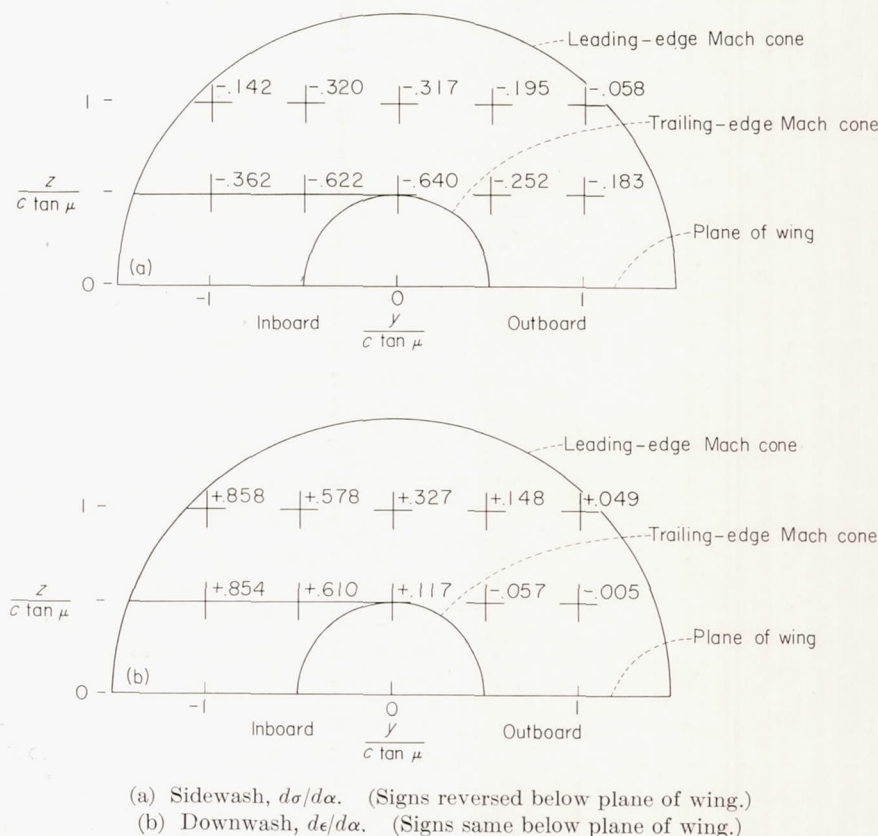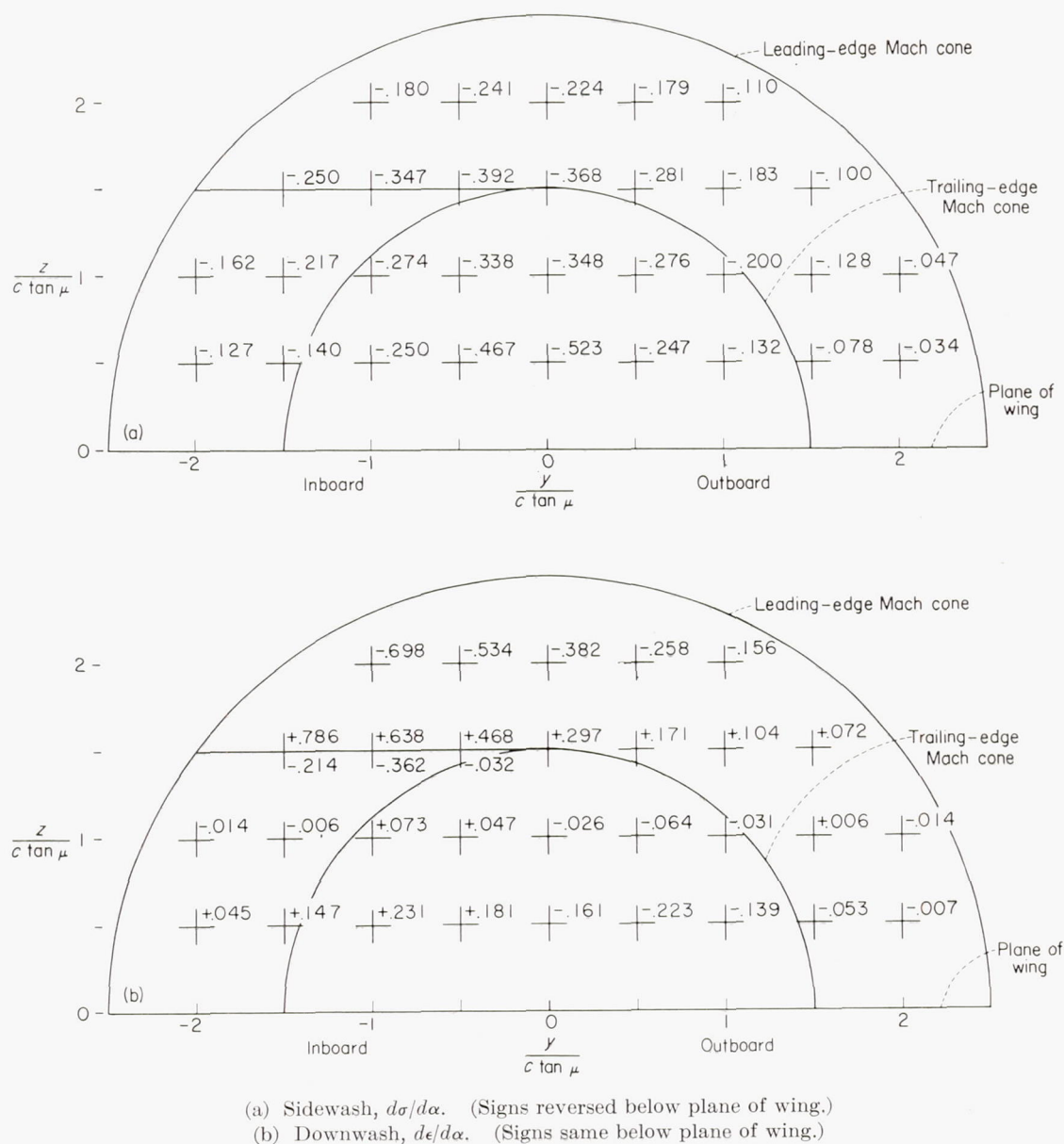
FIGURE 15.—Theoretical values of $d\sigma/d\alpha$ and $d\epsilon/d\alpha$ in a vertical plane 1.5 chords behind the trailing edge of a semi-infinite rectangular wing of zero thickness.

0.0839 chord ahead of the midchord point; hence, as the angle of attack of the wing was changed, the vertical location of the points of measurement relative to the wing trailing edge and the trailing vortex sheet varied. This type of test setup, which would therefore not directly correspond to the more conventional configuration of an aircraft with a fixed tail without modifications to the data, was used for this experiment as it made possible a larger-scale wing model. In addition, the results could be more readily compared with theory. Near angles of attack of 0°, a direct comparison between the experimental and theoretical results could be made for identical locations above and below the plane of the wing. At higher angles of attack, if a horizontal plane through the wing trailing edge (the point of origin of the trailing vortex sheet) is taken as the datum plane, it can be seen that the location of this datum plane will vary with angle of attack relative to the fixed test points. Also, with

the wing at an angle of attack, the self-induced displacement and distortion of the trailing vortex sheet with distance downstream complicates the locating of the datum plane for comparison of theoretical and experimental results.

Downwash results.—Figure 18 contains curves of downwash angle ϵ plotted against α. Each part of figure 18 shows the results obtained at each spanwise station for vertical locations 0.363 chord above the tunnel axis, on the tunnel axis, and 0.363 chord below the tunnel axis. As mentioned previously, the flexibility of the supporting arm allowed slight variations in the actual z-location of each test point and, although, for convenience, each specified vertical location of the curves is referred to as either on the center line or 0.363 chords above or below this center line, the actual vertical locations as measured by a cathetometer at each test point are presented in table I.

(a)

Leading-edge Mach cone

3 — $\quad$ −.112 $\quad$ −.168 $\quad$ −.191 $\quad$ −.187 $\quad$ −.162 $\quad$ −.118 $\quad$ −.072

−.178 $\quad$ −.250 $\quad$ −.294 $\quad$ −.298 $\quad$ −.285 $\quad$ −.249 $\quad$ −.200 $\quad$ −.149 $\quad$ −.088

2 — $\quad$ −.178 −.202 −.199 −.208 −.213 −.219 −.223 −.202 −.178 −.117 −.062

Trailing-edge Mach cone

$\dfrac{z}{c\,\tan\mu}$ — −.128 −.151 −.153 −.168 −.207 −.234 +.237 −.209 −.163 −.150 −.126 −.073 −.029

1 — −.085 −.101 −.111 −.154 −.230 −.304 −.317 −.232 −.151 −.112 −.093 −.063 −.028

−.056 −.052 −.069 −.103 −.243 −.479 −.537 −.233 −.106 −.064 −.042 −.036 −.008

Plane of wing

0 — $\quad$ −3 $\quad$ −2 $\quad$ −1 $\quad$ 0 $\quad$ 1 $\quad$ 2 $\quad$ 3

Inboard $\qquad\qquad \dfrac{y}{c\,\tan\mu} \qquad\qquad$ Outboard

(b)

Leading-edge Mach cone

3 — +.787 +.635 +.512 +.404 +.309 +.215 +.127

+.800 +.682 +.567 +.453 +.349 +.263 +.187 +.126 +.084
−.200 −.318 −.433 +.047

Trailing-edge Mach cone

2 — +.137 +.097 −.041 −.001 +.010 +.003 +.023 +.056 +.080 +.061 +.050

$\dfrac{z}{c\,\tan\mu}$ — −.069 −.020 +.025 +.054 +.059 +.025 −.028 −.050 −.045 −.019 +.015 +.019 +.011

1 — −.003 +.047 +.086 +.120 +.124 +.061 −.045 −.117 −.115 −.085 −.041 −.006 +.006

+.010 +.072 +.129 +.195 +.252 +.185 −.191 −.273 −.184 −.129 −.078 −.030 .000

Plane of wing

0 — $\quad$ −3 $\quad$ −2 $\quad$ −1 $\quad$ 0 $\quad$ 1 $\quad$ 2 $\quad$ 3

Inboard $\qquad\qquad \dfrac{y}{c\,\tan\mu} \qquad\qquad$ Outboard

(a) Sidewash, $d\sigma/d\alpha$. (Signs reversed below plane of wing.)
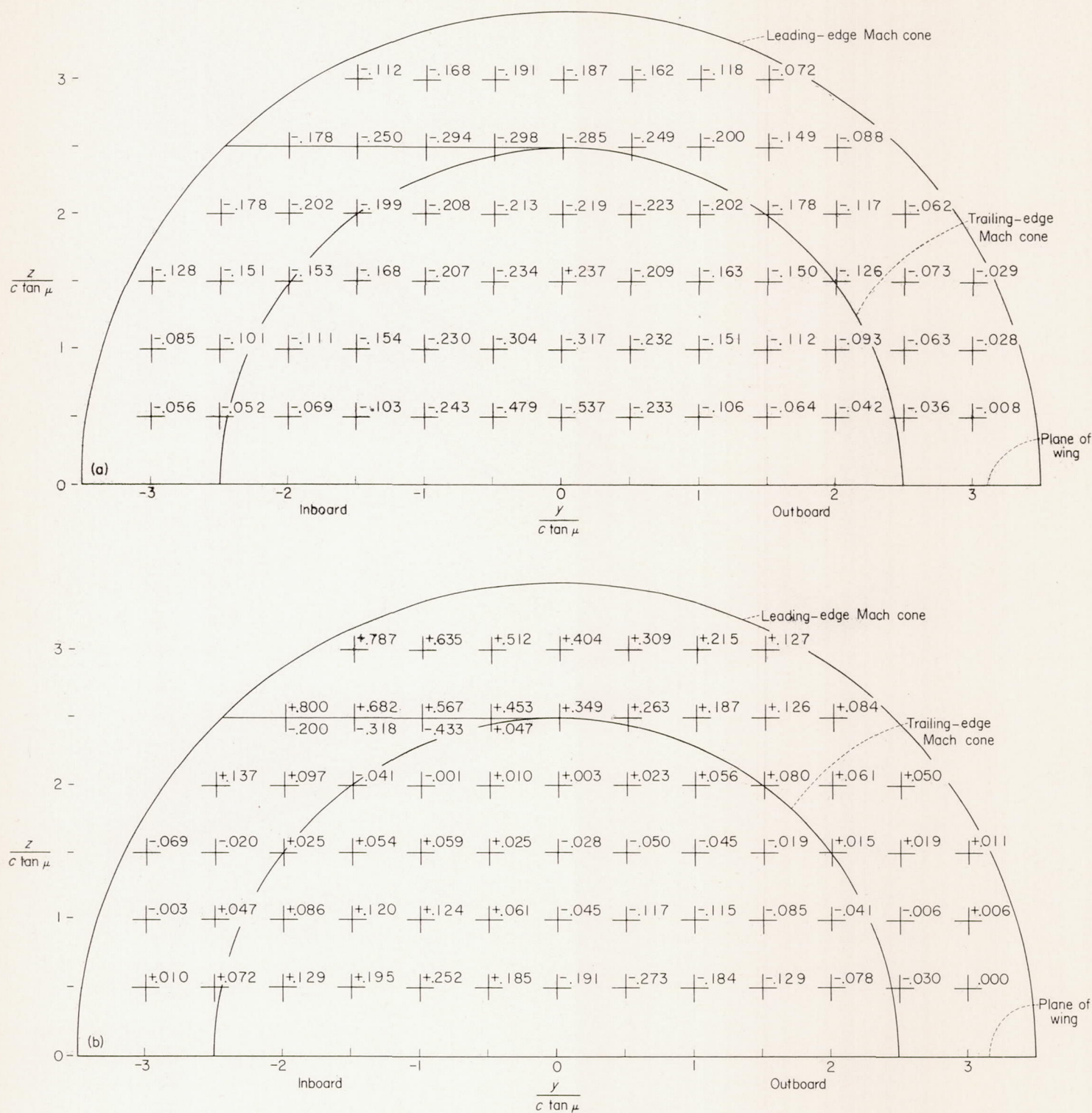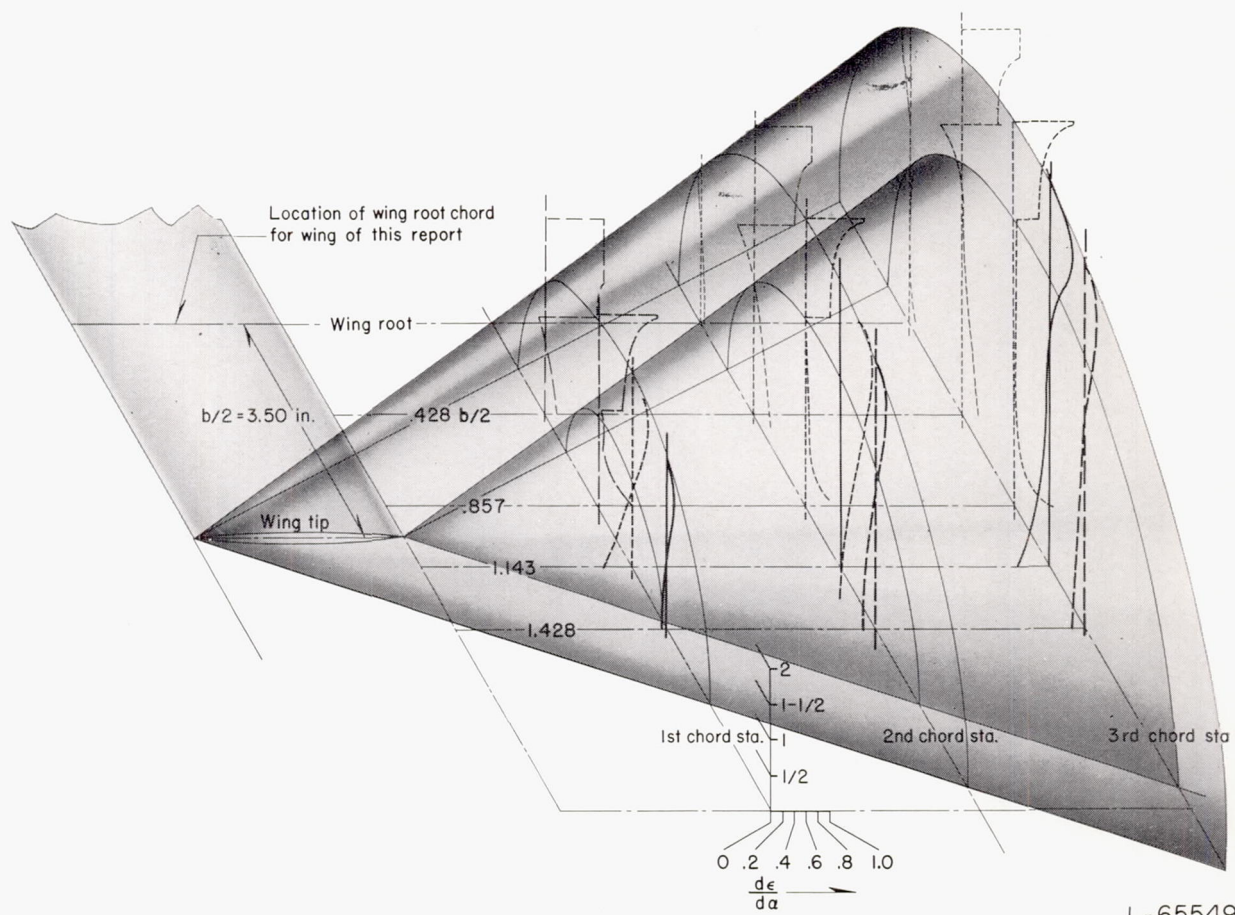(b) Downwash, $d\epsilon/d\alpha$. (Signs same below plane of wing.)

FIGURE 16.—Theoretical values of $d\sigma/d\alpha$ and $d\epsilon/d\alpha$ in a vertical plane 2.5 chords behind trailing edge of a semi-infinite rectangular wing of zero thickness.
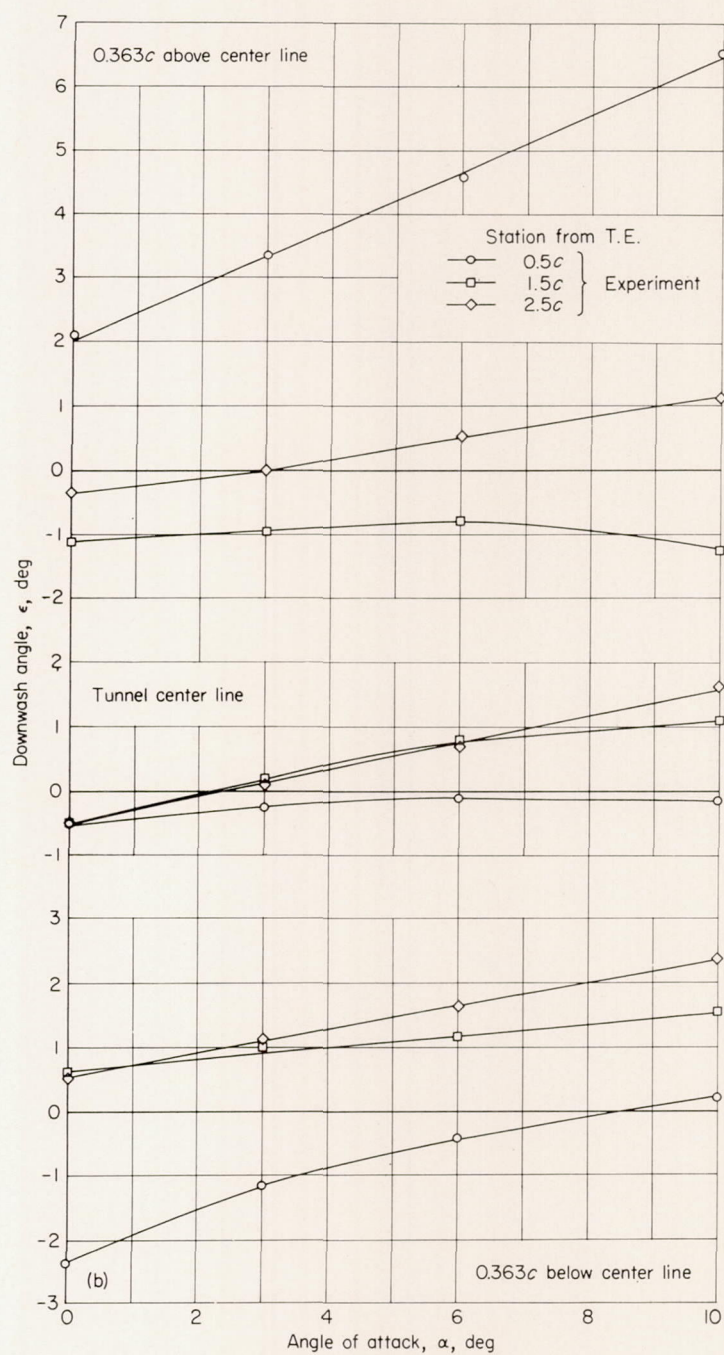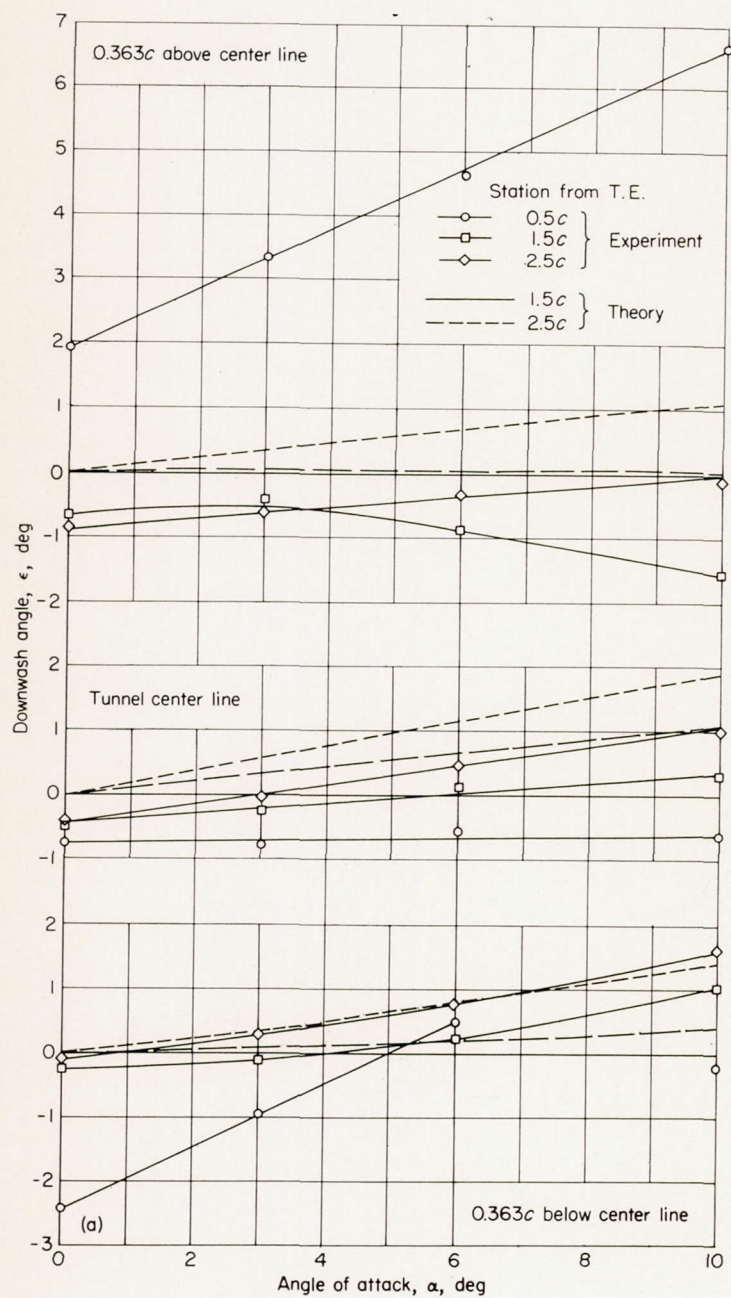
FIGURE 17.—Oblique view of theoretical $d\epsilon/d\alpha$ distribution behind a semi-infinite rectangular wing of zero thickness. $M=2.41$.
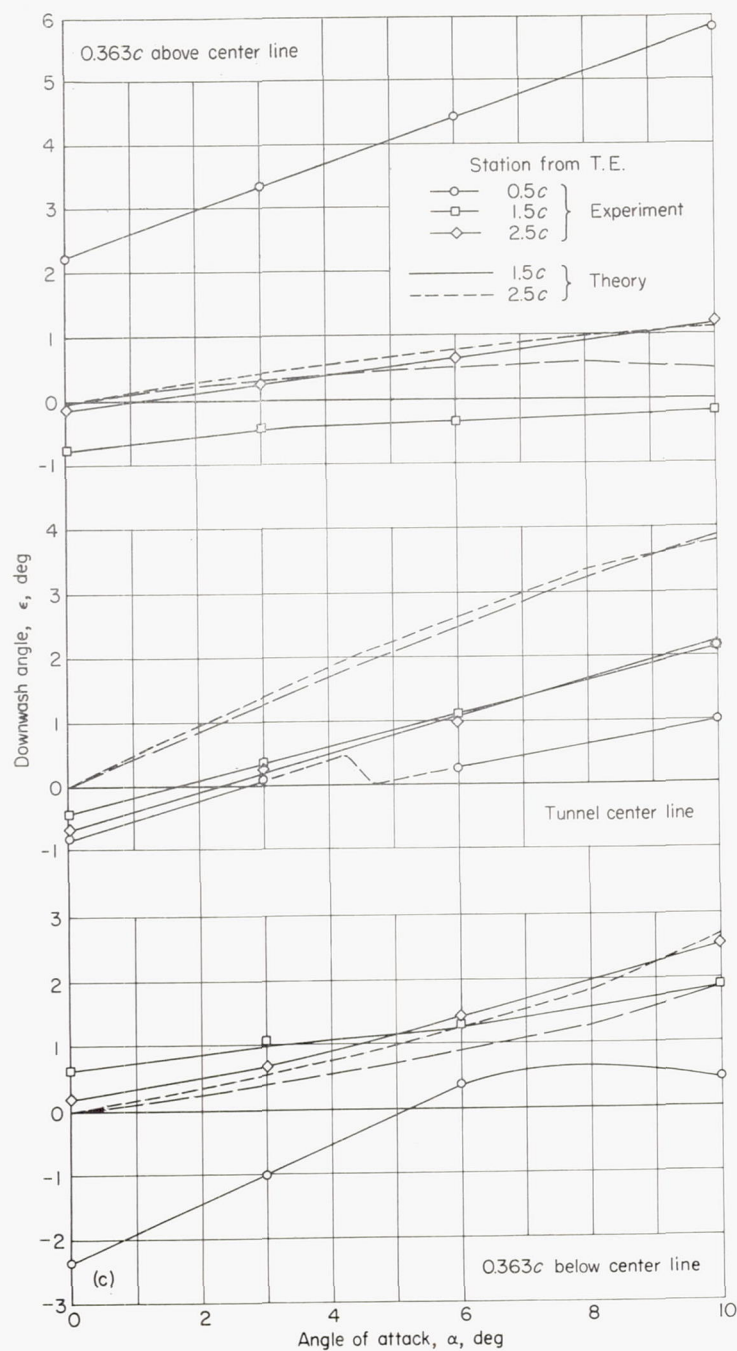
(a) Spanwise station, $0.286\frac{b}{2}$. (Slight curvature of theoretical curves is due to trailing-edge displacement relative to fixed test-point locations.)
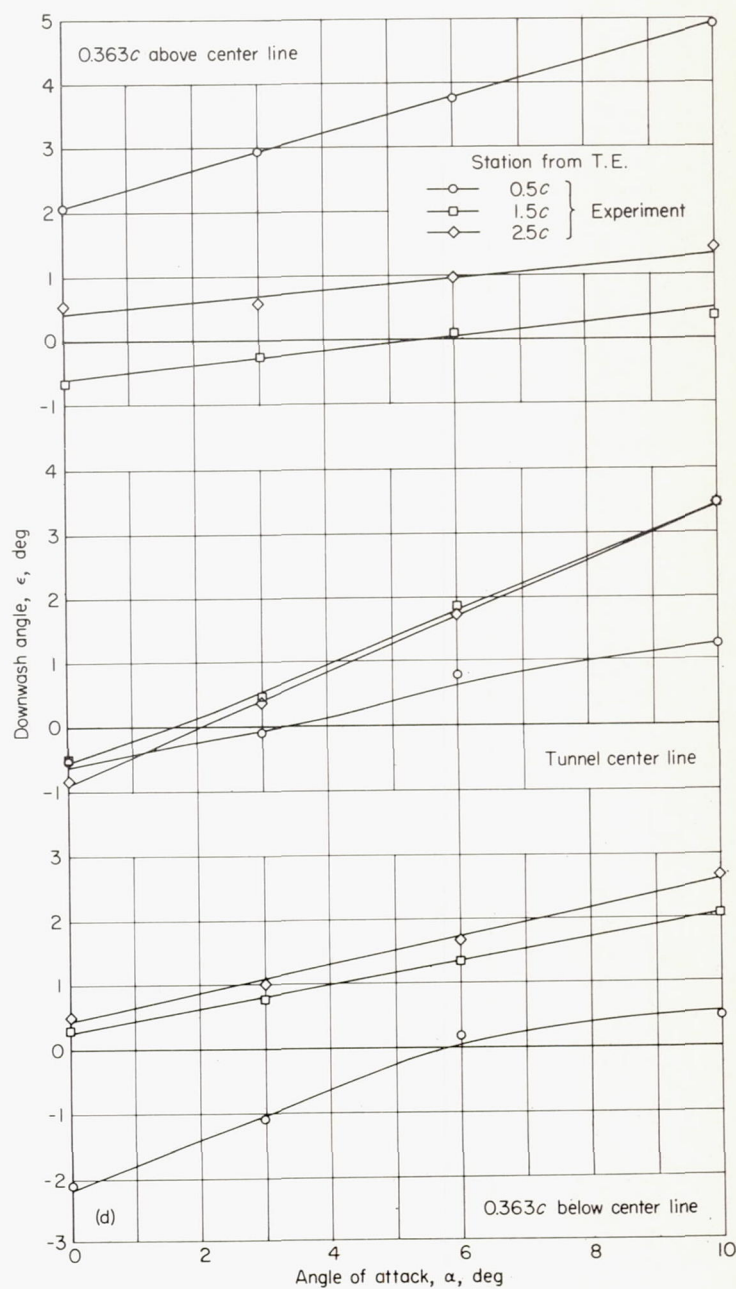
(b) Spanwise station, $0.428\frac{b}{2}$.
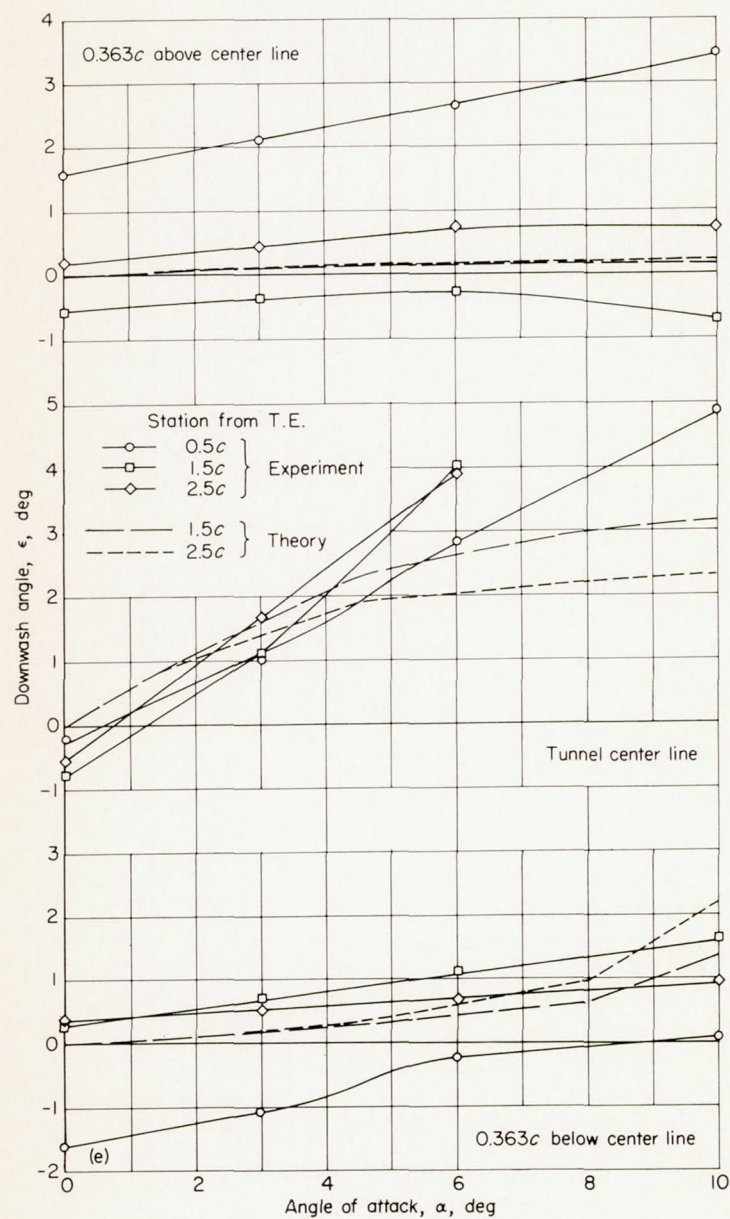
Figure 18.—Variation of ϵ with α.

(c) Spanwise station, $0.571\frac{b}{2}$. (Slight curvature of theoretical curves is due to correction for displacement of trailing vortex sheet at $0.571\frac{b}{2}$ station.)
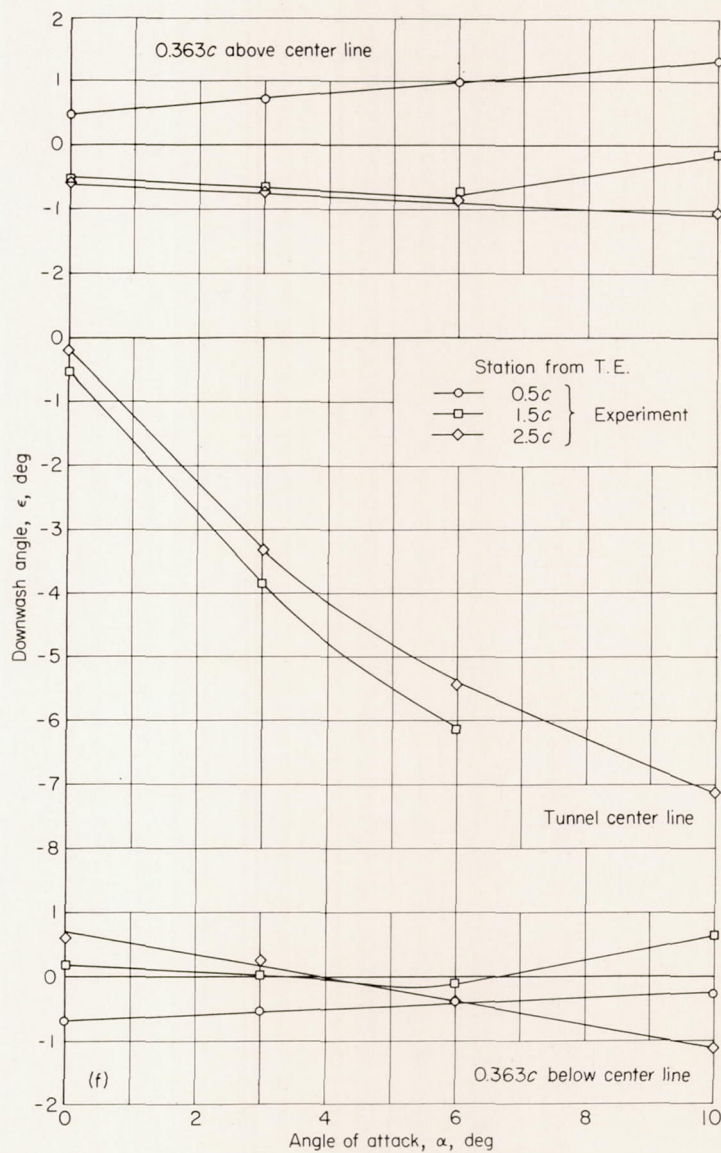
(d) Spanwise station, $0.714\frac{b}{2}$.

FIGURE 18.—Continued.

(e) Spanwise station, $0.857\frac{b}{2}$. (Curvature of theoretical curves is due to correction for displacement of trailing vortex sheet at $0.857\frac{b}{2}$ station.)

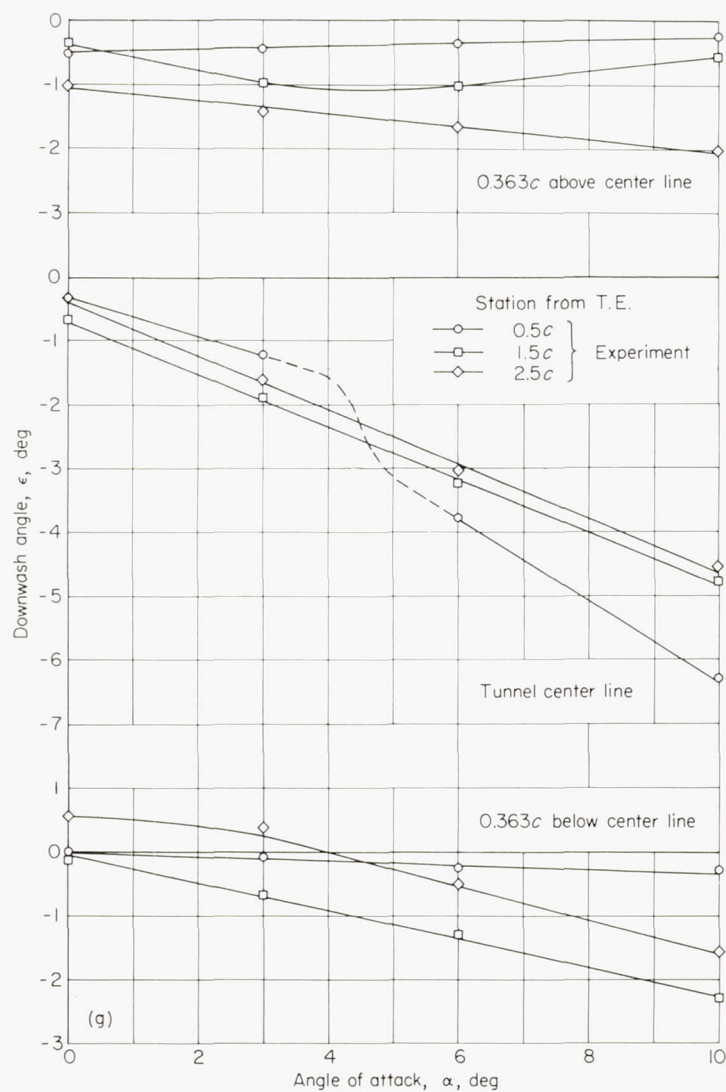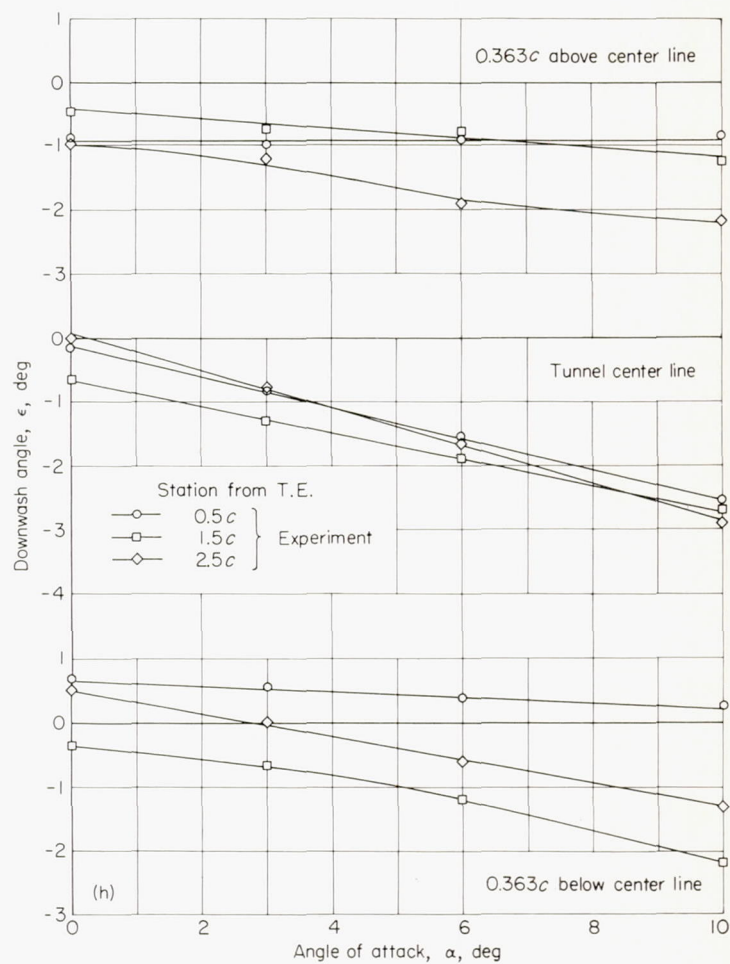(f) Spanwise station, $1.000\frac{b}{2}$.

FIGURE 18.—Continued.

(g) Spanwise station, $1.143\dfrac{b}{2}$.

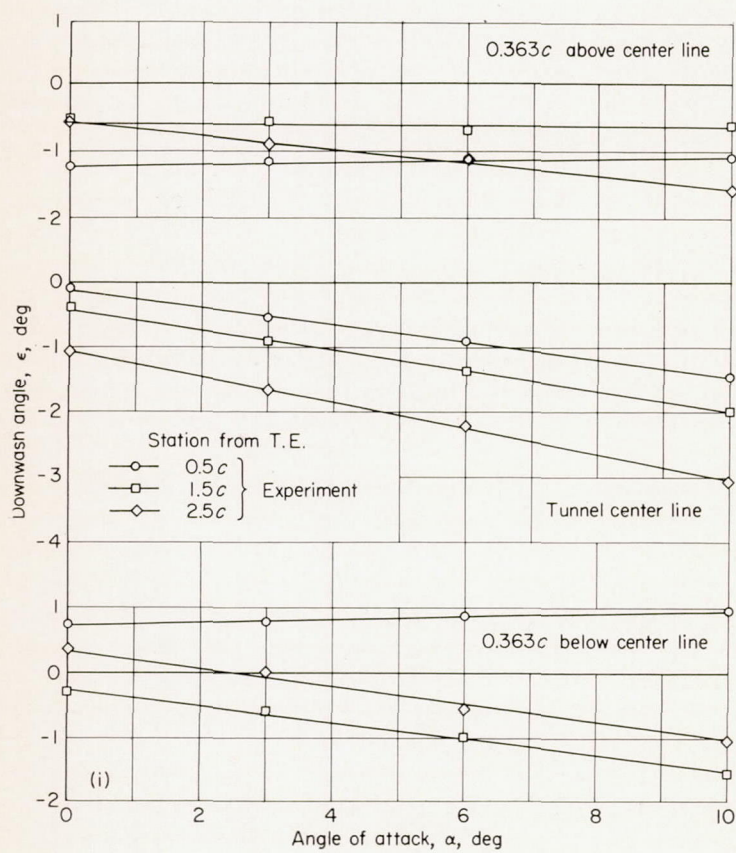(h) Spanwise station, $1.286\dfrac{b}{2}$.

FIGURE 18.—Continued.
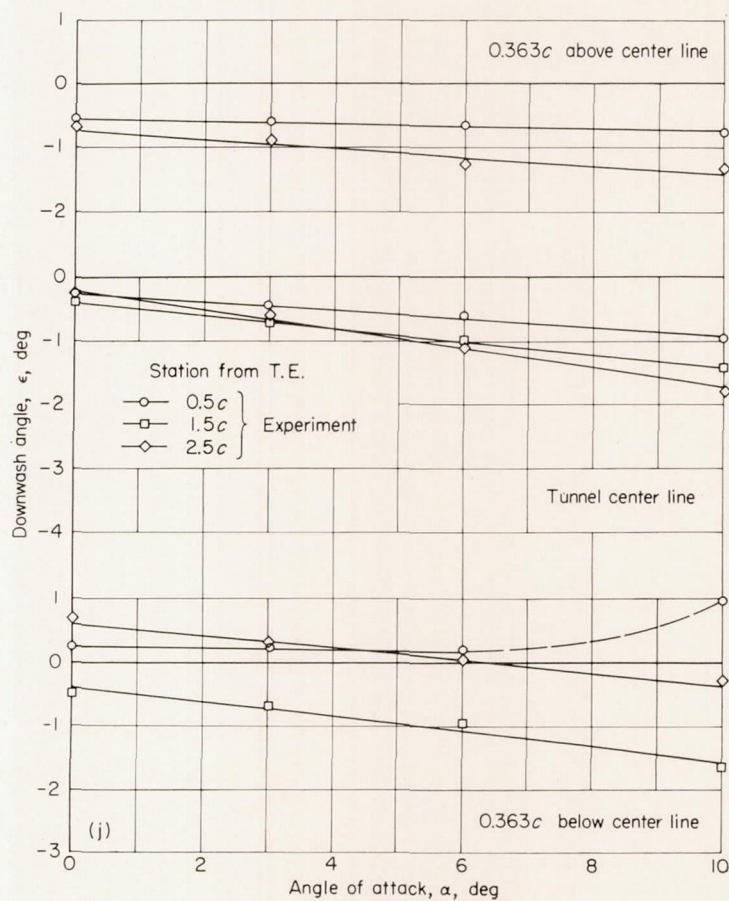
(i) Spanwise station, $1.428\frac{b}{2}$.

(j) Spanwise station, $1.571\frac{b}{2}$.

FIGURE 18.—Concluded.

TABLE I

VERTICAL LOCATIONS $\left(\dfrac{z}{c}\right)$ OF EACH OF THE TEST POINTS FOR THE DOWNWASH AND SIDEWASH MEASUREMENTS REFERRED TO TUNNEL CENTER LINE

α, deg	z/c at $\dfrac{y}{b/2}=$									
	0.286	0.428	0.571	0.714	0.857	1.000	1.143	1.286	1.428	1.571
0.5 chord behind wing trailing edge										
0	0.363 .002 −.393	0.363 .002 −.393	0.363 −.003 −.393	0.363 −.008 −.403	0.363 −.002 −.403	0.367 −.407	0.363 .012 −.403	0.373 .007 −.403	0.373 .010 −.400	0.373 .008 −.400
3	0.363 .002 −.393	0.363 .002 −.393	0.363 −.003 −.393	0.363 −.008 −.403	0.363 −.002 −.403	0.367 −.407	0.363 .012 −.403	0.373 .007 −.403	0.373 .010 −.400	0.373 .008 −.400
6	0.363 .002 −.393	0.363 .002 −.393	0.363 −.003 −.393	0.363 −.008 −.403	0.363 −.002 −.403	0.367 −.407	0.363 .012 −.403	0.373 .007 −.403	0.373 .010 −.400	0.373 .008 −.400
10	0.363 .002 −.393	0.363 .002 −.393	0.363 −.003 −.393	0.363 −.008 −.403	0.363 −.002 −.403	0.367 −.407	0.363 .012 −.403	0.373 .007 −.403	0.373 .010 −.400	0.373 .008 −.400
1.5 chords behind wing trailing edge										
0	0.357 .003 −.378	0.353 −.007 −.383	0.357 −.007 −.383	0.357 −.007 −.383	0.357 .007 −.382	0.363 .007 −.380	0.363 −.007 −.373	0.363 −.003 −.372	0.363 −.003 −.375	−.003 −.372
3	0.357 .003 −.378	0.353 −.007 −.383	0.357 −.007 −.383	0.357 −.007 −.383	0.357 .007 −.382	0.363 .007 −.380	0.363 .007 −.373	0.363 −.003 −.372	0.363 −.003 −.375	−.003 −.372
6	0.357 .003 −.378	0.353 −.007 −.383	0.357 −.007 −.383	0.357 −.007 −.383	0.357 .007 −.382	0.363 .007 −.380	0.363 .007 −.373	0.363 −.003 −.372	0.363 −.003 −.375	−.003 −.372
10	0.357 .003 −.378	0.353 −.007 −.383	0.357 −.007 −.383	0.357 −.007 −.383	0.357 .007 −.382	0.363 .007 −.380	0.363 .007 −.373	0.363 −.003 −.372	0.363 −.003 −.375	−.003 −.372
2.5 chords behind wing trailing edge										
0	0.363 .035 −.352	0.359 .043 −.358	0.363 .043 −.358	0.383 .043 −.358	0.379 .047 −.358	0.409 .045 −.355	0.416 .046 −.355	0.416 .039 −.355	0.426 .049 −.355	0.426 .039 −.355
3	0.363 .035 −.352	0.359 .043 −.358	0.363 .043 −.358	0.383 .043 −.358	0.379 .047 −.358	0.409 .045 −.355	0.416 .046 −.355	0.416 .039 −.355	0.426 .049 −.355	0.426 .039 −.355
6	0.363 .035 −.352	0.359 .043 −.358	0.363 .043 −.358	0.383 .043 −.358	0.379 .047 −.358	0.409 .045 −.355	0.416 .046 −.355	0.416 .039 −.355	0.426 .049 −.355	0.426 .039 −.355
10	0.363 .035 −.352	0.359 .043 −.358	0.363 .043 −.358	0.383 .043 −.358	0.379 .047 −.358	0.409 .045 −.355	0.416 .046 −.355	0.416 .039 −.355	0.426 .049 −.355	0.426 .039 −.355

At $\alpha=0°$, for those points falling within the region of two-dimensional flow and ahead of the trailing-edge shocks (i.e., at the distance of 0.5 chord to the rear of the trailing edge of the wing and 0.363 chord above and below the plane of the wing), the flow-deflection angles as measured are of the order of $\pm 2°$. These flow deflections are almost exactly what would be expected if the direction of flow at the respective stations were assumed to equal the slope of the wing surface at the point where Mach lines passing through the stations meet the wing surface. The plots of ϵ against α for these two stations gave straight lines, each having a slope numerically equal to 0.5, whereas linearized theory predicts the slope in this region to be unity. That this discrepancy was a direct result of wing thickness was borne out by a simple calculation in which, at a number of wing angles of attack, the angle of downflow was calculated at the station 0.5 chord rearward of the trailing edge and 0.363 chord above the plane of the wing, two-dimensional flow being assumed and curvature of the leading-edge shock being ignored. At each angle of attack, the flow at the point was assumed to be parallel to

the wing surface at that point at which the characteristic through the point meets the wing surface. The plot of ϵ against α calculated in this manner agreed almost exactly with experiment.

It can be seen in figure 18 that, for locations downstream of the trailing-edge shocks, the curves of ϵ plotted against α do not, in general, go through $0°$ at $\alpha=0°$. As mentioned previously, this result is due to several effects, of which the influence of the wake on the downwash field is believed to be of the greatest significance.
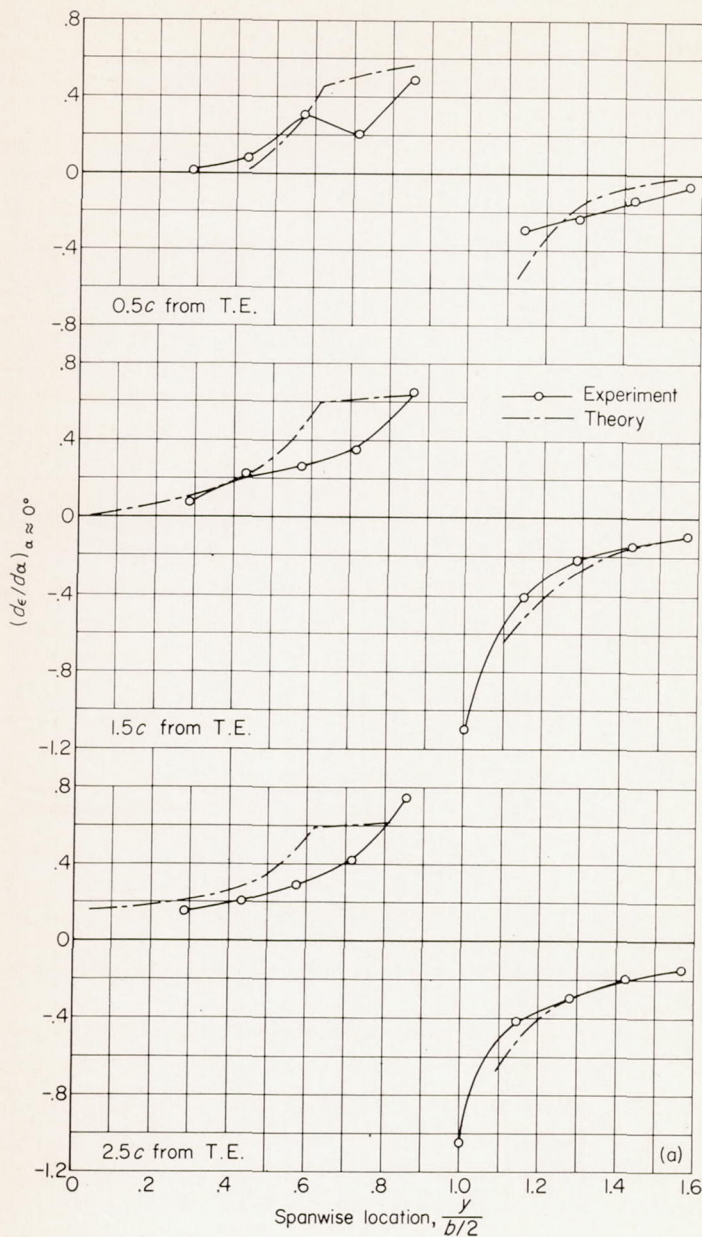
In certain of the plots of ϵ against α, discontinuities in slope are present. In each case, these discontinuities are the result of the passing of the point at which the flow measurements were being made from one region of flow to another, as the wing angle of attack is changed. Tracing these discontinuities to their source is facilitated by reference to figures 6 and 7, previously described, in which the boundaries separating the various regions of flow are shown.

Values of $d\epsilon/d\alpha$ are plotted against spanwise location for the three chordwise stations behind the trailing edge and the three vertical locations in figure 19. The values of $d\epsilon/d\alpha$ were obtained by measuring the slopes of the curves of ϵ against α. The slopes of the curves of ϵ against α near $\alpha=0°$ are compared directly with theory in figures 19 (a) and 19 (b), and the slopes near $\alpha=10°$ are compared with theory, which has been modified to account for the displacement and distortion of the trailing vortex sheet, in figures 19 (c) and 19 (d).

Comparison of downwash data with theoretical results.—It was mentioned previously that the effect of thickness reduces the values of $d\epsilon/d\alpha$ for the two-dimensional region between the leading- and trailing-edge shocks by a factor of 0.5 for the 6-percent-thick wing of these tests. (This factor is of course dependent on wing profile and the test-point location.) Although a theoretical value for $d\epsilon/d\alpha$ can be found readily in the strictly two-dimensional region with thickness taken into account, at points farther outboard where the tip effect is felt, no ready means are available for calculating the effect of thickness on $d\epsilon/d\alpha$. In obtaining the theoretical curve of figure 19 (a), for the location 0.363 chord above and below the wing and only 0.5 chord behind the trailing edge, the assumption was made that values of downwash in the tip region would be reduced in the same proportion as in the two-dimensional region. When this assumption is used, good agreement between theory and experiment is obtained.

For the downwash field downstream of the trailing-edge shock, it is evident in figure 19 (a), which is for angles of attack near $0°$, that only in a region just inboard of the tip, in the plane of the wing, does theory differ markedly from experiment. The disparity between theory and experiment existing in this region is due to the proximity of the test points in this region to the shed vortex sheet and to the probable difference in the spanwise distribution of vorticity from that predicted by theory. Even near an angle of attack of $0°$ separation effects on the wing, especially near the tip, would influence the spanwise load distribution and consequently the spanwise vortex distribution. This effect, as well as the redistribution of vorticity with distance downstream,

(a) Near $\alpha=0°$, plane through tunnel center line.

FIGURE 19.—Spanwise $d\epsilon/d\alpha$ variation.

(b) Near $\alpha=0°$, planes 0.363 chord above and below tunnel center line.

FIGURE 19.—Continued.

wash at a wing angle of attack of 0°. The wake pitot profiles, however, do not indicate any appreciable change in shape or size with angle of attack, except near the tip where the vortex sheet rolls up, so that the only effect of the wake on the variation of downwash with angle of attack results from its displacement.

The displacement and distortion of the trailing vortex sheet produced the curvature of the theoretical curves of ϵ against α of figures 18 (c) and 18 (e) (linear theory, of course, predicts a straight-line variation). The spanwise station shown in figure 18 (e) is near enough to the tip to be in a region of sizable downwash angles and, consequently, an appreciable displacement of the trailing vortex sheet occurs. The theoretical curves, which are for an inboard station (fig. 18 (a)), were computed with only the displacement of the wing trailing edge relative to the fixed test points with angle of attack being taken into account.

The corrections accounting for the displacement and distortion of the trailing vortex sheet are based on a location of the vortex sheet at a particular spanwise station, which is computed from the theoretical downwash values of that spanwise station in a manner described in more detail in appendix B. In figures 19 (c) and (d) the experimental $d\epsilon/d\alpha$ values, which are for an angle of attack near 10°, are compared with the theoretical values at each spanwise station. One of the two theoretical curves shown in these figures is corrected inboard of the tip for the displacement of the vortex sheet, the vertical location of which was determined from theoretical $d\epsilon/d\alpha$ values at each spanwise station. The other theoretical curve, which is in much better agreement with experiment, was obtained by considering the vertical location of the vortex sheet at each

would account for the fact that the vortex distribution is other than that predicted by linear theory. For illustrative purposes, the degree of influence of the spanwise tip loading on the downwash distribution is brought out in figure 20, in which various types of tip loadings and their corresponding downwash distribution in the Trefftz plane are shown. It is seen that, except in the plane of the wing inboard of the tip (i.e., the region in the immediate neighborhood of the vortex elements), the values are little influenced by loading. In the region inboard of the tip large changes in the downwash field result from the different spanwise load distributions illustrated. These spanwise load distributions were merely selected at random and, since pressure measurements on the wing were not made, a correlation between theory and experiment in this region is not attempted.

It was mentioned previously that the presence of the wake is believed to have considerable effect on values of down-
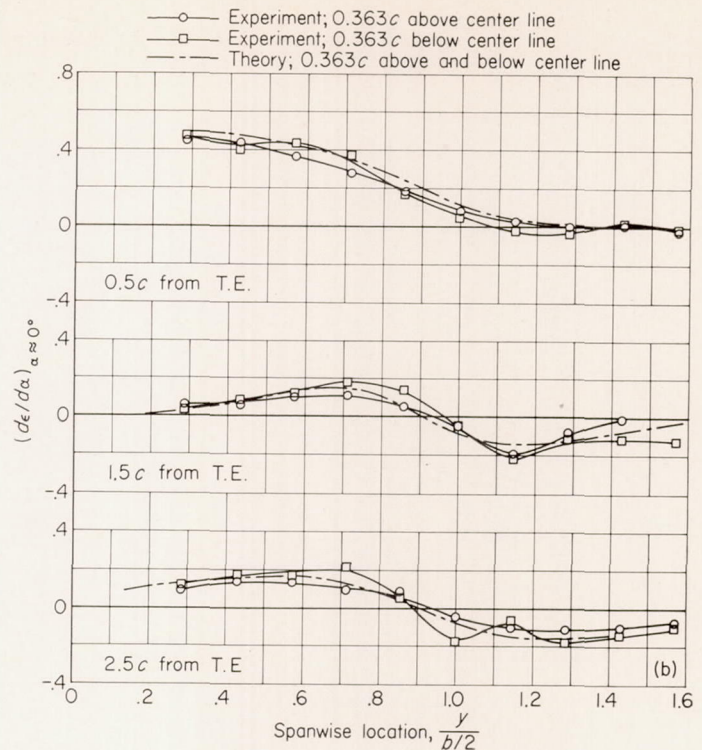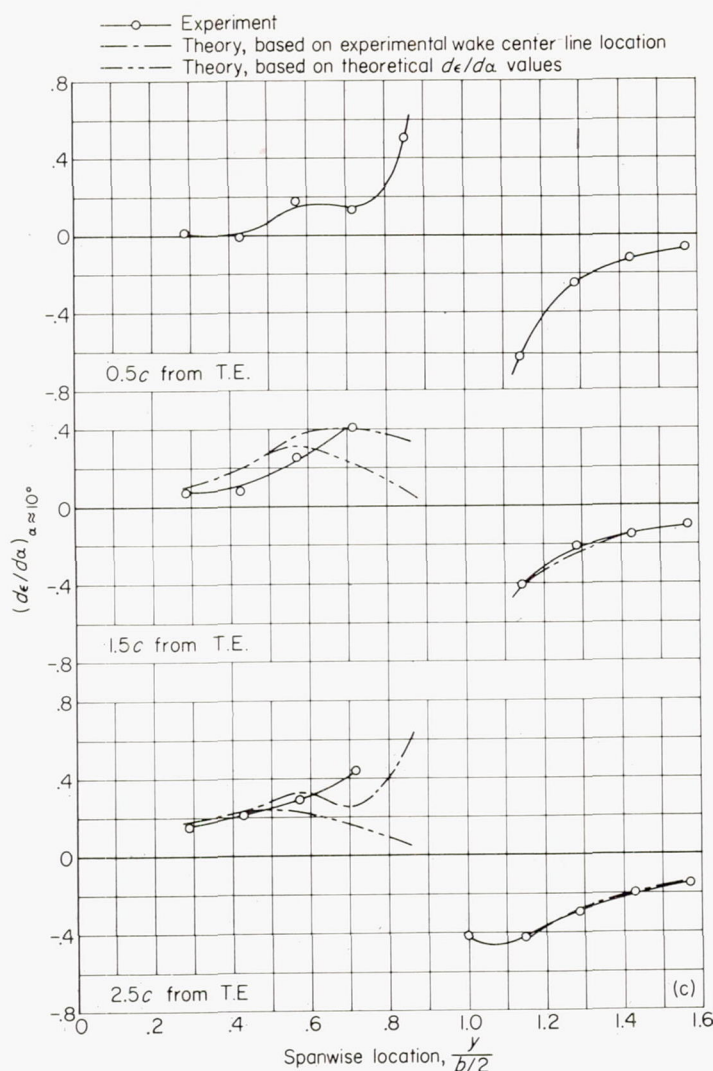
(c) Near $\alpha=10°$, plane through tunnel center line.

FIGURE 19.—Continued.

(d) Near $\alpha=10°$, planes 0.363 chord above and below tunnel center line.

FIGURE 19.—Concluded.

separate spanwise station inboard of the tip to be coincident with the experimentally determined wake-center-line location. For all the stations outboard of the tip the datum plane of the theoretical $d\epsilon/d\alpha$ distribution was assumed to be coincident with a horizontal plane through the wing trailing edge. It can be seen that excellent agreement exists between theory and experiment outboard of the tip and that inboard of the tip, wherever it is important that the displacement and distortion of the vortex sheet be accounted for, such as the stations 0.363 chord below the tunnel axis, the method based on theoretical $d\epsilon/d\alpha$ values is very poor. The disagreement between theory and experiment in figure 19 (a) for locations in the plane of the wing inboard of the tip, where the experimental $d\epsilon/d\alpha$ values are much less than theory, partly accounts for the failure of trailing vortex sheet (as evidenced by the vertical locations of the wake center line) to be displaced as much as theory predicts. Another consideration which would make the displacement of the trailing vortex sheet less than theory predicts is that the overexpansion phenomena from the high-
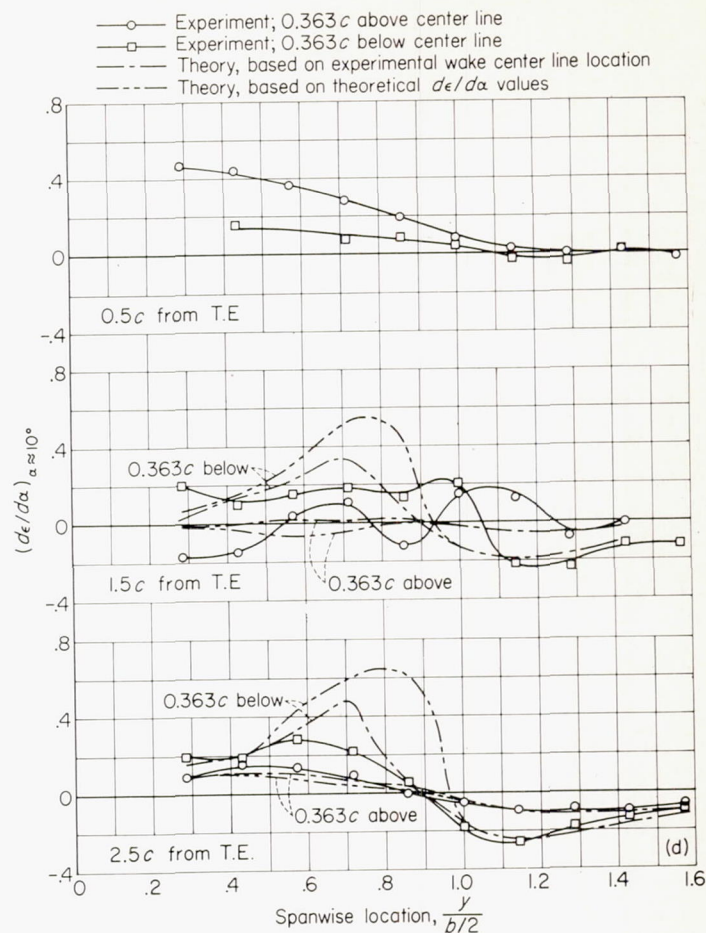
pressure side of the wing trailing edge would displace the effective trailing edge downstream and upward. The low Reynolds number of the test might tend to exaggerate this effect for the present experiment. The effect of Reynolds number on the separation point is pointed out in reference 10.

Sidewash results.—Values of sidewash angle σ are plotted against wing angle of attack α in figure 21. For the most part these curves are essentially linear. Departures from linearity are attributable to the same displacement of the trailing edge and trailing vortex sheet as was mentioned in connection with the downwash. Discontinuities resulting from the passing of the point of measurement from one region of flow to another can be traced to their source by using figures 6 and 7. In general, the plots of σ against α do not pass through the origin (at $\alpha=0$ sidewash flow angles as high as 3° were observed). This result is at variance with linearized theory for a flat plate. The departures of the sidewash angles from zero at $\alpha=0°$ is brought out in figure 22 where curves of sidewash angle, measured at $\alpha=0°$, are plotted against spanwise location. The slopes of the curves of σ against α near $\alpha=0°$ are plotted against spanwise location in figures 23 (a) and 23 (b), and their slopes near $\alpha=10°$ are plotted in figures 23 (c) and 23 (d).
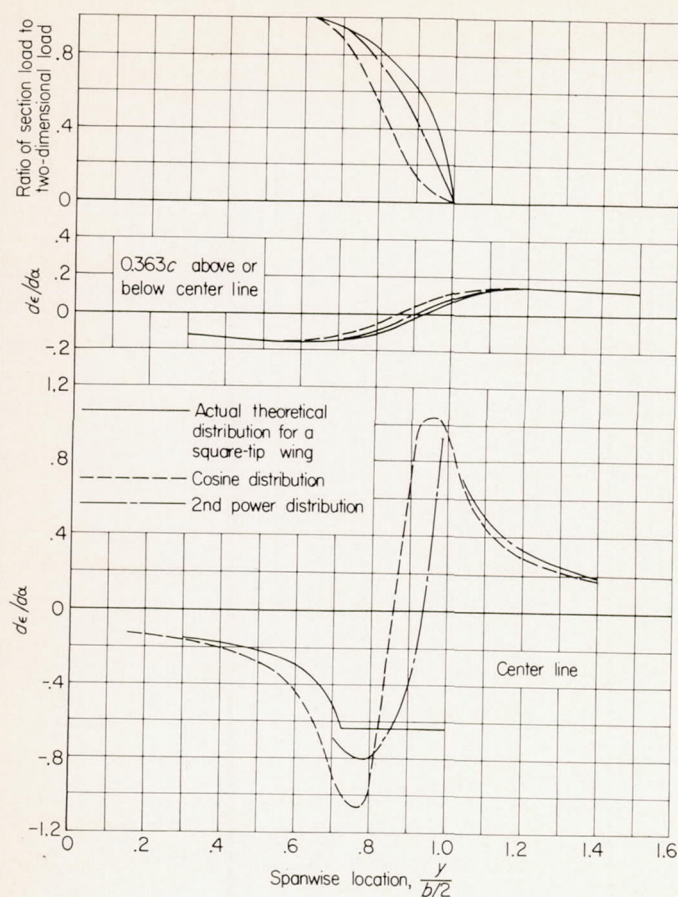
FIGURE 20.—Theoretical curves of $d\epsilon/d\alpha$ against span in the Trefftz plane behind a rectangular wing, showing effect of spanwise load distribution on downwash values.

Comparison of sidewash data with theoretical results.—
The theoretical values of the rate of change of sidewash with wing angle of attack $d\sigma/d\alpha$ have been computed at a large number of points distributed throughout the entire flow field downstream of the rectangular wing. The results of these computations are presented in nondimensional form in figures 14, 15, and 16. By their use, the sidewash at any point in the field of flow of a rectangular wing may be readily evaluated by interpolation for any desired value of chord and Mach number.

In describing the experimental results obtained in these tests, attention has already been drawn to the fact that the curves of σ plotted against α did not, in general, pass through the origin for the condition of 0° wing angle of attack. Three possible causes are: (a) wing thickness, (b) presence of wing wake, and (c) unsymmetrical boundary-layer-shock interaction effects occurring on the bypass plate and resulting from the intersection of the wing and the bypass plate.

An estimate of the effect of the finite thickness of the wing was made by distributing sources of strength proportional to the slope of the wing surface over the wing plan form and calculating the resulting sidewash field. The details of the calculation are given in appendix B. The results of these computations are superimposed on figure 22. Agreement is rather poor although at the station 0.5 chord back from the trailing edge the trends are apparent.
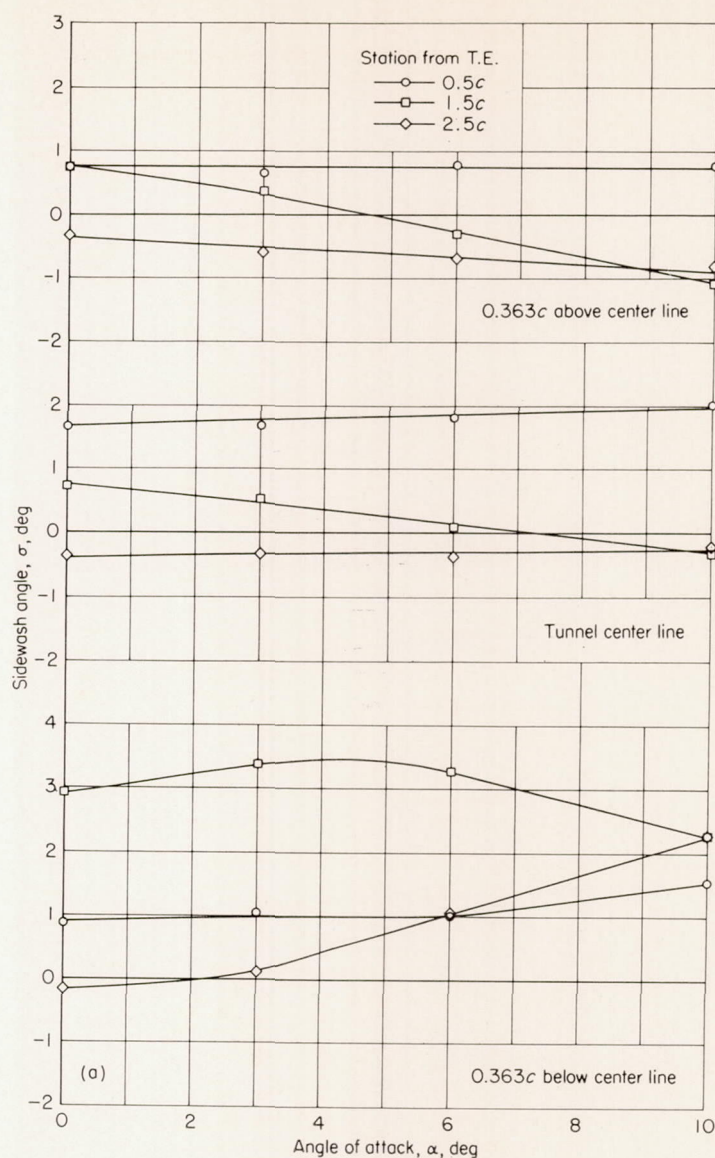
(a) Spanwise station, $0.286\dfrac{b}{2}$.

FIGURE 21.—Variation of σ with α.

The influence of the wake on the sidewash field would be expected to be appreciable only in the neighborhood of the tip vortices. Elsewhere in the flow field the wake might be expected to have its largest effect on downwash and it seems unlikely that the wake can account for the large sidewash angles encountered. It would thus appear that the boundary-layer and shock interaction effects in the sidewash direction at and to the rear of the intersection of the wing and the bypass plate are an important factor contributing to the observed values of sidewash. This conclusion is to some extent borne out by the better comparison of the trends between theory and experiment at the 0.5-chord station (where the supersonic flow would not be affected by the divergence of the stream contours in the sidewash direction at the intersection of the wing and the bypass plate) than the comparison at stations farther downstream.
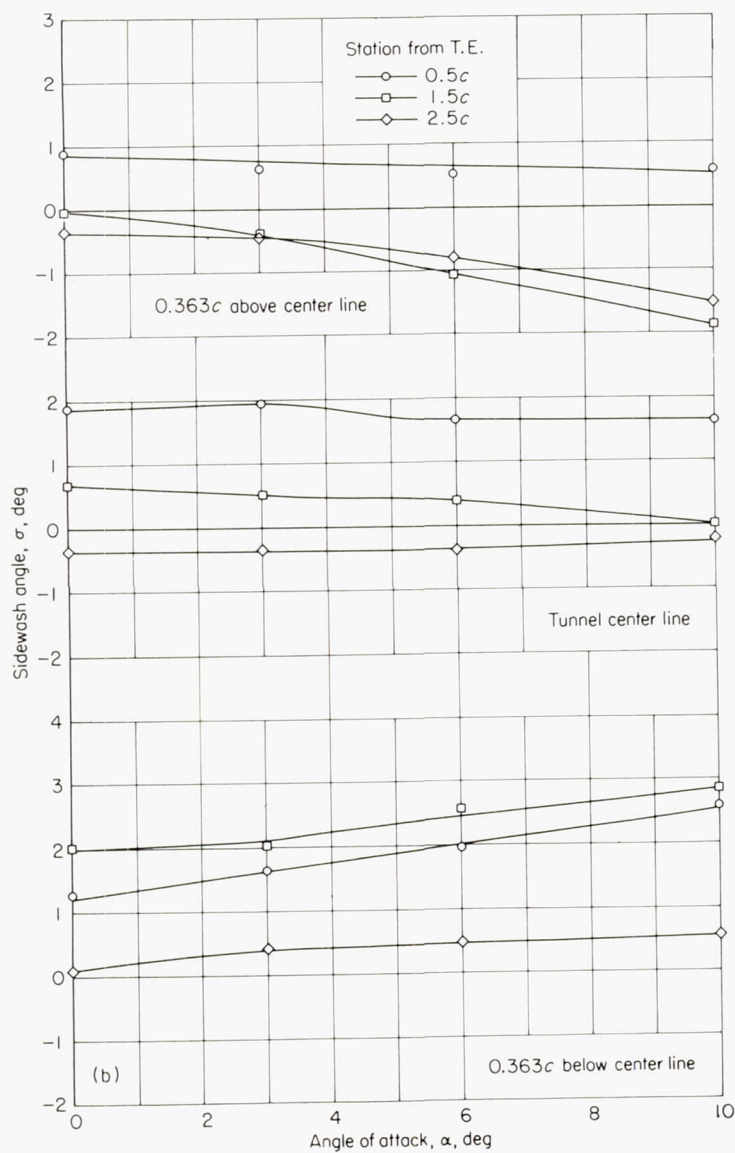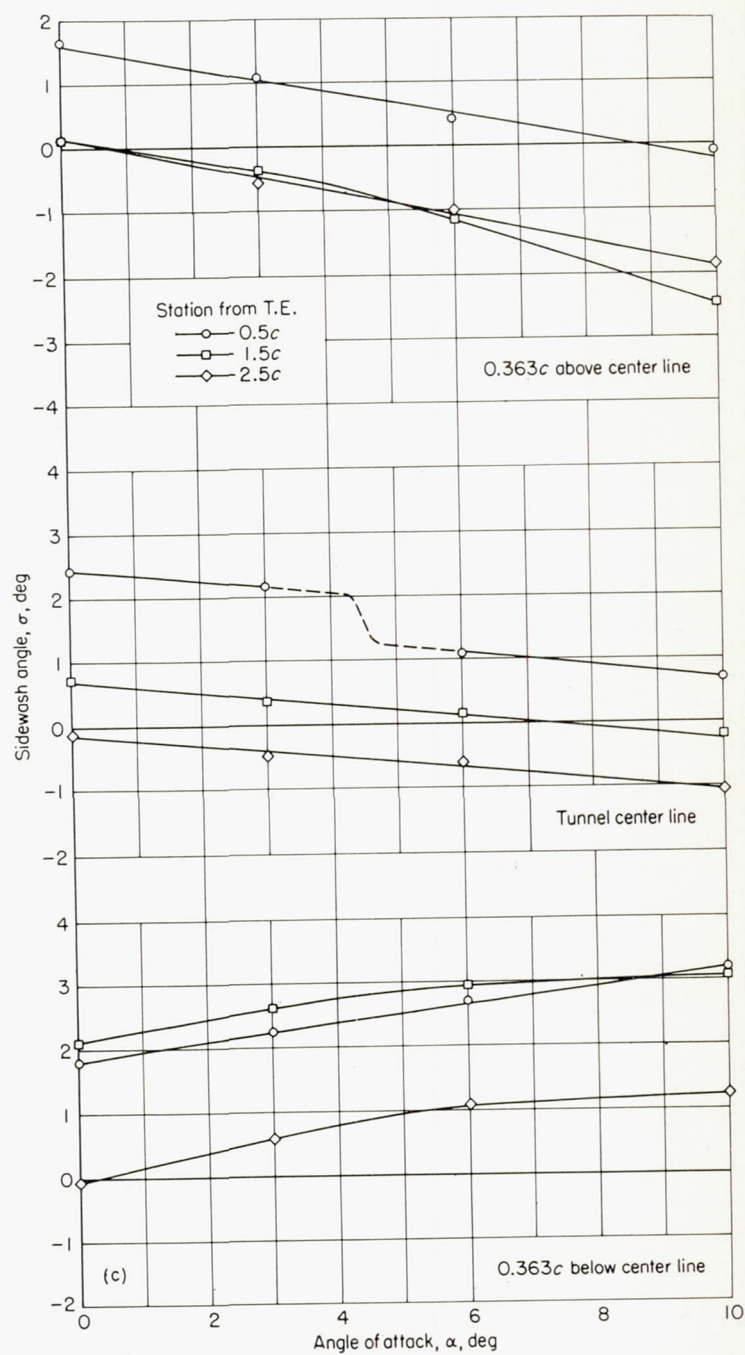
(b) Spanwise station, $0.428\frac{b}{2}$.   (c) Spanwise station, $0.571\frac{b}{2}$.
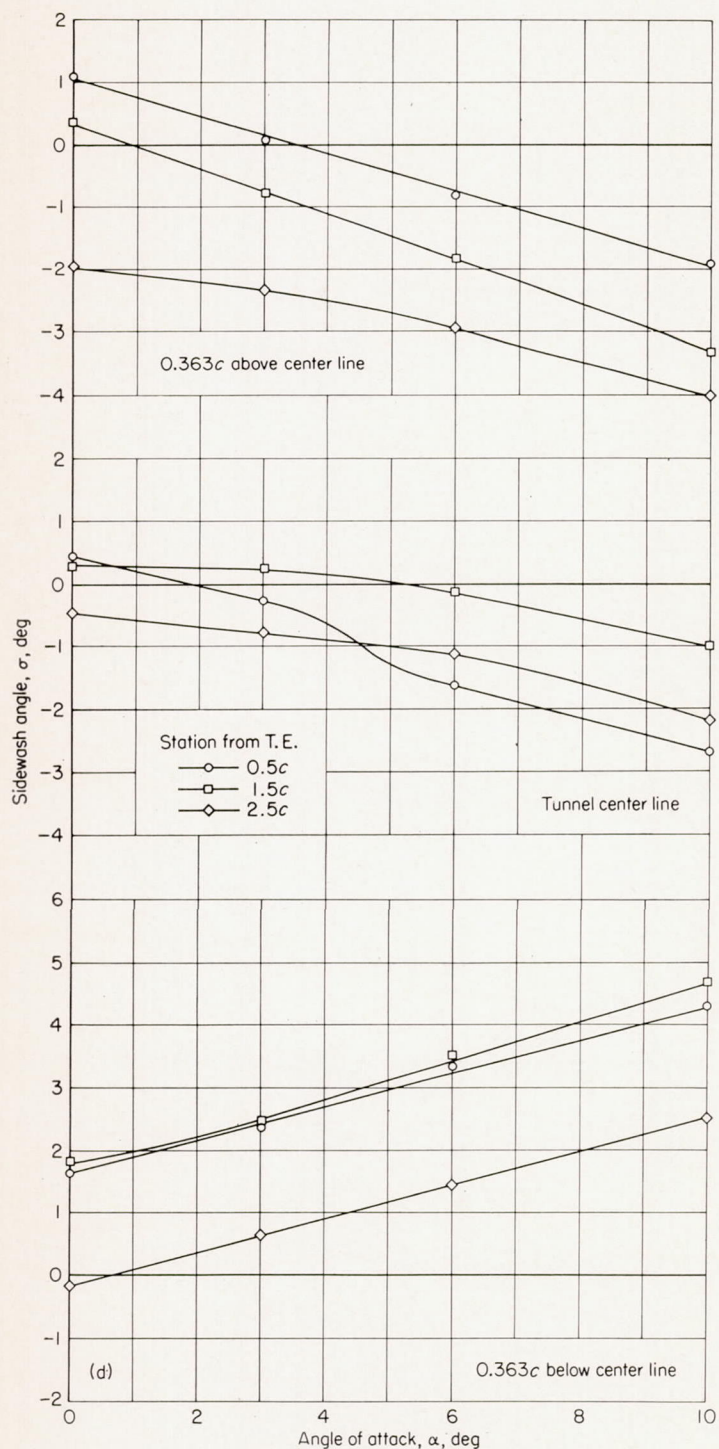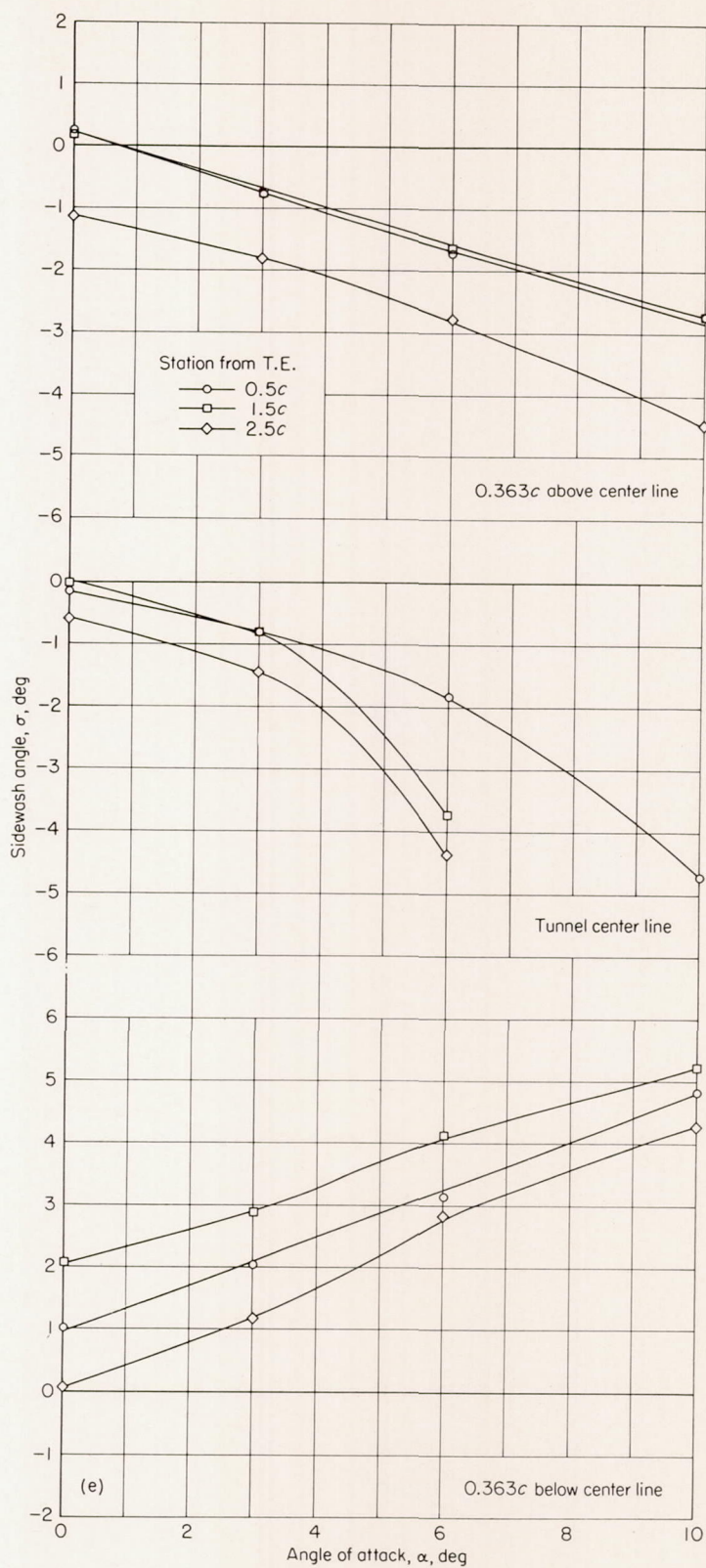
FIGURE 21.—Continued.

(d) Spanwise station, $0.714\frac{b}{2}$.

(e) Spanwise station, $0.857\frac{b}{2}$.

FIGURE 21.—Continued.

(f) Spanwise station, $1.000\frac{b}{2}$.
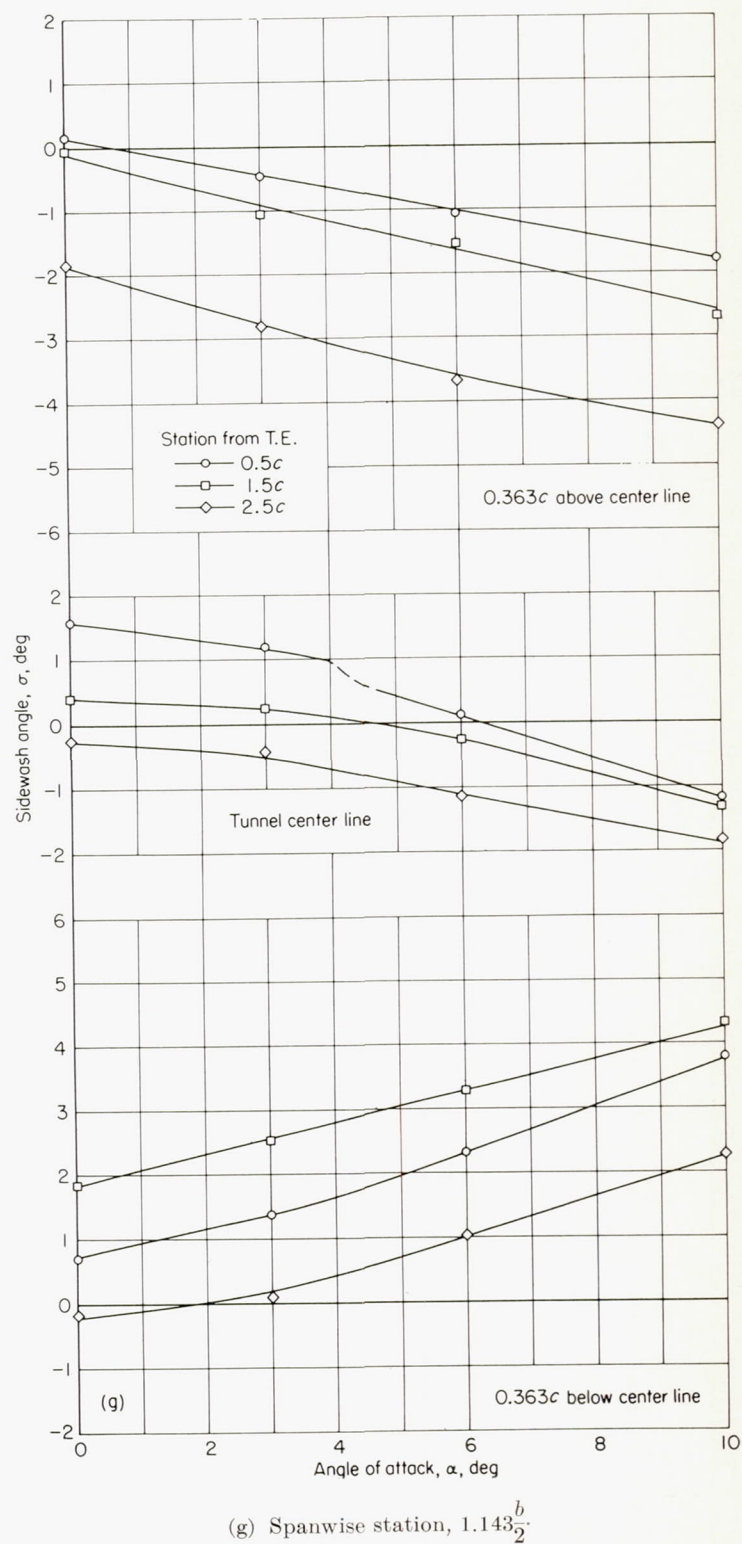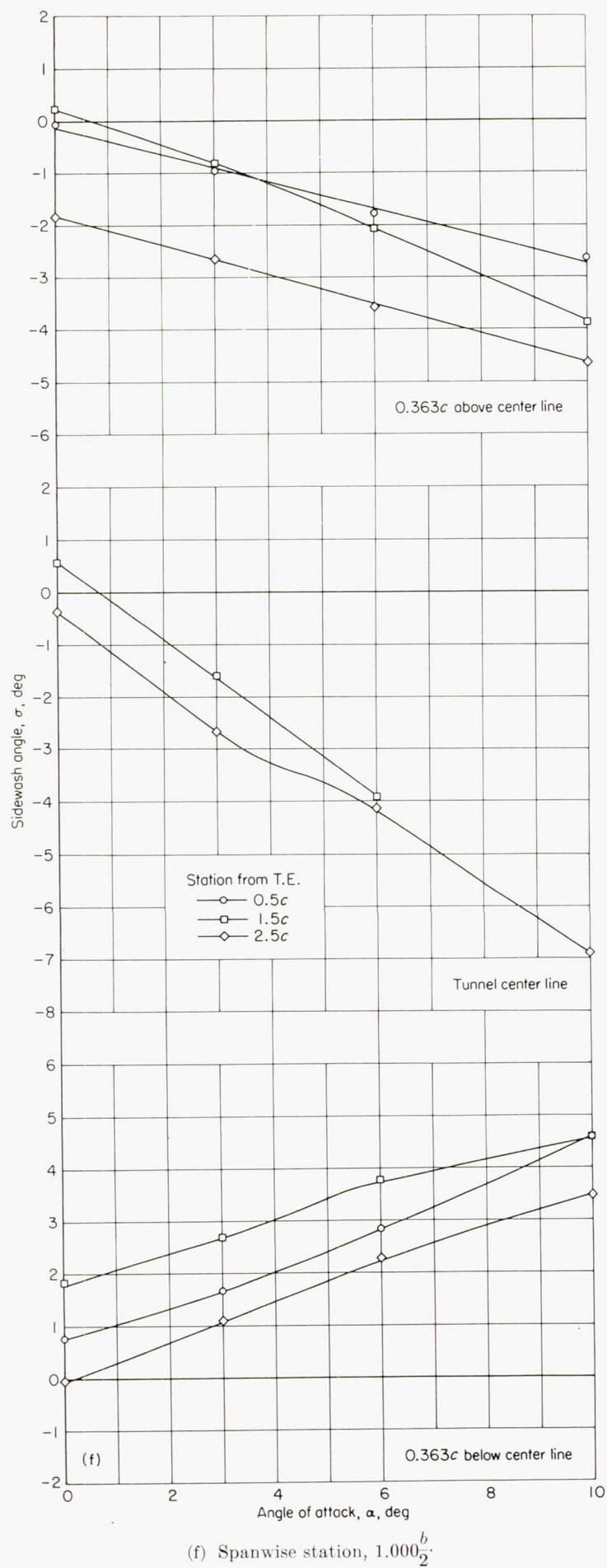
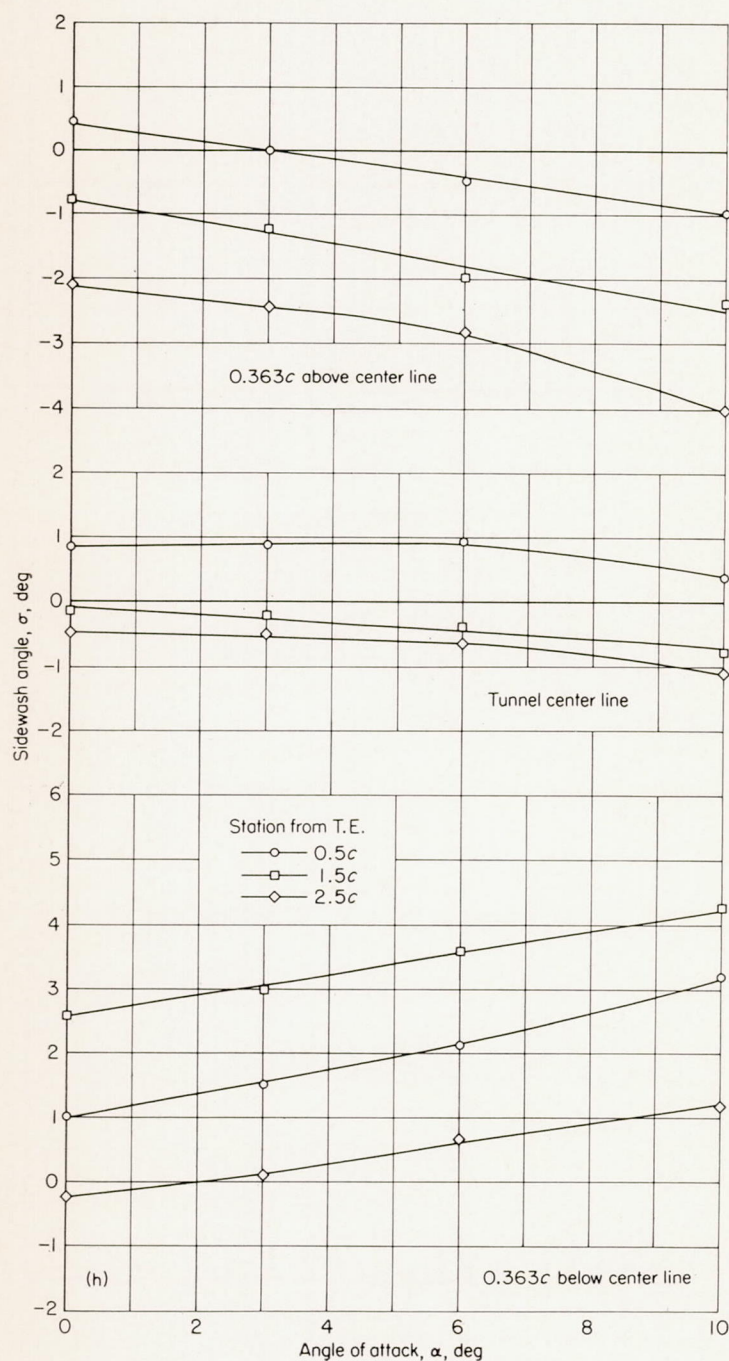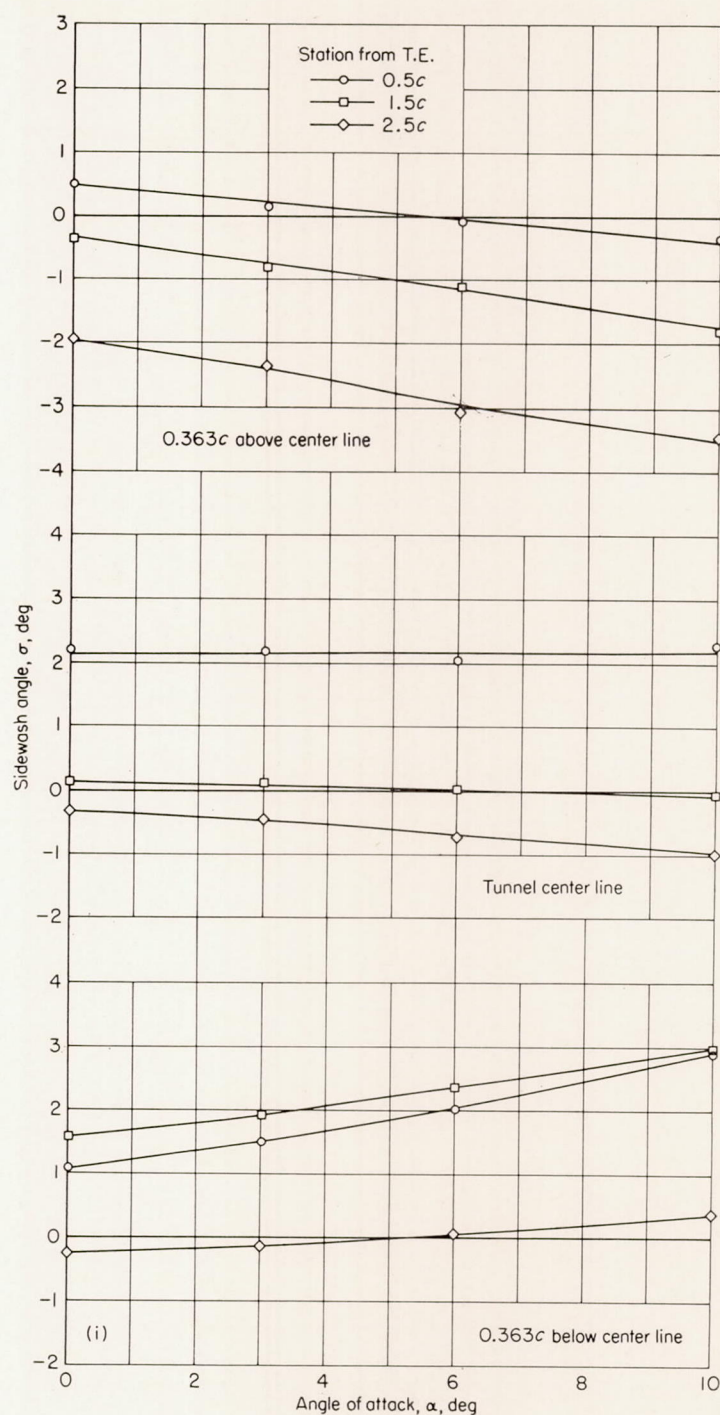(g) Spanwise station, $1.143\frac{b}{2}$.

FIGURE 21.—Continued.

(h) Spanwise station, $1.286\frac{b}{2}$.

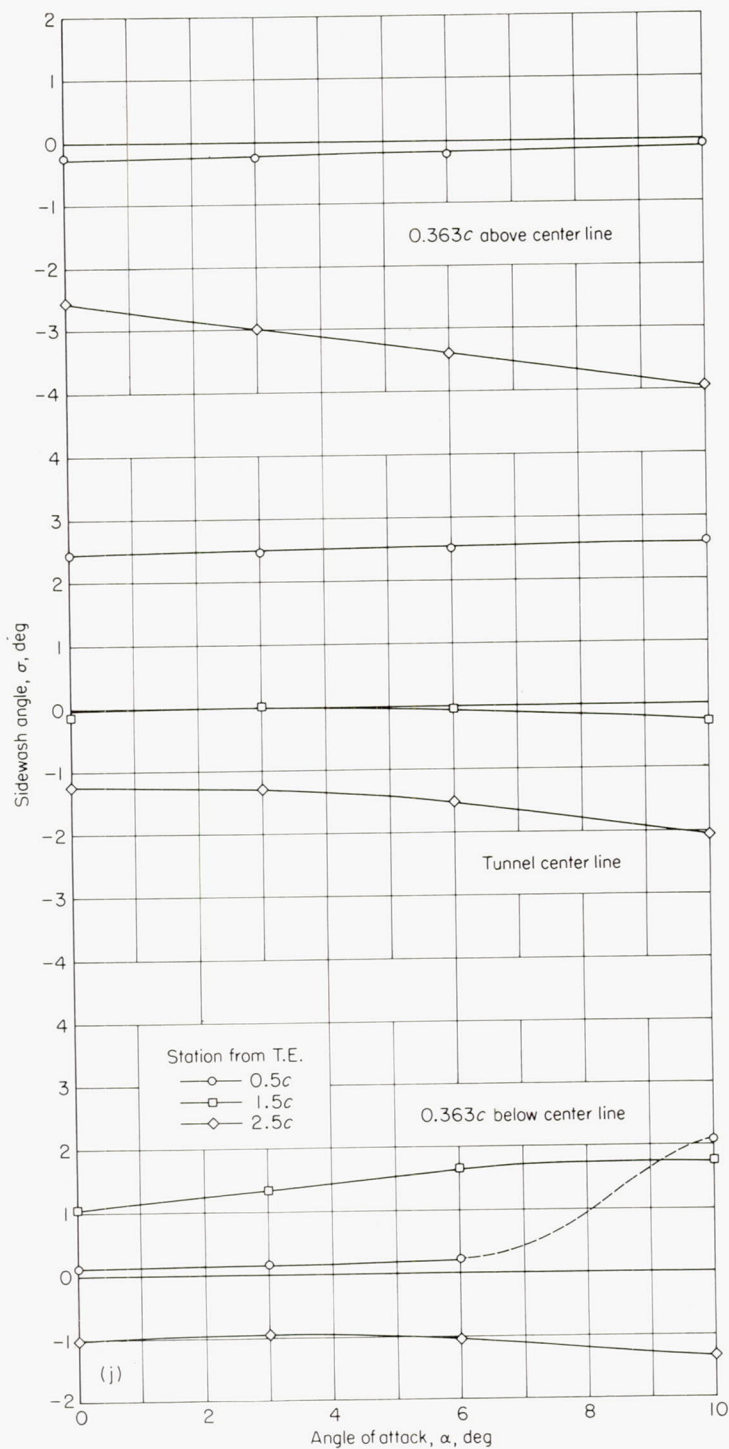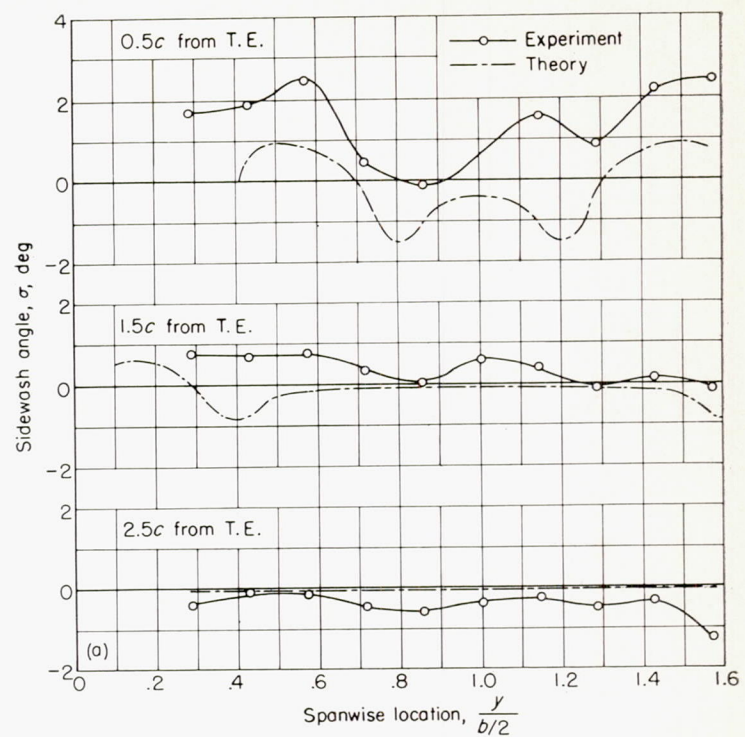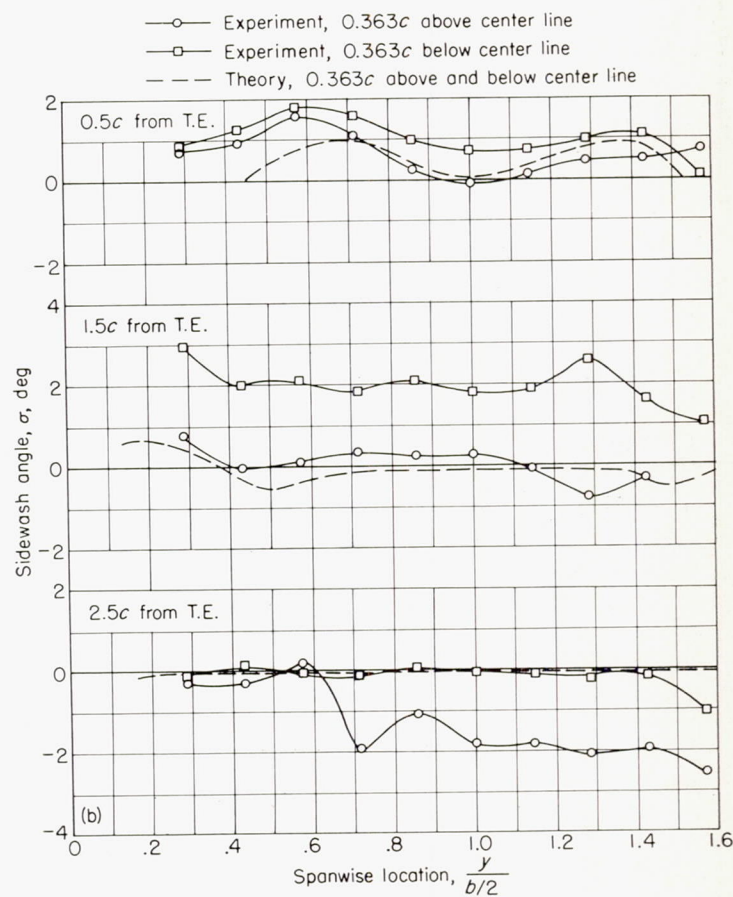(i) Spanwise station, $1.428\frac{b}{2}$.

FIGURE 21.—Continued.

(j) Spanwise station, $1.571\frac{b}{2}$.

FIGURE 21.—Concluded.

(a) On tunnel center line.

(b) Locations $0.363c$ above and below tunnel center line.

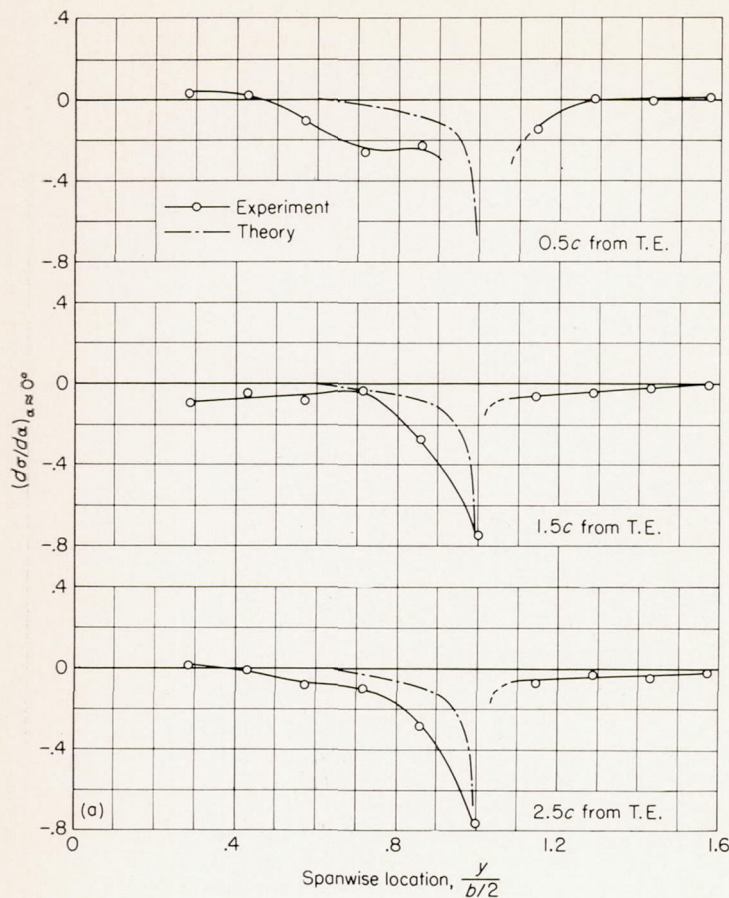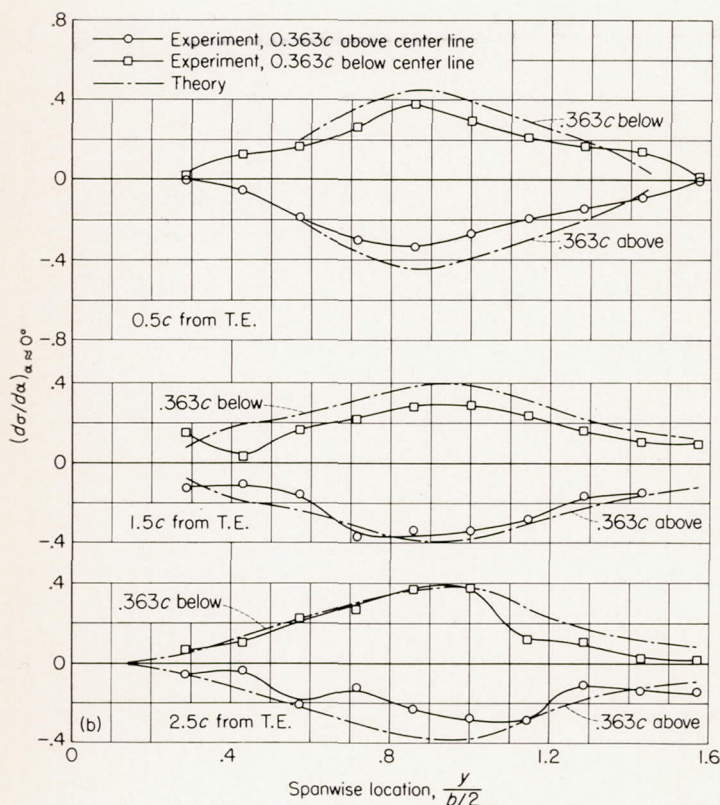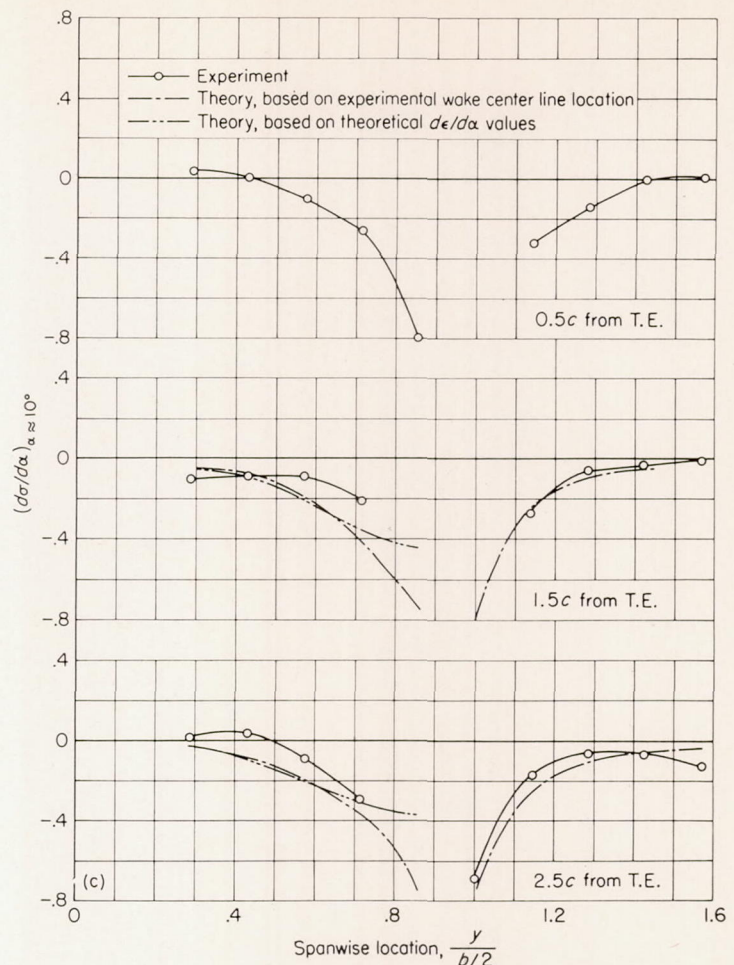FIGURE 22.—Spanwise variation in sidewash angle at a wing angle of attack of 0°.

(a) Near $\alpha=0°$, plane through tunnel center line.

(b) Near $\alpha=0°$, planes 0.363 chord above and below tunnel center line.

FIGURE 23.—Spanwise $d\sigma/d\alpha$ variation.

(c) Near $\alpha=10°$, plane through tunnel center line.

FIGURE 23.—Continued.

The theoretical values of $d\sigma/d\alpha$ have been superimposed on the experimental curves in figure 23. The comparison between theory and experiment near an angle of attack of $0°$, where the displacement of the wing trailing edge and of the trailing vortex sheet need not be considered, is shown in figures 23 (a) and 23 (b). It can be seen that for locations above and below the plane of the wing there is general agreement as to shape, but the experimental values of $d\sigma/d\alpha$ are consistently smaller numerically than the theoretical values. For the locations in the plane of the wing the theory of reference 2 predicts $d\sigma/d\alpha$ to be zero outboard of the tip, to be infinity at stations directly behind the tip, and to have finite values rapidly decreasing to zero inboard of the tip. Also the theory predicts that this $d\sigma/d\alpha$ distribution will remain unchanged in the streamwise (x) direction. This type of distribution is, of course, not fully realized for the experimental case; however, the general agreement can be seen in figure 23 (a).

Near an angle of attack of $10°$ the displacement of the trailing edge and of the trailing vortex sheet must be considered for any comparison between theory and experiment. In figures 23 (c) and 23 (d) the experimental curves are compared with theoretical results calculated by the same two methods for location of the trailing vortex sheet as in the case of downwash, namely, (1) the vortex-sheet location based on the theoretical $d\epsilon/d\alpha$ distribution of each spanwise

(d) Near $\alpha = 10°$, planes 0.363 chord above and below tunnel center line.

FIGURE 23.—Concluded.

station, integrated in the streamwise direction from the trailing edge to the test-point location, and (2) the trailing-vortex-sheet location as determined from the experimental location of the wake center line. It can be seen that when any appreciable difference is found in the results based on the two methods, such as for the location 2.5 chords behind the wing trailing edge and 0.363 chord below (fig. 23 (d)), the method based on the wake-center-line location produces better agreement with experiment.

General considerations of downwash, sidewash, and wake.—Figure 24 is a vector representation of the components of the flow velocities in planes normal to the stream for the locations 1.5 and 2.5 chords behind the wing trailing edge. Each vector was constructed from the experimental downwash and sidewash measurements. Figure 24 (a) presents the values with the wing at 0° angle of attack. The finite size of the values results from previously mentioned effects. Figures 24 (b) and 24 (c) represent the change in flow velocities within these planes resulting from an increase in angle
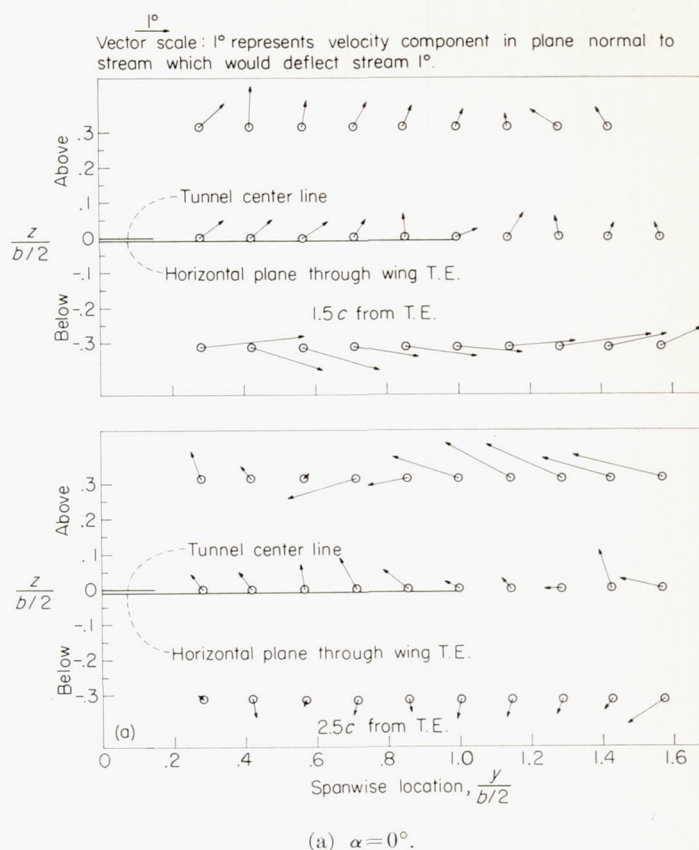
(a) $\alpha = 0°$.
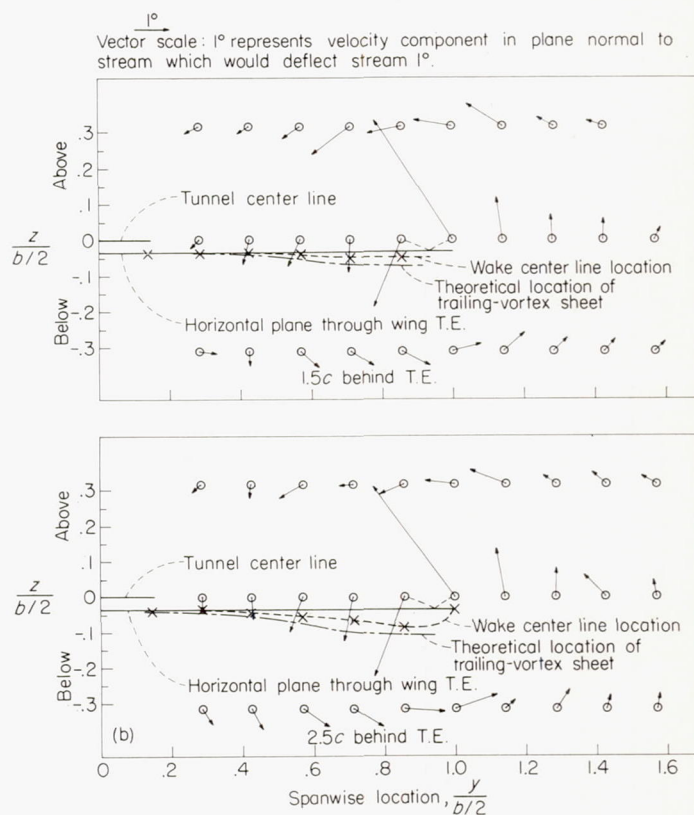
(b) $\alpha = 3°$.

FIGURE 24.—Vector representation of flow velocities in planes normal to free stream, 1.5 and 2.5c behind wing trailing edge.

Vector scale: 1° represents velocity component in plane normal to stream which would deflect stream 1°.

1.5c behind T.E.

2.5c behind T.E.

Spanwise location, $\frac{y}{b/2}$

(c) $\alpha = 6°$.

FIGURE 24.—Concluded.

of attack from $\alpha = 0°$ to $\alpha = 3°$, and from $\alpha = 0°$ to $\alpha = 6°$, respectively. Thus, when the values at $\alpha = 0°$ are used as the datum, the effects other than those of angle of attack are eliminated.

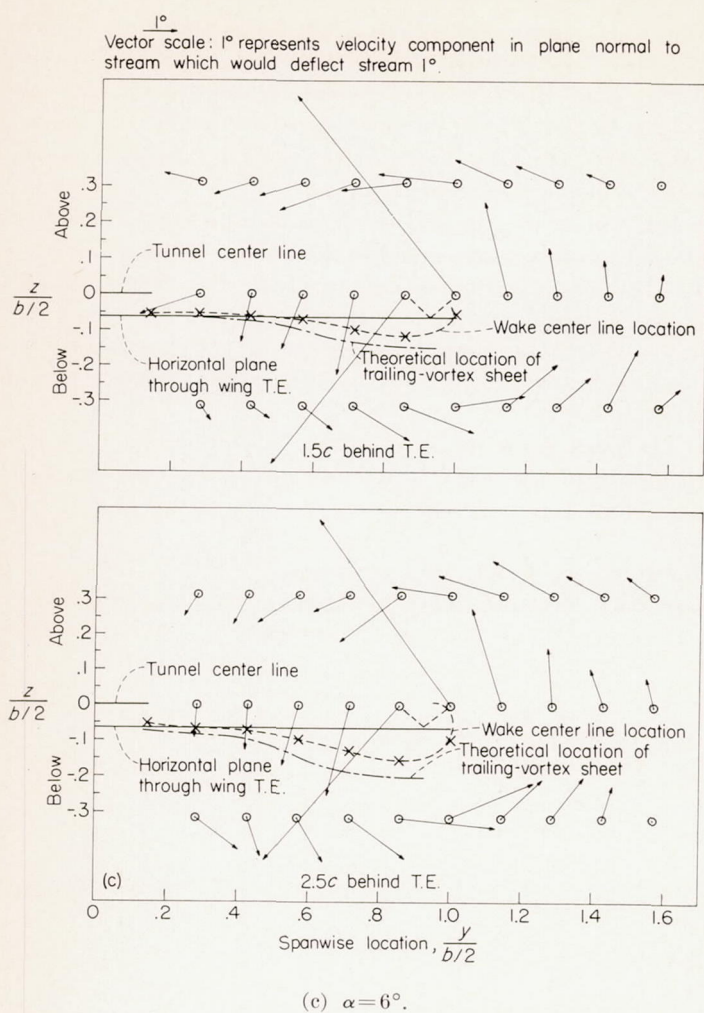This type of figure provides a good means for study of the rolling-up of the trailing vortex sheet. If the vorticity in these planes had been concentrated within a single vortex filament, the induced velocity at any point would be perpendicular to the line joining the point in question to the filament and of magnitude inversely proportional to the length of the line. The cross-flow components of velocity as given in figure 24 are not induced by a single vortex filament but by a distribution of vortex filaments, so that this component at the wing trailing edge is proportional to the rate of change of loading along the wing span. Of course for a rectangular wing the strength is greatest near the tip and, in addition, the vortex sheet rolls up with distance downstream concentrating more vorticity into this localized region downstream of the tip. The growth in the size of the two vectors near the tip with distance downstream results from the rolling-up of the trailing vortex sheet. The two large vectors are believed to be close enough to the region of strong vorticity that the intersection of their normals determines its location. It can be seen that the location of

this region of strong vorticity remains in a horizontal plane through the wing trailing edge (i.e., it is not displaced down as is the case of the inboard part of the trailing vortex sheet) and that this localized region of strong vorticity moves inward with distance downstream. Correspondingly, the size of the two large tip vectors varies inversely as their distance from the center of strong vorticity.

Also plotted in figure 24 are the locations of the intersection of the trailing vortex sheet with the planes normal to the stream represented by the figure. The location of this intersection was determined experimentally by the vertical locations of the wake pressure deficiency peaks (the dashed line through the crosses) and was calculated from the theoretical downwash distribution (indicated by the dotted dashed line). It can be seen that there is an appreciable difference between the two locations and that the use of the latter in correcting downwash values for the displacement and distortion of the vortex sheet would introduce large errors at locations inboard of the tip in the vicinity of the vortex sheet. The data of reference 7, which were obtained at a different Mach number, indicated a disparity between the location of the wake pressure deficiency peaks and the theoretical location of the trailing vortex sheet of the same order of magnitude as of this experiment, when the distances were plotted in dimensionless coefficients.

CONCLUSIONS

Surveys of the flow behind a wing of rectangular plan form, aspect ratio 2.34, and 6-percent-thick circular-arc section at a Mach number of 2.41 indicated the following conclusions:

1. Downstream of the trailing-edge shocks, there was good agreement near zero lift between experimental and theoretical values of the rate of change of downwash with angle of attack $d\epsilon/d\alpha$ except in the plane of the wing just inboard of the tip; in this region the proximity of the vortex sheet caused the downwash to be sensitive to the effects of spanwise load distribution which in turn might be greatly influenced by separation effects on the wing surface, particularly near the tip. At angles of attack near 10°, it was necessary to correct for the displacement and distortion of the vortex sheet at points near the sheet. The measured location of the vortex sheet differed greatly from that computed from the theoretical downwash distribution and, consequently, corrections to the theoretical downwash based on the theoretical location gave poor agreement with experiment. Corrections based on the measured location of the trailing vortex sheet produced much better agreement with experiment.

2. Upstream of the trailing-edge shocks, experimental values of $d\epsilon/d\alpha$ departed from the linear theory because of the effects of wing thickness and profile. In the region of two-dimensional flow, the experimental values were 0.5 instead of 1, in close agreement with calculated two-dimensional values for the particular airfoil section and Mach number. For locations outboard of the two-dimensional region the same correction factor of 0.5 gave good agreement between linear theory and experiment.

3. Experimental values of the rate of change of sidewash with angle of attack $d\sigma/d\alpha$ were in general qualitative agreement with the theory, but the magnitudes of the values measured about 0.4 chord above and below the plane of the wing were somewhat less than those predicted by theory.

4. Comparatively high values of sidewash were measured at zero lift. Calculations made by replacing the wing with a distribution of sources indicated that these values were largely attributable to the effect of wing thickness; however, the boundary-layer-shock interaction effects at the intersection of the wing and the bypass plate might be expected to affect the sidewash component of the flow angle more than the downwash component and to be more pronounced as the distance downstream increases.

5. Detailed surveys of the viscous wake showed that the trailing vortex sheet rolled up as it moved downstream. These wake surveys and the measurements of cross-flow velocities showed that the vortex core from the wing tip moved inward with increasing angle of attack and distance downstream but remained in a streamwise plane through the trailing edge, unlike the inboard portion of the sheet, which was displaced downward.

6. The wake thickness was essentially constant across the span near zero lift. At higher angles of attack the thickness increased considerably near the wing tip, but the total-pressure deficiency decreased.

7. Inboard of the tip region, the wake thickness increased much more rapidly than in subsonic flow for a short distance behind the wing; farther downstream the rate of increase of thickness became less than for the subsonic case. The wake thickness was little affected by angle of attack, but increasing the angle of attack deflected the center of the wake below the trailing edge.

8. The peak value of total-pressure deficiency in the wake was roughly of the same order as that of smooth wings in subsonic flow.

LANGLEY AERONAUTICAL LABORATORY,
    NATIONAL ADVISORY COMMITTEE FOR AERONAUTICS,
        LANGLEY FIELD, VA., *July 26, 1950.*

APPENDIX A

CALIBRATION OF MIRROR NORMALS AND METHOD OF REDUCING OPTICAL DATA TO DOWNWASH AND SIDEWASH

CALIBRATION OF MIRROR NORMALS

The equipment essential for making the measurements of the orientation of the normals to the mirror surfaces relative to the vane axis of rotation is illustrated in figure 25. The parallel light used in these calibrations was that from the tunnel schlieren apparatus. The two 6-inch-square mirrors to which the vane holder and vane were clamped were alined normal to the light by causing the image from the cross hairs across the lower hole in the screen of figure 25 to reflect back on the same cross hairs. Simultaneously the axis of rotation of the head of the vise (AA' in fig. 25) was set normal to the vertical reference axis painted on the screen by adjusting the whole vise and the horizontal turntable of the vise so that the image of the cross hairs across the lower hole of the screen always fell on the vertical reference axis of the screen, whether the 6-inch mirrors were in their vertical position or tilted up or down 22.5°.

The spindle of the vane was alined with the vertical reference axis of the screen by placing a small point source of light behind the vane, so that a greatly magnified shadow of the vane shaft fell on the screen. The 6-inch mirrors, vane holder, and vane were then rotated as a unit about axis BB' in figure 25 until the shadow cast by the vane spindle coincided with the vertical reference axis on the screen.

With the axis AA' of the tilting head of the vise normal to the vertical reference axis on the screen and with the vane spindle parallel to this vertical reference axis, the head of the vise was tilted 22.5° ±1' from the position in which the
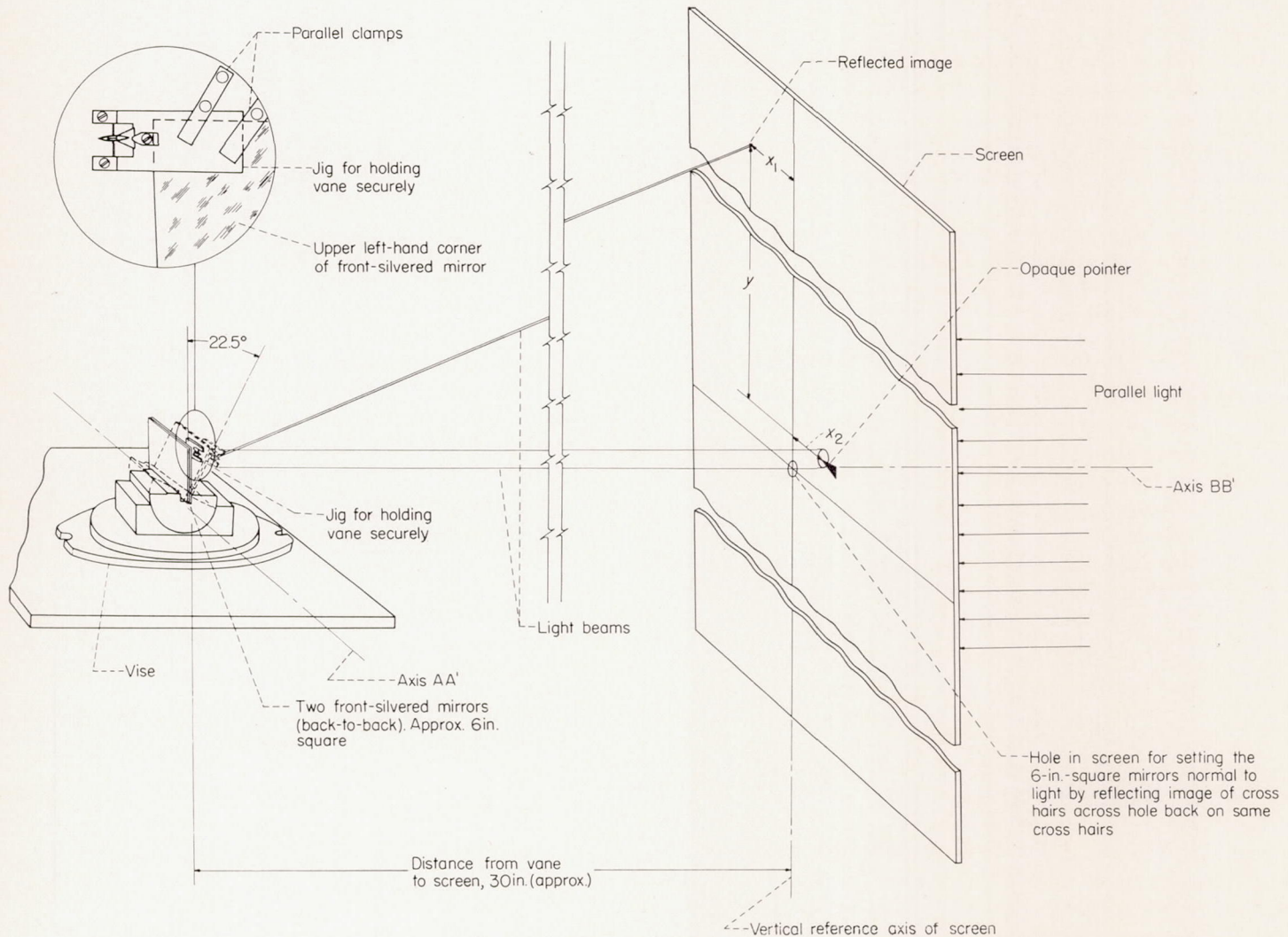

FIGURE 25.—Sketch of setup used for measuring the angles between vane axis and normals to each mirror-polished surface of vane.

6-inch mirrors were normal to the parallel light. The coordinates of the light spot thrown onto the screen by one of the polished flats of the vane were then measured. In measuring these coordinates the apex of a small opaque pointer was located in the plane of the screen in such a way that its shadow fell upon the vane mirror under calibration. This pointer was used as a reference datum to measure the coordinates from which the mirror normals could be readily determined.

METHOD OF REDUCING OPTICAL DATA TO DOWNWASH AND SIDEWASH

After the mirror surface calibration measurements were made as just described and the perpendicular distance of the grid from the vane (80 in. for these tests) and also the location of the light source relative to the grid were fixed, it was possible to compute charts whereby the angle ϕ (which the vane spindle made with the horizontal) and the angles α_B or α_T (the angle of rotation of the vane about its spindle) could be accurately determined from the measurements in inches of the x- and y-coordinates of the point of the grid illuminated by the light beam proceeding from the light source and reflected from the mirror surface of the vane. (See fig. 25.) With the vane mounted in the manner already described, namely, with its spindle inclined at approximately 45° with the horizontal, the rotation of the vane about its spindle produces an almost horizontal displacement of the light spot (for small angles) and thus is determined by the x-coordinate of the light spot and a slight rotation of the spindle in the vertical plane results in a vertical displacement of the light spot which is therefore determined by measuring the y-coordinate of the light spot.

The actual steps made in reducing the experimental data are outlined as follows:

Charts giving y, α_B, α_T, and $\left(\dfrac{d\phi}{dy}\right)_{45°}$ for values of x were computed where

x horizontal displacement of light spot

y vertical displacement of light spot

α_B angle of rotation of vane about its spindle when the bottom mirror is exposed to the incident light beam

α_T the angle of rotation of the vane about its spindle when the top mirror of the vane is exposed to the incident light beam

ϕ angle which the spindle makes with the horizontal

$\left(\dfrac{d\phi}{dy}\right)_{45°}$ the rate of change of ϕ with vertical location of light spot when the spindle is actually inclined at 45° to the horizontal

With the vane located at each of the experimental stations in turn, the x- and y-coordinates of the light spot were measured. From the prepared charts, the rotation of the vane about its spindle could be obtained in terms of x. The angle of rotation of the vane about its spindle having thus been determined, the y-coordinate of the light beam corresponding to a spindle inclination of 45° could then be obtained by referring to another set of prepared charts.

The actual inclination of the axis during tests differed slightly from 45° and hence the y-coordinate actually measured differed somewhat from the value thus obtained. The amount by which the inclination of the vane axis differed from 45° is obtained from the relation:

$$\phi_{\text{actual}}-45°=\frac{d\phi}{dy}\left(y_{\text{actual}}-y_{\text{corresponding to 45°}}\right)$$

Details of the construction of the charts of y, x, and $\dfrac{d\phi}{dy}$ corresponding to various values of vane angle of deflection α_T are given below: In sketch 1 used in calibration calculations of the vane, X, Y, and Z are reference axes fixed with respect to the tunnel, where X is parallel to the tunnel longitudinal axis, Y is the transverse axis, normal to the tunnel side walls, and Z is the vertical axis. The axes x, y, and z are fixed with respect to the vane, where x is coincident with the longitudinal axis of the vane, y with the vane spindle, and z with the normal to both x and y.
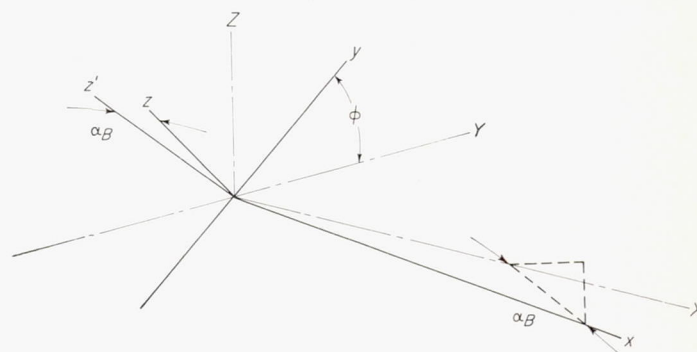
Sketch 1

The axis z' is mutually normal to the axes X and y (i.e., X, y, and z' is the orientation of the body axes when α_B equals 0°). The direction cosines of the normal to the mirror (previously measured) relative to the vane axes x, y, and z are denoted by l, m, and n, respectively. The direction cosines of the normal to the mirror with respect to X, y, and z' axes are:

$$l_1=l\cos\alpha_B+n\sin\alpha_B$$

$$m_1=m$$

$$n_1=-l\sin\alpha_B+n\cos\alpha_B$$

The direction cosines of the normal to the mirror with respect to tunnel axes X, Y, and Z are:

$$l_2=l_1$$

$$m_2=m_1\cos\phi_B-n_1\sin\phi_B$$

$$n_2=m_1\sin\phi_B+n_1\cos\phi_B$$

When the light beam which was installed in the ZY-plane is directed onto the mirror at a known angle β, it may be shown that the direction cosines of the reflected light beam

relative to the tunnel axes X, Y, and Z will be:

$$\bar{l}=-2l_2m_2\cos\beta+2l_2n_2\sin\beta$$

$$\bar{m}=-\cos\beta+2m_2{}^2\cos\beta-2m_2n_2\sin\beta$$

$$\bar{n}=-\sin\beta+2n_2{}^2\sin\beta-2m_2n_2\cos\beta$$

There exist also the relations:

$$x=D\frac{\bar{l}}{\bar{m}} \qquad (A1)$$

$$y=D\frac{\bar{n}}{\bar{m}} \qquad (A2)$$

When β, ϕ_B, and D and the direction cosines l, m, and n of the normal to the mirror with respect to the body axes are known, x and y can be evaluated in terms of α_B. Differentiating equations (A1) and (A2) with respect to ϕ, gives the expressions for $\left(\dfrac{\partial x}{\partial\phi}\right)_{45°}$ and $\left(\dfrac{\partial y}{\partial\phi}\right)_{45°}$. The former is found to be a second-order quantity and can be omitted from consideration.

The manner of obtaining downwash and sidewash is indicated in sketch 2 of the front view of the vane in its two positions where $\bar{\alpha}_T$ is the cross-flow velocity such that $\tan^{-1}\dfrac{\bar{\alpha}_T}{U}=\alpha_T$ and correspondingly $\alpha_B=\tan^{-1}\dfrac{\bar{\alpha}_B}{U}$:
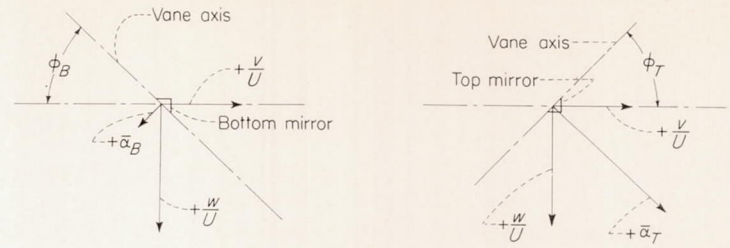
Sketch 2

For the bottom mirror it can be seen that the angular deflection of the vane is

$$\alpha_B=-\frac{v}{U}\sin\phi_B+\frac{w}{U}\cos\phi_B$$

and for the top mirror

$$\alpha_T=+\frac{v}{U}\sin\phi_T+\frac{w}{U}\cos\phi_T$$

From these two equations the downwash and sidewash can be evaluated as follows:

$$\epsilon=\frac{w}{U}=\frac{\alpha_B\sin\phi_T+\alpha_T\sin\phi_B}{\sin(\phi_B+\phi_T)}\approx\frac{1}{\sqrt{2}}(\alpha_B+\alpha_T)$$

$$\sigma=\frac{v}{U}=\frac{\alpha_T\cos\phi_B-\alpha_B\cos\phi_T}{\sin(\phi_B+\phi_T)}\approx\frac{1}{\sqrt{2}}(\alpha_T-\alpha_B)$$

APPENDIX B

THEORETICAL EVALUATION OF DOWNWASH AND SIDEWASH

Several methods exist for the evaluation of flow fields of wings in supersonic flow. The methods using doublet distributions, or vortex distributions, were discarded in favor of the superposition method of reference 2, which is the more rapid for a wing having the rectangular plan form of the tests of this report. A detailed explanation is given in reference 2 of the superposition principles on which this method is based.

In reference 2 values of $d\epsilon/d\alpha$ have been computed at various points within the plane of the wing and by interpolation, values of $d\epsilon/d\alpha$ could be obtained at those stations within the plane of the wing corresponding to the measurements of this investigation. For the purpose of comparing values predicted by linearized theory with the experimental values not in the plane of the wing, additional computations had to be made.

Once the flow field in the neighborhood of the tip of a semi-infinite rectangular wing has been evaluated, it is a simple matter to obtain by superposition the flow field of a finite rectangular wing. (See ref. 2.) Hence the problem of evaluating downwash and sidewash virtually reduces to solving the flow in the region of the tip of a semi-infinite rectangular wing.

The method used for making these computations is outlined in the following sections.

EVALUATION OF DOWNWASH $d\epsilon/d\alpha$

The evaluation of downwash in the tip region of a semi-infinite rectangular wing is made by use of the diagram shown as sketch 3:
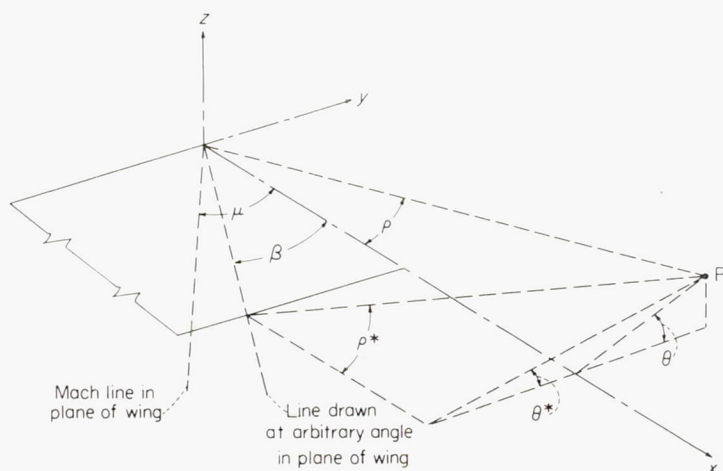
Sketch 3

The following identities are useful in this analysis:

$$a = \frac{\tan \beta}{\tan \mu}$$

$$r = \frac{\tan \rho}{\tan \mu} = \frac{\sqrt{y^2 + z^2}}{x \tan \mu}$$

$$\theta = \tan^{-1} \frac{z}{y}$$

$$r^* = \frac{\tan \rho^*}{\tan \mu} = \frac{\sqrt{\left(\dfrac{y}{c \tan \mu} - a\right)^2 + \left(\dfrac{z}{c \tan \mu}\right)^2}}{\dfrac{x}{c} - 1}$$

$$\theta^* = \tan^{-1} \frac{\dfrac{z}{c \tan \mu}}{\dfrac{y}{c \tan \mu} - a}$$

The evaluation proceeds in two parts:

(1) Downwash associated with the wing covering the planar semi-infinite quadrant can be expressed in closed form, and its evaluation presents no difficulties, thus,

$$-\frac{d\epsilon}{d\alpha} = \frac{2}{\pi}\left(\frac{1-r}{r}\right)^{\frac{1}{2}} \cos\frac{\theta}{2} + \frac{1}{\pi}\left(\tan^{-1}\frac{2\sqrt{r(1-r)}\cos\dfrac{\theta}{2}}{1-2r\cos^2\dfrac{\theta}{2}}\right) - 1 \quad \text{(B1)}$$

(2) Downwash associated with wings of constant lift distribution superimposed along the trailing edge is next to be considered (for details, refer to ref. 2). This contribution is obtained by evaluating the integral

$$\frac{d\epsilon}{d\alpha} = \frac{1}{\pi}\int_{-1}^{0} G(a, r^*, \theta^*)\, \frac{da}{\sqrt{-a(1+a)}} \quad \text{(B2)}$$

where a, r^*, and θ^* are as previously defined. The function $G(a, r^*, \theta^*)$ is a rather complicated one; namely,

$$G(a, r^*, \theta^*) = \frac{1}{\pi}\left(\frac{1}{a}\log_e R^* + \tan^{-1}\frac{2R^*\cos\theta^*}{1 - R^{*2}} + \right.$$
$$\left. \frac{B^2-1}{4B}\log_e \frac{R^{*2}+B^2-2BR^*\cos\theta^*}{1+B^2R^{*2}-2BR^*\cos\theta^*} - \frac{\pi}{2}\right) \quad \text{(B3)}$$

where

$$B = \frac{1 - \sqrt{1-a^2}}{a}$$

and

$$R^*=\frac{1-\sqrt{1-r^{*2}}}{r^*}$$

The integral (B2) was not evaluated in closed form, so that graphical methods were used. Before this evaluation can be made, the integral must be put into another form, since, as it stands, the integrand tends to infinity at both the upper and lower limits of integration.

One modified form of the integral (B2) which eliminates these infinities at the limits of integration and which can therefore be used for the purpose of making a graphical evaluation is given in the following equation where $G(0,r_0,\theta_0)$ and $G(-1,r_1,\theta_1)$ are the values of $G(a,r^*,0^*)$ at $a=0$ and -1, respectively:

$$\frac{1}{\pi}\int_{-1}^{0}G(a,r^*,\theta^*)\frac{da}{\sqrt{-a(1+a)}}=\frac{1}{\pi}\int_{-1}^{0}[G(a,r^*,\theta^*)+aG(-1,r_1,\theta_1)-$$

$$(1+a)\,G(0,r_0,\theta_0)]\frac{da}{\sqrt{-a(1+a)}}-$$

$$G(-1,r_1,\theta_1)\frac{1}{\pi}\int_{-1}^{0}\frac{a\,da}{\sqrt{-a(1+a)}}+$$

$$G(0,r_0,\theta_0)\frac{1}{\pi}\int_{-1}^{0}\frac{(1+a)da}{\sqrt{-a(1+a)}}$$

$$=\frac{1}{\pi}\int_{-1}^{0}[G(a,r^*,\theta^*)+aG(-1,r_1,\theta_1)-$$

$$(1+a)\,G(0,r_0,\theta_0)]\frac{da}{\sqrt{-a(1+a)}}-$$

$$\frac{1}{2}[G(-1,r_1,\theta_1)+G(0,r_0,\theta_0)]\quad(B4)$$

As a preliminary step in the evaluation of the downwash field, a number of charts were made, corresponding to values of a ranging from -1 to 0 in intervals of 0.1. Each of these charts consisted of plots of $G(a,r^*,\theta^*)$ against r at a constant value of θ^*.

The actual steps taken in computing downwash at any point in the flow field are enumerated below:

(1) At each value of a (from -1 to 0 in intervals of 0.1) the values of r^* and θ^* can be measured from a scale drawing or computed by using the coordinates of the point in question. Referring to the appropriate a chart permits the value of the function $G(a,r^*,\theta^*)$ to be obtained directly.

(2) Plot

$$[G(a,r^*,\theta^*)+aG(-1,r_1,\theta_1)-(1+a)\,G(0,r_0,\theta_0)]\frac{1}{\sqrt{-a(1+a)}}$$

against a and obtain the area under this curve from -1 to 0. This process gives the value of the integral

$$\int_{-1}^{0}[G(a,r^*,\theta^*)+aG(-1,r_1,\theta_1)-(1+a)\,G(0,r_0,\theta_0)]\frac{da}{\sqrt{-a(1+a)}}$$

(3) Evaluate the remaining terms of equation (B4) and add them to the result of step (2) to obtain

$$\frac{1}{\pi}\int_{-1}^{0}G(a,r^*,\theta^*)\frac{da}{\sqrt{-a(1+a)}}$$

(4) Adding this contribution to that resulting from the presence of the basic quadrant (equation (B1)) yields the final value of $d\epsilon/d\alpha$.

EVALUATION OF SIDEWASH $d\sigma/d\alpha$

As in the case of downwash, the flow about a semi-infinite wing is obtained by superimposing the flow about a lifting quadrant with the flows about wings of constant lift distribution as described in reference 2.

The sidewash associated with a lifting quadrant is given in finite terms by the formula:

$$\frac{d\sigma}{d\alpha}=-\frac{2}{\pi}\left(\frac{1-r}{r}\right)^{1/2}\sin\frac{\theta}{2}\qquad(B5)$$

The wings of constant lift distribution, which are placed along the trailing edge to cancel the pressure discontinuity existing downstream of the trailing edge, make the following contribution to $d\sigma/d\alpha$:

$$\frac{d\sigma}{d\alpha}=-\frac{1}{\pi}\int_{-1}^{0}F(a,r^*,\theta^*)\frac{da}{\sqrt{-a(1+a)}}$$

where a, r^*, and θ^* have already been defined and

$$F(a,r^*,\theta^*)=\frac{1}{\pi}a\left[\theta-\tan^{-1}\frac{2R^*\sin\theta^*\left(R^*\cos\theta^*-\frac{1}{a}\right)}{R^{*2}(\cos^2\theta^*-\sin^2\theta^*)-2\frac{R^*}{a}\cos\theta^*+1}\right]$$

In this case, as in the case of the integral used in evaluating downwash, the integrand becomes infinite at the upper and lower limits. The same artifice is used here as is used in the case of the downwash integral and the integral is changed to the form

$$\frac{d\sigma}{d\alpha}=-\frac{1}{\pi}\int_{-1}^{0}F(a,r^*,\theta^*)\frac{da}{\sqrt{-a(1+a)}}$$

$$=-\frac{1}{\pi}\int_{-1}^{0}[F(a,r^*,\theta^*)+aF(1,r_1,\theta_1)-$$

$$(1+a)F(0,r_0,\theta_0)]\frac{da}{\sqrt{-a(1+a)}}-\frac{1}{2}[F(-1,r_1,\theta_1)+F(0,r_0,\theta_0)]$$

where $F(0,r_0,\theta_0)$ and $F(-1,r_1,\theta_1)$ are the values of $F(a,r^*,\theta^*)$ at $a=0$ and -1, respectively. In the special case $a=0$, $F(a,r^*,\theta^*)$ assumes the special form

$$F(0,r_0,\theta_0)=-\frac{R^{*2}}{2\pi R^*}\sin\theta^*$$

The actual computation proceeds along the same lines as that in the computation of downwash.

CORRECTIONS TO BE APPLIED TO LINEARIZED THEORY

The calculations that have been discussed up to the present have been concerned with the estimation of basic downwash and sidewash as predicted by linearized theory. In those instances where linearized theory fails to explain the experimental data, certain refinements have been made to the basic theory in an endeavor to explain the departure from linearized theory; these refinements include, (1) the effect of distortion of the vortex sheet and (2) the effect of the wing thickness on sidewash.

The method of making such calculations is described in the following sections.

Method of applying corrections for distortion of vortex sheet.—In supersonic, as in subsonic flow, the vortex sheet deforms as it proceeds downstream from the trailing edge. The distortion of the vortex sheet in subsonic compressible flow has been the subject of various investigations, some of which are enumerated in reference 12. It is common practice, in this subsonic case, to compute the distortion of the vortex filament springing from the midspan point of the trailing edge. All vortex filaments are then assumed to be deformed in like manner. In other words, the vortex sheet is curved in a lengthwise direction but remains flat across its width. This assumption has proved valid enough in the subsonic case because in the conventional subsonic configuration the tail span is much less than the wing span. For cases where the wing and tail spans are more nearly equal, as is the case for most supersonic missile configurations, this assumption is no longer valid. The example of references 7 and 8 has been followed in this paper in evaluating the distortion separately in each of several vertical planes parallel to the stream direction. The distortion within each plane is obtained by calculating, on the basis of linearized theory, the downwash at a number of points along a line lying within the plane and passing through the wing trailing edge. The slope of the distorted sheet is then assumed to be at all points parallel to the direction of flow predicted by linearized theory. This process may be expressed in mathematical form thus:

$$\Delta z = \int_{T.E.}^{x} \frac{d\epsilon}{d\alpha}\, dx$$

where Δz is the vertical displacement of sheet at a point a distance x behind the trailing edge.

Sidewash resulting from wing thickness.—Linearized lifting-surface theory presupposes the wing to be infinitely thin and hence at $\alpha=0°$ predicts all sidewash and downwash effects to be entirely absent. In the practical case, however, the finite thickness of the wing results in an appreciable disturbance to the flow even at $\alpha=0°$. An endeavor has been made in this report to analyze the sidewash flow in the neighborhood of the tip of the rectangular wing of these tests at $\alpha=0°$ in order to ascertain whether this thickness effect would explain in part the rather large sidewash angles measured in the flow field at $\alpha=0°$.

The theoretical calculations of the thickness effect on the sidewash field at $\alpha=0°$ consist in first determining the manner in which to distribute sources over the wing plan form to simulate the flow over the 6-percent-thick, circular-arc section of the wing, and then, by use of this source distribution, in computing the sidewash in the neighborhood of the tip. If the flow is to follow the contour of the wing, it may readily be shown that, for a thin wing, the flow at the wing surface is given by

$$\frac{w}{U} = 2\frac{t}{c}\left(1-2\frac{\xi}{c}\right)$$

where
w velocity of upflow
t/c wing thickness ratio
ξ, η, ζ coordinates (see sketch 4)
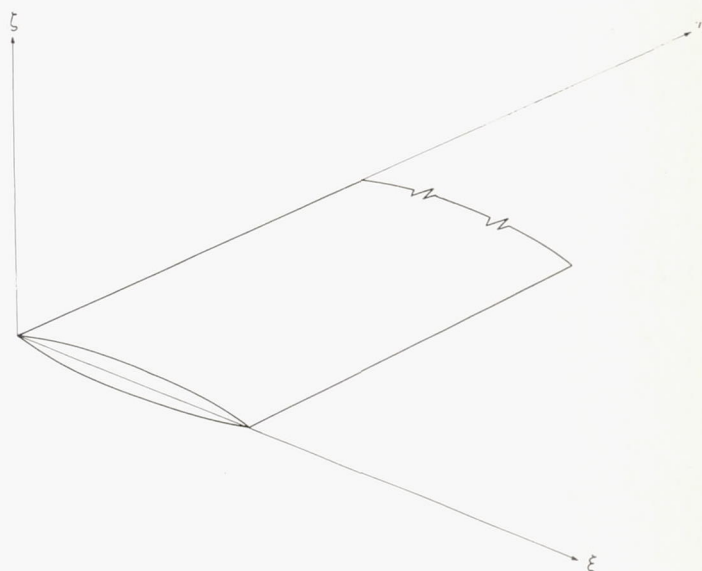
Sketch 4

The source distribution downstream of ξ_0 that will provide the desired w/U values is given by the following equation:

$$f(\xi,\eta) = -\frac{1}{\pi}w = -\frac{2}{\pi}U\frac{t}{c}\left(1-2\frac{\xi}{c}\right) = \phi(\xi)$$

This equation expresses the distribution of sources required to simulate the flow over the circular-arc wing.

The potential at any point P having the coordinates (x,y,z) can be obtained from the integral

$$\phi_P = \iint \frac{\phi(\xi)d\xi\,d\eta}{\sqrt{(x-\xi)^2 - B^2(y-\eta)^2 - B^2 z^2}}$$

The integration extends over that part of the wing surface contained within the part of the Mach forecone opening ahead of the point.

Performing these integrations and differentiating partially with respect to η yields the following expressions for the

ratio v/U (where v is the sidewash velocity and its ratio to the free-stream velocity is the tan σ). For the point lying outside the trailing-edge tip cone and inside the leading-edge tip cone

$$\frac{v}{U}=\frac{2}{\pi}\frac{t}{c}\left[-2\sqrt{\left(\frac{x}{c}\right)^2-\beta\left(\frac{y}{c}\right)^2-\beta\left(\frac{z}{c}\right)^2}+\right.$$

$$\left.\left(1-2\frac{x}{c}\right)\cosh^{-1}\frac{\frac{x}{c}}{\beta\sqrt{\left(\frac{y}{c}\right)^2+\left(\frac{z}{c}\right)^2}}\right]$$

For the point lying inside the trailing-edge tip cone,

$$\frac{v}{U}=\frac{2}{\pi}\frac{t}{c}\left[2\sqrt{\left(\frac{x}{c}-1\right)^2-\beta\left(\frac{y}{c}\right)^2-\beta\left(\frac{z}{c}\right)^2}+\right.$$

$$\left(1-2\frac{x}{c}\right)\cosh^{-1}\frac{\frac{x}{c}-1}{\beta\sqrt{\left(\frac{y}{c}\right)^2+\left(\frac{z}{c}\right)^2}}-$$

$$\left.2\sqrt{\left(\frac{x}{c}\right)^2-\beta^2\left(\frac{y}{c}\right)^2-\beta^2\left(\frac{z}{c}\right)^2}-\left(1-2\frac{x}{c}\right)\cosh^{-1}\frac{\frac{x}{c}}{\sqrt{\left(\frac{y}{c}\right)^2+\left(\frac{z}{c}\right)^2}}\right]$$

REFERENCES

1. Silverstein, Abe, Katzoff, S., and Bullivant, W. Kenneth: Downwash and Wake Behind Plain and Flapped Airfoils. NACA Rep. 651, 1939.

2. Lagerstrom, P. A., Graham, Martha E., and Grosslight, G.: Downwash and Sidewash Induced by Three-Dimensional Lifting Wings in Supersonic Flow. Rep. No. SM–13007, Douglas Aircraft Co., Inc., April 14, 1947.

3. Lagerstrom, P. A., and Graham, Martha E.: Methods for Calculating the Flow in the Trefftz-Plane Behind Supersonic Wings. Rep. No. SM–13288, Douglas Aircraft Co., Inc., July 28, 1948.

4. Mirels, Harold, and Haefeli, Rudolph C.: Line-Vortex Theory for Calculation of Supersonic Downwash. NACA Rep. 983, 1950.

5. Lomax, Harvard, Sluder, Loma, and Heaslet, Max A.: The Calculation of Downwash Behind Supersonic Wings With an Application to Triangular Plan Forms. NACA Rep. 957, 1950.

6. Ellis, Macon C., Jr., and Grigsby, Carl E.: Aerodynamic Investigation at Mach Number 1.92 of a Rectangular Wing and Tail and Body Configuration and Its Components. NACA RM L9L28a, 1950.

7. Perkins, Edward W., and Canning, Thomas N.: Investigation of Downwash and Wake Characteristics at a Mach Number of 1.53. I—Rectangular Wing. NACA RM A8L16, 1949.

8. Perkins, Edward W., and Canning, Thomas N.: Investigation of Downwash and Wake Characteristics at a Mach Number of 1.53. II—Triangular Wing. NACA RM A9D20, 1949.

9. Cummings, J. L., Mirels, H., and Baughman, L. E.: Downwash in Vortex Region Behind Trapezoidal-Wing Tip at Mach Number of 1.91. NACA RM E9H15, 1949.

10. Czarnecki, K. R., and Mueller, James N.: Investigation at Mach Number 1.62 of the Pressure Distribution Over a Rectangular Wing With Symmetrical Circular-Arc Section and 30-Percent-Chord Trailing-Edge Flap. NACA RM L9J05, 1950.

11. Czarnecki, K. R., and Mueller, James N.: An Approximate Method of Calculating Pressures in the Tip Region of a Rectangular Wing of Circular-Arc Section at Supersonic Speeds. NACA TN 2211, 1950.

12. Sprieter, John R., and Sacks, Alvin H.: The Rolling Up of the Trailing Vortex Sheet and Its Effect on the Downwash Behind Wings. Jour. Aero. Sci., vol. 18, no. 1, Jan. 1951.